

This is to certify that the

dissertation entitled

The Effect of Experimental Nonidealities on the Results of Electrode Kinetics Experiments

presented by

Edward W. Schindler, Jr.

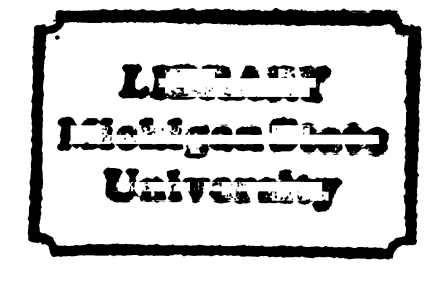
has been accepted towards fulfillment of the requirements for

Ph. D. degree in Chemistry

Date August 31, 1982

MSU is an Affirmative Action/Equal Opportunity Institution

0-12771





RETURNING MATERIALS:
Place in book drop to remove this checkout from your record. FINES will be charged if book is returned after the date stamped below.

THE EFFECT OF EXPERIMENTAL NONIDEALITIES ON THE RESULTS OF ELECTRODE KINETICS EXPERIMENTS

Ву

Edward W. Schindler, Jr.

A DISSERTATION

Submitted to

Michigan State University
in partial fulfillment of the requirements

for the degree of

DOCTOR OF PHILOSOPHY

Department of Chemistry

rat

theo

(ċį

tio to

ten

Sal Sim

of,

fin sub

the

ABSTRACT

THE EFFECT OF EXPERIMENTAL NONIDEALITIES ON THE RESULTS OF ELECTRODE KINETICS EXPERIMENTS

By

Edward W. Schindler, Jr.

Experiments designed to measure fast electrochemical reaction rates cannot be performed exactly as they are described by the theory. Factors such as instrumental nonidealities and the electrostatic interaction between the electrode and the charged reactant (diffuse-layer adsorption) have negligible effects under most conditions, but might exert a greater influence as the method is pushed to measure faster rates. It is of interest to determine to what extent these factors affect the accuracy of the measured rate constants.

The transient techniques which were studied include coulostatics, galvanostatic double pulse, and potential-step experiments. A parallel simulation method was used to generate transients showing the influence of weak reactant adsorption or an instrumental nonideality such as finite potentiostat risetime. These simulated transients were then subjected to data analysis procedures to determine the accuracy of the extracted rate constants.

Вс

found :

rent is

ing cur

time po

decreas:

volts b

Hete data bor

transie:

the valu

errors (

constant

Sma

and the to both

The sha

The conv

was four

rate con

could ot

Both reactant adsorption and finite potentiostat risetime were found to affect the shape of normal pulse polarograms when the current is sampled at or below the 1 ms time scale. Peaks resembling d.c. polarographic maxima were found for both cases. The true limiting current was attained with adsorbed reactant, while finite risetime polarograms exhibited a plateau region in which the current decreased toward the true limiting value for many hundreds of millivolts beyond the wave.

Heterogeneous rate constants were derived from these simulated data both by nonlinear regression on the chronoamperometric decay transients and by a pulse polarographic method. The accuracies of the values obtained by both methods were comparable, showing large errors (10 - 100%) for typical experimental conditions and large rate constants (>0.1 cm/s).

Small-perturbation methods were also studied in a similar manner, and the derived rate constants were found to be extremely sensitive to both instrumental and chemical nonidealities for fast reactions. The shapes of the nonideal transients showed no anomalous features. The conventional analysis for galvanostatic double pulse experiments was found to be superior to other analyses, yielding fairly accurate rate constants even under conditions such that no reasonable value could otherwise be derived.

Mic

thr

ACKNOWLEDGMENT

The author would like to express his thanks to Professor Michael Weaver for offering helpful suggestions and advice throughout the course of this work.

EDUCATIONAL GENEALOGY

- M. J. Weaver
 - D. Inman
- J. O. Bockris
- H. J. T. Ellingham
 - A. J. Allmand
 - W. H. Nernst
 - W. Ostwald
 - C. Schmidt
 - J. Liebig
- J. L. Gay-Lussac
- C. L. Berthollet

TABLE OF CONTENTS

Chapter
LIST OF TABLES
LIST OF FIGURES
LIST OF SYMBOLS
CHAPTER 1. INTRODUCTION
1.1. Phenomenological Electron-Transfer Kinetics
1.2. Experimental Techniques Used to Study Fast Electrode Kinetics
1.3. Instrumental Nonidealities
1.4. Weak Reactant Adsorption
1.5. Summary of Dissertation
CHAPTER 2. METHODS
2.1. Digital Simulation
2.2. Accuracy of Digital Simulation
2.3. Parallel Simulation Method
2.4. Details of Simulation Programming 41
2.5. Nonlinear Regression Analysis 41
2.6. Error Function Evaluation
CHAPTER 3. POTENTIAL-STEP EXPERIMENTS FOR THE STUDY OF IRREVERSIBLE ELECTRODE REACTIONS
3.1. Description of Experiment
3.2. Analysis of Data from Potential- Step Experiments

CHA CHAI

Chapter		Page
3.3.	Unique Aspects of Simulation	. 54
3.4.	Effect of Finite Potential Risetime	. 55
3.5.	Effect of Weak Reactant Adsorption	. 62
3.6.	Effect of Coupled Risetime/Adsorption	. 68
3.7.	Effect of Nonidealities on Normal Pulse Polarography	. 70
3.8.	Correlation of Model with Experimental Data	. 79
CHAPTER 4	. POTENTIAL-STEP EXPERIMENTS FOR THE STUDY OF QUASI-REVERSIBLE ELECTRODE REACTIONS	. 85
4.1.	Description of Experiment	. 86
4.2.	Conventional Data Analysis	. 87
4.3.	Unique Aspects of Simulation	. 88
4.4.	Effect of Risetime on Small-Step Chronoamperometry	. 89
4.5.	Effect of Adsorption on Small-Step Chronoamperometry	93
4.6.	Comparison of the Effect of Risetime on Normal Pulse Polarography and Large-Step Chronoamperometry	99
4.7.	Comparison of the Effect of Adsorption on Normal Pulse Polarography and Large-Step Chronoamperometry	103
4.8.	Implications for the Use of Normal Pulse Polarography	108
CHAPTER 5	. COULOSTATICS EXPERIMENTS	114
5.1.	Description of Experiment	115
5.2.	Analysis of Data from Coulostatics Experiments	118
5 2	Unique Aspects of Simulation	110

Chapter							Page
5.4. Effect of Finite Charge Injection Time	•	•	•	•	•	•	121
5.5. Effect of Weak Reactant Adsorption	•	•	•	•		•	127
CHAPTER 6. GALVANOSTATIC DOUBLE PULSE EXPERIMENTS	•	•	•	•	•	•	143
6.1. Description of Experiment	•	•		•	•	•	144
6.2. Analysis of Data from G.D.P. Experiments	•	•	•	•	•		146
6.3. Unique Aspects of Simulation	•	•	•	•	•	•	149
6.4. Shape of Deviations due to Reactant Adsorption	•	•	•	•	•	•	150
6.5. Initial Investigations	•			•	•	•	152
6.6. Effect of Adsorption in Nonlinear Regression Analysis	•	•	•	•		•	153
6.7. Effect of Adsorption in Conventional Analysis	•	•	•	•	•	•	160
6.8. Implications for the Use of Small-Step Methods	•	•	•	•	•	•	166
CHAPTER 7. SUGGESTIONS FOR FURTHER RESEARCH	•	•	•	•	•	•	169
7.1. Extension to Other Adsorption Isotherms	•	•	•	•	•	•	170
7.2. Alternative Analysis Procedures	•	•	•	•	•	•	171
APPENDIX. A SAMPLE SIMULATION PROGRAM	•	•	•	•	•	•	173
LIST OF REFERENCES		•					180

3.

3.

3.

3,5

3.6

LIST OF TABLES

Table		Page
3.1	Error in Rate Constants Derived from	
	Chronoamperometric Transients for Ir-	
	reversible Reactions Due to Finite Po-	
~	tentiostat Risetime	58
3.2	Comparison of Results of Standard and	
	"Time-shift" Analyses of Chronoampero-	
	metric Transients with Finite Risetime	61
3.3	Error in Rate Constants Derived from	
	Chronoamperometric Transients Due to	
	Weak Reactant Adsorption	65
3.4	Error in Rate Constants Derived from	
	Chronoamperometric Transients with	
	Varying Amounts of Weak Reactant Ad-	
	sorption	67
3.5	Error in Rate Constants Derived from	
	Chronoamperometric Transients Due to	
	Both Finite Risetime and Weak Reactant	
	Adsorption	69
3.6	Comparison of Results from Pulse Polar-	
	ographic and Chronoamperometric Analyses	
	of Transients with Finite Disetime	73

Table		Page
3.7	Comparison of Results from Pulse Polaro-	
	graphic and Chronoamperometric Analyses	
	of Transients with Weak Reactant Adsorp-	
	tion	. 78
3.8	Rate Constants for $Cr_{(aq)}^{3+}$ Reduction Derived	
	by Pulse Polarographic and Chronoampero-	
	metric Analyses	. 81
3.9	Results of Simulation Analysis of $Cr_{(aq)}^{3+}$	
	Data	. 83
, ,	Town to Date Contacts Darks 1 form	
4.1	Error in Rate Constants Derived from	
	Chronoamperometric Transients for Quasi-	
	Reversible Reactions Due to Finite Rise-	
	time	. 92
4.2	Error in Rate Constants Derived from	
	Chronoamperometric Transients Due to	
	Weak Reactant Adsorption	95
4.3	Error in Rate Constants Derived from	
	Chronoamperometric Transients Due to	
	Weak Reactant Adsorption (Kox + Kred)	97
4.4	Error in Rate Constant Derived from	
	Chronoamperometric Transients Due to	
	Weak Reactant Adsorption (C + C red)	98
4.5	Comparison of Chronoamperometric and	
	Pulse Polarographic Analysis of Transients	
	with Finite Risetime	102

Table			Page
4.6	Comparison of Chronoamperometric and		
	Pulse Polarographic Analyses of Tran-		
	sients with Weak Reactant Adsorption		109
5.1	Error in Rate Constants Derived from		
	Coulostatic Transients Due to Finite		
	Injection Time	• •	124
5.2	Error in Double-Layer Capacitances		
	Derived from Coulostatic Transients		
	Due to Finite Injection Time		128
5.3	Error in Rate Constants Derived from		
	Coulostatic Transients Due to Weak		
	Reactant Adsorption		133
5.4	Effect of Varying Reactant Concentration		
	on Error in Rate Constant Derived from		
	Coulostatic Data with Weak Reactant		
	Adsorption		135
5.5	Effect of Varying Adsorption Coef-		
	ficients on Error in Rate Constant		
	Derived from Coulostatic Data		136
5.6	Error in Double-Layer Capacitance		
	Derived from Coulostatic Transients		
	Due to Weak Reactant Adsorption		139
5.7	Effect of Varying Reactant Concentra-		
	tion on Error in Double-Layer		

6. 6. 6.6

6.

[able		Page
	Capacitance Derived from Coulostatic	
	Data with Weak Reactant Adsorption	• 140
5.8	Effect of Varying Adsorption Co-	
	efficients on Error in Double-Layer	
	Capacitance Derived from Coulostatic	
	Data	. 141
6.1	Effect of Adjustable Experimental	
	Parameters on Error in Rate Constant and	
	Double-Layer Capacitance Derived from	
	G.D.P. Transients with Weak Reactant	
	Adsorption	. 154
6.2	Error in Rate Constants Derived from	
	G.D.P. Transients Due to Weak Reac-	
	tant Adsorption (K _{ox} = K _{red})	. 155
6.3	Error in Double-Layer Capacitance	
	Derived from G.D.P. Transients Due to	
	Weak Reactant Adsorption (K = K red)	. 156
6.4	Error in Rate Constant Derived from	
	G.D.P. Transients Due to Weak Reactant	
	Adsorption (K _{ox} ≠ K _{red})	. 159
6.5	Error in Rate Constants Derived from	
	G.D.P. Transients Due to Weak Reactant	
	Adsorption (C _{ox} ≠ C _{red})	. 161
6.6	Results of Conventional Analysis of G.D.P.	
	Data with Weak Reactant Adsorption	. 165

LIST OF FIGURES

Figure		Page
1.1	Diffuse-layer adsorption coefficient	
	K _{ad} (calculated from Equation 1.11)	
	vs. potential for a 3+ ion in 1 M	
	KF at a mercury electrode	. 18
1.2	Diffuse-layer adsorption coefficient	
	K (calculated from Equation 1.11)	
	vs. potential for a 3+ ion in 0.1 M	
	KF at a mercury electrode	. 19
2.1	Summary of the process used to determine	
	the effects of nonidealities upon the re-	
	sults of electrode kinetics experiments	. 26
2.2	Basic elements of digital simulation	
	of electrochemical experiments	. 29
2.3	Standard deviation of simulation $vs.$	
	simulation parameter Δx_1 for typical	
	systems. Curve 1: conventional simulation.	
	Curve 2: parallel simulation	. 39
2.4	Standard deviation of simulation vs.	
	computation time for typical systems.	
	Curve 1: conventional simulation.	
	Curve 2: parallel simulation	. 40

Figure		Page
2.5	Experimental process modified to	
	reflect the parallel simulation method	42
2.6	Functions of g(z) to obtain f(z) in	
	four quadrants	47
3.1	Chronoamperometric transients for	
	irreversible reactions illustrating the	
	effects of potentiostat risetime, with	
	$k_f = 0.3 \text{ cm/s}, C = 1 \text{ mM}, D = 1 \times 10^{-5}$	
	cm^2/s , $E_{step} = -500 \text{ mV}$. Curve 1:	
	ideal system. Curve 2: τ = 20 μs.	
	Curve 3: τ = 50 μs	56
3.2	Chronoamperometric transients illustrat-	
	ing the effects of weak reactant adsorpton,	
	with parameters as in Figure 3.1, ex-	
	cept k _f = 0.1 cm/s. Curve 1: ideal	
	system. Curve 2: $K_{ad}^{1} = K_{ad} = 2 \times 10^{-5}$	
	cm. Curve 3: $K_{ad}^{1} = 2 \times 10^{-5}$ cm, $K_{ad} = 0$.	
	Curve 4: $K_{ad}^1 = 0$, $K_{ad} = 2 \times 10^{-5}$ cm	63
3.3	Pulse polarograms illustrating the ef-	
	fects of finite risetime, with α =	
	0.5, $C = 1 \text{ mM}$, $D = 1 \times 10^{-5} \text{ cm}^2/\text{s}$.	
	Curve 1: ideal system, 100 µs sampling	
	time. Curve 2: τ = 20 μ s, 100 μ s	
	sampling time. Curve 3: ideal system,	
	1 ms sampling time. Curve 4: τ =	
	20 Mg 1 mg gamoling time	71

Figure	Page

3.4	Pulse polarograms illustrating the ef-	
	fects of reactant adsorption, with	
	$\alpha = 0.5$, $C = 1$ mM, $D = 1 \times 10^{-5}$ cm ² /s.	
	Curve 1: ideal system, 100 µs sampling	
	time. Curve 2: $K_{ad}^{1} = K_{ad} = 2 \times 10^{-5}$	
	cm, 100 μ s sampling time. Curve 3:	
	ideal system, 1 ms sampling time.	
	Curve 4: $K_{ad}^{i} = K_{ad} = 2 \times 10^{-5} \text{ cm}, 1 \text{ ms}$	
	sampling time	75
3.5	Pulse polarograms illustrating the ef-	
	fects of reactant adsorption, with α =	
	0.5, $C = 1 \text{ mM}$, $D = 1 \times 10^{-5} \text{ cm}^2/\text{s}$, 100	
	μs sampling time. Curve 1: ideal	
	system. Curve 2: $K_{ad}^{i} = 2 \times 10^{-5}$ cm,	
	$K_{ad} = 0$. Curve 3: $K_{ad}^{1} = 0$, $K_{ad} =$	
	2×10^{-5} cm	77
3.6	Rate constants for Cr(OH ₂) ₆ ³⁺ reduc-	
	tion derived from experimental chrono-	
	amperometric transients using simula-	
	tion analysis, vs. potential. Line is	
	least-squares fit of lower six points	82
4.1	Chronoamperometric transients for	
	quasi-reversible reactions illustrating	
	the effects of finite risetime, with k std	
	= 0.1 cm/s, α = 0.5, E_{step} = -10 mV,	

		4
		,
		4

Figure Page

	$C_{\text{ox}} = C_{\text{red}} = 1 \text{ mM}, D_{\text{ox}} = D_{\text{red}} =$
	$1 \times 10^{-5} \text{ cm}^2/\text{s}$. Curve 1: ideal system.
	Curve 2: τ = 50 μs 90
4.2	Chronoamperometric transients il-
	lustrating the effects of reactant
	adsorption, with k std = 0.1 cm/s,
	α = 0.5, E _{step} = -10 mV, C _{ox} = C _{red}
	= 1 mM, $D_{ox} = D_{red} = 1 \times 10^{-5} \text{ cm}^2/\text{s}$.
	Curve 1: ideal system. Curve 2:
	$K_{\text{ox}} = K_{\text{red}} = 2 \times 10^{-5} \text{ cm}$
4.3	Pulse polarograms illustrating the ef-
	fects of finite risetime, with k std =
	0.1 cm/s, α = 0.5, E_{std} = 0 mV, C_{ox} =
	1 mM, $D_{ox} = D_{red} = 1 \times 10^{-5} \text{ cm}^2/\text{s}$,
	100 μs sampling time. Curve 1: ideal
	system. Curve 2: $\tau = 10 \mu s$. Curve
	3: τ = 20 μs
4.4	Pulse polarograms illustrating the ef-
	fects of reactant adsorption, with k std
	= 0.1 cm/s, α = 0.5, E_{std} = 0 mV,
	$C_{ox} = 1 \text{ mM}, D_{ox} = D_{red} = 1 \times 10^{-5}$
	${\rm cm}^2/{\rm s}$, 100 $\mu{\rm s}$ sampling time. Curve 1:
	ideal system. Curve 2: $K_{ox}^{i} = K_{ox} =$
	2×10^{-5} cm. Curve 3: $K_{ox}^{i} = 2 \times 10^{-5}$
	cm, $K_{ox} = 0$. Curve 4: $K_{ox}^{i} = 0$, $K_{ox} =$
	2×10^{-5} cm

4.5	Pulse polarograms illustrating the	
	effects of reactant adsorption at the	
	onset of reversibility, with $\alpha = 0.5$,	
	$E_{std} = 0 \text{ mV}, C_{ox} = 1 \text{ mM}, D_{ox} = D_{red}$ = 1 x 10 ⁻⁵ cm ² /s, $K_{ox}^{1} = K_{ox} = 2 \times 10^{-5}$	
	cm, 100 µs sampling time. Curve 1:	
	k _{std} = 3 cm/s. Curve 2: k _{std} = 0.1	
	cm/s	107
5.1	Coulostatic transients illustrating	
	the effects of finite charge injection	
	time, with $k_{std} = 1 \text{ cm/s}, C_{d1} =$	
	20 $\mu F/cm^2$, $Q_{inj} = 1 nC$, area = 0.02	
	cm^2 , $C_{ox} = C_{red} = 1 mM$, $D_{ox} = D_{red}$	
	= 1×10^{-5} cm ² /s. Curve 1: ideal	
	charge injection. Curve 2: t _{inj} =	
	500 ns	122
5.2	Relative error in standard rate	
	constant vs. ratio τ_c/τ_d . Curve 1:	
	$t_{inj}/\tau_c = 0.0188$. Curve 2: t_{inj}/τ_c	
	= 0.0565. Curve 3: $t_{inj}/\tau_c = 0.133$.	
	Curve 4: $t_{inj}/\tau_c = 0.188$	126
5.3	Relative error in double-layer capaci-	
	tance vs. ratio τ_c/τ_d . Curve 1: $t_{inj}/$	
	$\tau_{c} = 0.0188$. Curve 2: $t_{inj}/\tau_{c} = 0.0565$.	
	Curve 3: $t_{inj}/\tau_c = 0.133$. Curve 4:	
	$t_{inj}/\tau_c = 0.188 \dots \dots \dots \dots$	129

Page

Figure

Figure Page

```
5.4
          Coulostatic transients illustrating the
          effects of reactant adsorption, with
          k_{std} = 1 \text{ cm/s}, C_{d1} = 20 \mu \text{F/cm}^2, Q_{ini}
          = 1 nC, area = 0.02 \text{ cm}^2, C_{\text{ox}} = C_{\text{red}} =
          1 mM, D_{ox} = D_{red} = 1 \times 10^{-5} \text{ cm}^2/\text{s}.
          Curve 1: ideal system. Curve 2: K
          = K_{red} = 1 \times 10^{-6} cm. Curve 3: K_{ox} =
          K_{\text{red}} = 5 \times 10^{-6} \text{ cm.} \dots \dots \dots
                                                                                 131
6.1
          Galvanostatic double pulse transients
          illustrating the effects of reactant
          adsorption, with k_{std} = 0.3 cm/s,
          C_{d1} = 20 \mu F/cm^2, i_1 = 0.055 \text{ A/cm}^2,
          t_1 = 1 \mu s, i_2 = 0.002 \text{ A/cm}^2, C_{ox} =
          C_{red} = 1 \text{ mM}, D_{ox} = D_{red} = 1 \times 10^{-5}
          cm<sup>2</sup>/s. Curve 1: ideal system. Curve
          2: K_{ox} = K_{red} = 1 \times 10^{-6} cm. Curve 3:
          K_{ox} = K_{red} = 3 \times 10^{-6} cm. Curve 4:
          K_{ox} = K_{red} = 1 \times 10^{-5} \text{ cm.} \dots \dots \dots
                                                                                 151
          Overpotential minimum vs. t_1^{\frac{1}{2}} for con-
6.2
          ventional g.d.p. analysis, with k = =
          0.3 cm/s, C_{d1} = 20 \mu F/cm^2, i_2 = 0.003
          A/cm^2, C_{ox} = C_{red} = 1 \text{ mM}, D_{ox} = D_{red} =
          1 \times 10^{-5} \text{ cm}^2/\text{s}. Lines are least-
          squares best fit. Curve 1: ideal system.
          Curve 2: K_{ox} = K_{red} = 1 \times 10^{-5} \text{ cm} \dots \dots
                                                                                 163
```

Figure		Page
6.3	Overpotential minimum vs $t_1^{\frac{1}{2}}$ for con-	
	ventional g.d.p. analysis, with k std =	
	3 cm/s , $i_2 = 0.02 \text{ A/cm}^2$, other param-	
	eters as in Figure 6.2. Lines are	
	least-squares best fit. Curve 1:	
	ideal system. Curve 2: K = K =	
	1 x 10 ⁻⁵ cm	164

LIST OF SYMBOLS

Symbol	Meaning	Usual Units
A	electrode area	cm ²
		mol/cm ³
C	concentration	_
C _{bulk}	bulk concentration	mol/cm ³
Cox	bulk concentration of species Ox	mol/cm ³
Cred	bulk concentration of species Red	mol/cm ³
Co	concentration at electrode surface	mol/cm ³
C _x	concentration at distance x from surface	mol/cm ³
ci	concentration at discrete point i in solution	mol/cm ³
c_1	concentration at first discrete point in solution	mol/cm ³
Cdl	double-layer capacitance	μF/cm ²
D	diffusion coefficient	cm ² /s
Dox	diffusion coefficient of species Ox	cm²/s
Dred	diffusion coefficient of species Red	cm ² /s
E	electrode potential	v
EO	thermodynamic standard potential	V
Estd	standard electrode potential	V
E init	electrode potential prior to perturbation	V
E	potential step size	V
F	Faraday constant	coul/mol
f	F/RT	v ⁻¹
i	current	μ A
i sim	simulated current	μ A
icalc	calculated current	μ A
i _{lim}	polarographic limiting current	μA
i ₁	size of first pulse in g.d.p.	A/cm ²
1 ₂	size of second pulse in g.d.p.	A/cm ²
K	general equilibrium constant	

Symbol Symbol	Meaning	<u>Usual Units</u>
К.	adsorption coefficient	c m
"ad K ¹ ad	adsorption coefficient prior to perturbation	cm.
ad K	adsorption coefficient of species Ox	cm
K K ¹ ox	adsorption coefficient of species Ox prior to perturbation	cm
K red	adsorption coefficient of species Red	cm
Ki red	adsorption coefficient of species Red prior to perturbation	cm
k std	standard heterogeneous rate constant	cm/s
k _f	forward rate constant	cm/s
k f k f	forward rate constant for adsorbed species	s ⁻¹
k _{f,Estep}	forward rate constant at potential E step	cm/s
k _b	reverse rate constant	cm/s
k overal1	effective rate constant in the presence of adsorption	cm/s
n	number of electrons	
Pamp	size of current impulse in coulostatics	A
Q _{inj}	amount of injected charge in coulostatics	μC
q	total charge on electrode (inside o.H.p.)	μC/cmm ²
$\mathbf{q}^{\mathbf{m}}$	charge on electrode	μ C/cm²
q'	charge of specifically adsorbed ions	μ C/cm²
R	gas constant	J/mo1·K
$R_{\mathbf{u}}$	uncompensated resistance	Ω
T	temperature	K
t	time	s
t ₁	length of first pulse in g.d.p.	рв
t ₂	length of second pulse in g.d.p.	μв
t min	time at which minimum appears in g.d.p.	μ з
x	distance	cm
Z	charge on diffuse-layer adsorbed ion	
Z	charge on supporting electrolyte ion	
α	transfer coefficient	
β	dimensionless diffusion coefficient	

Symbol	Meaning	Usual Units
Γ	surface excess	mol/cm ²
Δt	simulation time increment	s
$\Delta \mathbf{x}$	simulation distance increment	cm
$^{\Delta\mathbf{x_{i}}}$	distance increment between discrete points i-1 and i	cm
Δx_1	first distance increment	c m
η	overpotential	mV
$\eta^{\mathbf{o}}$	initial overpotential in coulostatics	mV
η _{min}	minimum overpotential in g.d.p.	mV
η <mark>ο</mark> min	intercept of η_{\min} vs. $t_1^{\frac{1}{2}}$ plot in g.d.p.	mV
$\sigma_{ extsf{sim}}$	standard deviation of simulation	
τ	potentiostat rise time constant	μ з
$\tau_{\mathbf{c}}$	charge transfer time constant	μ ន
$\tau_{\mathbf{d}}$	diffusion time constant	μs
Φ	flux of reactant at electrode surface	mol/cm ² ·s
φ far	faradaic flux	mol/cm ² ·s
φ ₂	diffuse-layer potential at o.H.p.	mV .
$\phi_{\mathbf{x}}^{\mathbf{z}}$	diffuse-layer potential at distance x from o.H.p.	mV

CHAPTER 1

INTRODUCTION

Reactions involving the transfer of electrons between two redox centers are fundamental in many fields, from biochemistry (photosynthesis) to industrial processes (chlor-alkali technology). They are also the most basic type of reaction as there are no chemical bonds formed or broken. In many important systems, of course, the electron-transfer process is only one step in a mechanism involving several other, chemical steps, but it is generally the key step. Because these reactions are so basic, it is important to study their detailed mechanisms and rates so that the overall processes might be better understood.

Electrochemical reactions (heterogeneous electron-transfer reactions) occur at the surface of an electrode immersed in a solution of an oxidizable or reducible (electroactive) species. In this special case of electron-transfer reactions, the electrode acts as the other reactant in the redox reaction, supplying or accepting electrons as required. The advantages of studying the kinetics of redox species in this manner are that it is relatively easy to follow the rate of the reaction, only the chemistry of a single species needs to be considered, and finally that the thermodynamics of the system (electrode plus reactant) are continuously variable by adjustment of the electrode potential.

Various experimental techniques have been developed to study
the kinetics of electrode reactions, and, like their chemical kinetics
counterparts, they are subject to limitations based on the time scale

of the method. Steady state methods are useful for studying relatively slow reactions, while transient techniques are used for relatively fast rates. It is important to know under what conditions the theory of a given experiment breaks down and the results yield no useful information.

Electrochemical techniques, like all chemical experiments, are subject to minor experimental nonidealities. There are always factors which are not taken into account in the theory, but that do occur in the actual performance of an experiment. These effects must be minor, or the particular theory would not have general acceptance.

This dissertation will examine a variety of electrochemical transient techniques to determine whether the nonidealities that are inevitable in actual experiments affect the results as the method is used to determine faster and faster reaction rates. Effects which are largely negligible when slow reactions are studied could induce significant error as the technique is taken to its limits. This is because the rate of a fast electrode reaction is controlled more by the diffusion of reactant molecules to the electrode surface than by the actual kinetics of the charge-transfer process. A given experimental method must be sensitive enough to extract the small amount of kinetics information which is available in the data, and might therefore be more sensitive to nonideal experimental conditions.

Both the instrumentation and the chemical system itself must lead to variations from the theoretical conditions for an experiment. Instruments rarely perform ideally; for example, a potentiostat requires a period of time to attain a new cell potential, even though

a step-function is assumed in the derivation of the relevant equations.

Additionally, coulombic attractive or repulsive forces between the reactant ions and the electrode are virtually universal, but seldom considered.

Some previous work (1-4) has examined the effects of finite measurement precision and some instrumental limitations upon the results of many of the same electrode kinetics experiments which are examined here. These investigations simply used an explicit solution for the response of the system, rounded the results or otherwise modified the data to reflect the nonideal conditions, and derived the heterogeneous rate constants from these modified data. Thus, no nonidealities could be treated in this manner in the absence of an explicit solution. The work described in this dissertation removes that restriction by using the digital simulation of electrochemical systems, which allows a much wider variety of nonideal conditions to be examined.

Flanagan and Anson (5-7) examined some electrochemical systems to determine the effects of reactant adsorption for reversible systems. This work did not address the question of finite electron-transfer rates, but instead considered only deviations in the morphology response curves. They did, however, rely on digital simulation of the electrochemical experiments in some of their studies.

The remainder of this chapter is devoted to some basic concepts of electron-transfer kinetics, a description of some transient techniques used to study fast electrode reactions, and a discussion of both the instrumental and chemical nonidealities which must occur,

to at least some extent, in every experiment for the measurement of electrochemical reaction rates. The bulk of the dissertation examines the effects of these nonidealities on several common transient techniques and some general implications for the use of these methods.

1.1. Phenomenological Electron Transfer Kinetics

For a chemically irreversible process

$$0x + ne^{-k_f}$$
 Red (1.1)

occurring at an electrode surface, the rate constant $k_{\hat{f}}$ is known to be a function of the electrode potential:

$$k_f = k_{std} \exp \left[-\frac{\alpha nF}{RT} (E-E_{std})\right]$$
 (1.2)

For these irreversible processes, k_{std} is simply the heterogeneous rate constant at some arbitrary potential E_{std} . This expression is in fact a linear free energy relationship, correlating the rate of the electron-transfer reaction to the free energy driving force as it varies with the electrode potential ($\Delta G = -nFE$).

If the process is chemically reversible, however, we must also consider the rate of the reverse reaction,

$$0x + ne^{-} \stackrel{k_f}{\rightleftharpoons} Red \qquad (1.3)$$

$$k_b$$

The thermodynamic equilibrium of this redox process is governed by

the Nernst equation (neglecting activity coefficients),

$$E = E^{O} - \frac{RT}{nF} \ln \frac{[Red]}{[Ox]}$$
 (1.4)

which specifies the potential at which no net reaction occurs for a given ratio of product to reactant concentration (the equilibrium potential). Since the Nernst equation defines the equilibrium constant at a given electrode potential, and this equilibrium constant must be equal to the ratio of forward and reverse rate constants ($K = k_f/k_b$), it is possible to derive an expression for the rate constant for the reverse reaction as a function of potential,

$$k_{b} = k_{std} \exp\left[\frac{(1-\alpha)nF}{RT} (E-E_{std})\right]$$
 (1.5)

The standard potential, E_{std} , for these chemically reversible redox couples is now the thermodynamic E^{O} ; both the forward and reverse rate constants are equal to the standard rate constant at this potential. When this standard rate constant is very large (>10-100 cm/s), the couple is termed "reversible". At very small standard rate constants, the back reaction becomes insignificant (e.g., in order to force k_f to be large enough, the potential must be set sufficiently negative so that the reverse rate constant k_b is very small). Under these conditions, the system behaves as if it were chemically irreversible, and is termed "irreversible". Redox couples with standard rate constants between these extremes are usually referred to as "quasi-reversible".

1.2. Experimental Techniques Used to Study Fast Electrode Kinetics

Because of their speed, transient techniques (as opposed to steady-state methods) are usually used to study fast electrochemical reactions (9). These experiments involve, in the case of quasi-reversible reactions, a system at some equilibrium state to which a sudden perturbation is applied. The response of the system to the perturbation is followed, and rate parameters can be derived from these data. In the case of irreversible reactions, where no real redox equilibrium can exist, the perturbation usually involves a change in some experimental parameter which will initiate the electrochemical reaction. The perturbations in either type of chemical system can be steps of potential, current, or charge, or continuously applied waveforms, such as an ac signal or a triangle wave.

Potential-step experiments (10) are conceptually quite straightforward. An electrode in a solution of the species of interest is
held at a potential such that no reaction occurs and no current flows.

The potential is rapidly changed to a new value, the reaction begins,
and current flows. This current is monitored as a function of time.

Various modes of this type of experiment are possible, depending on
the chemistry of the reactant species. Large potential steps (several hundred millivolts) are needed if the reaction is irreversible

(10), as one must start at a potential which yields a negligible rate
constant and step to one which causes the reaction to proceed at
a faster rate.

Large potential steps can also be used for quasi-reversible reactions (10) if the concentration of one half of the redox couple is very small. A large step from the equilibrium potential is required in order to change the relative concentrations of the oxidized and reduced forms of the reactant enough to yield an observable current. This mode is used in the normal pulse polarographic study of quasi-reversible redox reactions, and is characterized by the addition of only one form of the redox couple to the solution.

Quasi-reversible reactions can also be studied when both the oxidized and reduced forms of the species are in solution at the start of the experiment (11). The electrode is held at the equilibrium potential for the system as given by the Nernst equation. A step in potential of several millivolts is applied, requiring the electrode reaction to proceed in order to adjust the concentration ratio of the reactants at the surface to that required by the Nernst equation.

Analogous to the small potential-step experiments are coulostatics experiments (12,13) in which the perturbation of the system is a fast injection of charge into the cell. The charge then leaks off into the solution at a rate controlled by the electrode reaction rate and by the diffusion of fresh reactant to the surface. The overpotential is followed as it decays, since it is impossible to measure the current itself because the flow of electrons occurs only from the electrode surface to the solution once the charge has been injected.

In small-step coulostatics for the study of quasi-reversible reactions (12,13), both the oxidized and reduced species are in the solution and the electrode is initially at the equilibrium potential.

The equations describing the overpotential decay are somewhat more
complicated, however, due to the fact that the potential (and hence

the rate constants) is changing continuously throughout the experiment.

The remaining step technique which has been commonly employed by electrode kineticists is galvanostatics (14). In these experiments, a system, again at such a potential that no current flows, is subjected to the sudden imposition of a constant current. The response of the system to this perturbation is a change in the overpotential sufficient to make the reactions proceed fast enough to consume these electrons as they flow through the cell. This overpotential—time transient contains information about the kinetics of the electron—transfer reaction.

Galvanostatic double pulse experiments were developed (15) to deal with very fast electrode reactions by precharging the electrode double layer with a fast, high current pulse. The overpotential-time data are recorded immediately thereafter during the application of a smaller current to the cell.

In addition to the step experiments, other types of transient signals have been used to measure electrochemical reaction rates. The application of an alternating potential waveform to a system at some equilibrium condition causes an alternating current to flow in response (16). Phase sensitive detection allows the extraction of heterogeneous rate data in these experiments. A potential ramp or triangular waveform can also be applied in techniques known as linear sweep voltammetry or cyclic voltammetry (17,18). A peak in the current is observed in the forward and reverse sweeps; the separation of these peaks can be related to the rate constant for the reaction of

interest.

The responses of any of the transient techniques are controlled by the rate of charge-transfer and that of diffusion, the former dominating at short times and the latter at longer times. The faster the charge transfer process, the sooner the diffusion of reactants controls the response. These transient techniques are useful, therefore, for the study of fast electrode reactions because the perturbation to the system can be made in a very small amount of time.

Of the step methods, potentiostatics is the slowest because of its high demands on the instrumentation. At the time of the step, the potentiostat must provide a large amount of current to charge the double-layer capacitance, yet it must be sensitive enough to measure the small currents due to faradaic processes. Because of this and problems with uncompensated resistance, the potential-step method is not used on much less than a 0.1 ms time scale, which is suitable only for the measurement of heterogeneous rate constants up to about 0.1 cm/s.

Charge-step methods are quite fast (indeed, this is the reason for their development), with the perturbation being applied in well under 1 µs, depending on the solution resistance. Galvanostatic methods also can be employed on the microsecond time scale. In both these methods, the capacitance of the electrode has a direct effect on the resulting transient; there is no need for the instrumentation to "beat out" the charging process as in potentiostatics. These methods have been claimed to be suitable for the measurement of rate constants in the 0.1 to 10 cm/s range.

AC methods are limited by the frequency which can be applied to the cell (16). At higher frequencies, the technique is affected by stray capacitances and other irreproducible nonidealities which render the signal virtually useless for kinetics purposes. The upper limit of the accessible rate constant is roughly the same as for coulostatics and galvanostatics.

Linear sweep methods are limited by the rate at which the potential can be scanned (17). At high sweep rates, the current which charges the double layer becomes quite large and deviations due to uncompensated resistance result, obscuring the kinetics information. Rate constants of about 0.1 cm/s are the maximum accessible with these methods.

1.3. Instrumental Nonidealities

The instrumentation used to perform these transient techniques is basically the same as that required for steady-state methods, except that optimizations for a fast response time must be included. A typical potentiostat (19) contains a potential control amplifier whose function is to hold the working electrode at some fixed potential relative to the reference electrode by supplying current to the cell. This current is measured by a second amplifier acting as a current to voltage converter.

The response of an ideal potentiostat to an instantaneous step function in the control potential is a simultaneous step in the cell potential. In a real potentiostat, however, the response time is limited by the time constants of both the cell and the potentiostat itself, as well as by the maximum current which can be supplied to

the auxillary electrode (20,22).

Uncompensated resistance between the reference electrode and the working electrode is another factor which prevents the applied potential from following the control potential (22). When current flows, the error in the cell potential is equal to iR_u. Since the most current flows at the moment the step is applied, the potential only approaches the control potential as the current decays.

Although the amount of uncompensated resistance varies with the solution composition (as does the cell time constant), it is present to at least some extent in all experiments since it can never be perfectly compensated. Because of this and the previously mentioned factors, all potential-step experiments must be to some degree non-ideal; an instantaneous potential step can never be applied to a real cell.

Solution resistance is also a problem in performing coulostatics experiments. The theory (15) calls for an instantaneous injection of charge into the cell, but in practice a finite amount of time is needed to accomplish this. Additionally, current impulse charge injection experiments (23) have an inherent injection time during which a current pulse is applied.

Galvanostatic experiments also suffer from iR drop errors in the measurement of the overpotential while current is applied. Not only is uncompensated resistance a problem, but the theory assumes that the current is initiated instantaneously (14). Again, instrumentation limitations prevent a perfect step function from being applied, leading to deviations from the ideal predictions.

These types of nonidealities are of interest here because they are inevitable when experiments are performed with real instrumentation. The nonidealities on which attention is focused in this work are finite potentiostat risetime and finite charge injection time in coulostatics. Uncompensated resistance effects were not considered because the effects in potentiostatics are similar to those of finite risetime.

1.4. Weak Reactant Adsorption

In most electrochemical experiments, we are dealing with charged reactant ions in solution in the vicinity of a charged electrode.

One would therefore expect some sort of electrostatic interaction to exist between them, either a concentration enhancement or reduction depending on the relative signs of the charges. A concentration enhancement due to these factors can be looked upon as a form of adsorption, and can be referred to as diffuse-layer adsorption.

This phenomenon is of interest because it must be present to at least some extent in almost all experiments which are designed to measure electrode kinetics (the exception being experiments which take place at a potential such that the total charge on the electrode is zero, e.g., the potential of zero charge, or p.z.c., in the absence of ionic specific adsorption). This electrostatic effect is well known in electrode kinetics through so-called double layer corrections of apparent heterogeneous rate constants, which consider the effect of the electrode charge on the relative stability of the transition state (24).

However, this correction does not consider the effect of the excess number of molecules at the surface of the electrode upon the diffusion profile created during electrochemical processes. This extra reactant, known as the surface excess, will cause distortions in the diffusion profile because electrons which should be reacting with species diffusing from the bulk solution will be used in the reaction of the adsorbed species. The derivations of the equations describing the transient responses assume the existance of an ideal, well-defined concentration gradient; hence, deviations from this ideal behavior will result. Because of the integrating effect of the diffusion profile, the transient will continue to be affected even after all the adsorbed species has reacted. It is of interest to determine the extent of the error in the rate constants which are derived from these distorted transients.

In this study we will consider this adsorption to be relatively weak and to follow the Henry adsorption isotherm (25),

$$\Gamma = K_{ad}C_{o}$$
 (1.6)

This is the isotherm typically used for weak adsorption because it does not consider adsorbate-adsorbate interactions, and hence implies surface coverages low enough to ensure the absence of any such interaction effects. It will be shown below that the Henry isotherm is consistent with Gouy-Chapman double-layer theory (26) when the enhancement is not large.

To determine the extent of the electrostatic interactions, we

must consider the structure of the aqueous electrolyte solution in the vicinity of the charged electrode. A fixed layer of water molecules or specifically adsorbed anions is found at the surface of the electrode. This "inner layer" limits the access of other ions in the solution to the surface, in that the ions can progress only as far as some "plane of closest approach", or "outer Helmholtz plane" (o.H.p.). Gouy-Chapman theory defines the potential at that point in the interfacial region, ϕ_2 , with respect to the bulk solution, as a function of the total charge inside the o.H.p. (the actual charge on the electrode, q^m , plus the charge of any adsorbed anions in the inner layer, q^*) to be

$$\phi_2 = \frac{51.39}{|z|} \sinh^{-1}[q/(11.74 c^{1/2})]$$
 (1.7)

for aqueous symmetrical electrolytes of charge z at 25 °C.

Since this potential is relative to the bulk solution, it must decay to zero with increasing distance from the electrode. It is this region of potential decay that is called the "diffuse layer". The function describing the shape of this decay is also given by Gouy-Chapman theory:

$$\phi_{x} = \frac{4}{|z|f} \tanh^{-1} \left[\tanh(\frac{\phi_{2}f|z|}{4}) \exp(-\kappa x) \right], \ \kappa = 3.3 \times 10^{7} |z| c^{\frac{1}{2}}$$
(1.8)

for aqueous z-z electrolytes at 25°C.

The concentration of an ion with a charge Z in this region will

be affected by this potential according to the following equation:

$$C_{x} = C \exp \left(-Zf\phi_{x}\right) \tag{1.9}$$

Using these equations, it is possible to calculate the enhancement or reduction in concentration of a given ion as a function of distance from an electrode of charge q, for a given supporting electrolyte composition. Note that the use of these equations implies that any ions in solution in addition to the supporting electrolyte must be at concentrations low enough that Equations 1.7 and 1.8 still apply.

We can now calculate the adsorption coefficients in the Henry isotherm. The surface excess Γ can be given as

$$\Gamma = \int_0^\infty (C_y - C) dx \qquad (1.10)$$

With the substitution of Equation 1.9, the expression for the surface excess takes the form of the isotherm:

$$\Gamma = C \int_0^{\infty} \left[\exp(-Zf \phi_x) - 1 \right] dx \qquad (1.11)$$

Equation 1.9 can be combined with experimental data for the charge on an electrode as a function of potential to give the potential dependence of the adsorption coefficient for each system (supporting electrolyte plus reactant) of interest. The results of these calculations for the adsorption of 3+ ions in 1 M KF are shown in

Figure 1.1, while those for the adsorption of 3+ ions in 0.1 M KF are given in Figure 1.2.

These results provide only an upper limit on the value of the adsorption coefficients due to the assumption that the presence of the higher-charged reactant ions does not change the double-layer structure as calculated for the 1+/1- electrolyte. A lower limit on these values may be obtained by assuming the supporting electrolyte charge is the same as the charge on the reacting ion. This calculation produces estimates of the adsorption coefficients which are far smaller than those calculated above. For example, the 3+/3- calculation for a constant amount of charge on the electrode surface (q^m + q') yields a value of K_{ad} of 3.5 x 10^{-8} cm, while the original 1+/1- approximation gives 2.4 x 10^{-6} cm (both for 1 M solutions). The 3+/3- values are clearly too low because they were calculated assuming that the more highly charged species was several orders of magnitude more concentrated than it would be in a typical experiment.

Unfortunately, the exact solutions for an arbitrary number of variously charged ions are not available in closed form, so it is quite difficult to calculate the values more closely. Some clues are available, however. It is possible to calculate values of ϕ_2 for these complex systems, and the variations are quite small with even a 1 mM addition of 3+ ions to a 0.1 M solution of 1+/1- supporting electrolyte. The calculation for 3+/3- supporting electrolytes underestimates the ϕ_2 values by a factor of 2 or 3, which would have a drastic effect on the calculated surface excess.

The Debye length, $1/\kappa$, describes the distance through which the

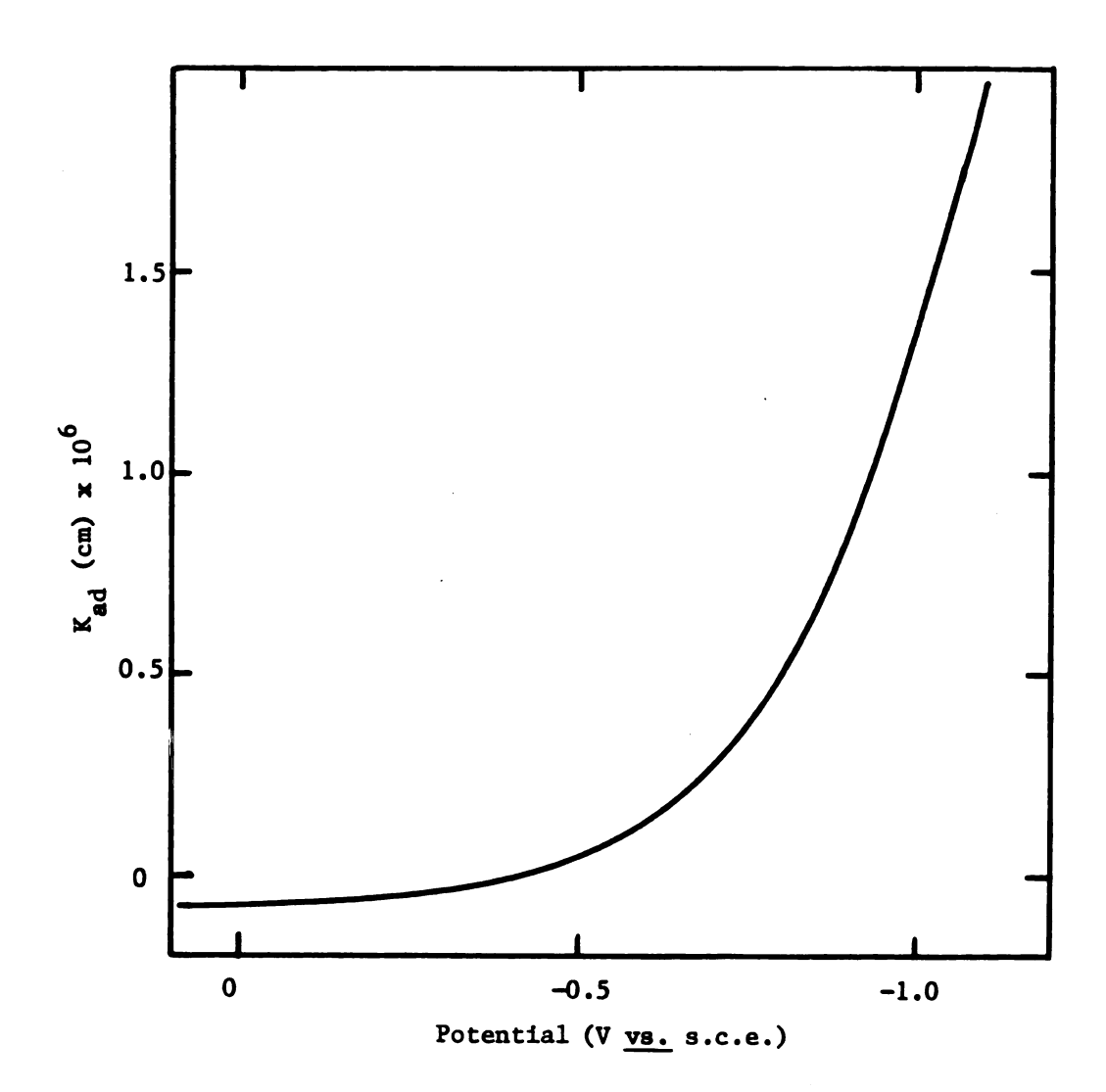


Figure 1.1. Diffuse-layer adsorption coefficient K_{ad} (calculated from equation 1.11) <u>vs.</u> potential for a 3+ ion in 1 M KF at a mercury electrode.

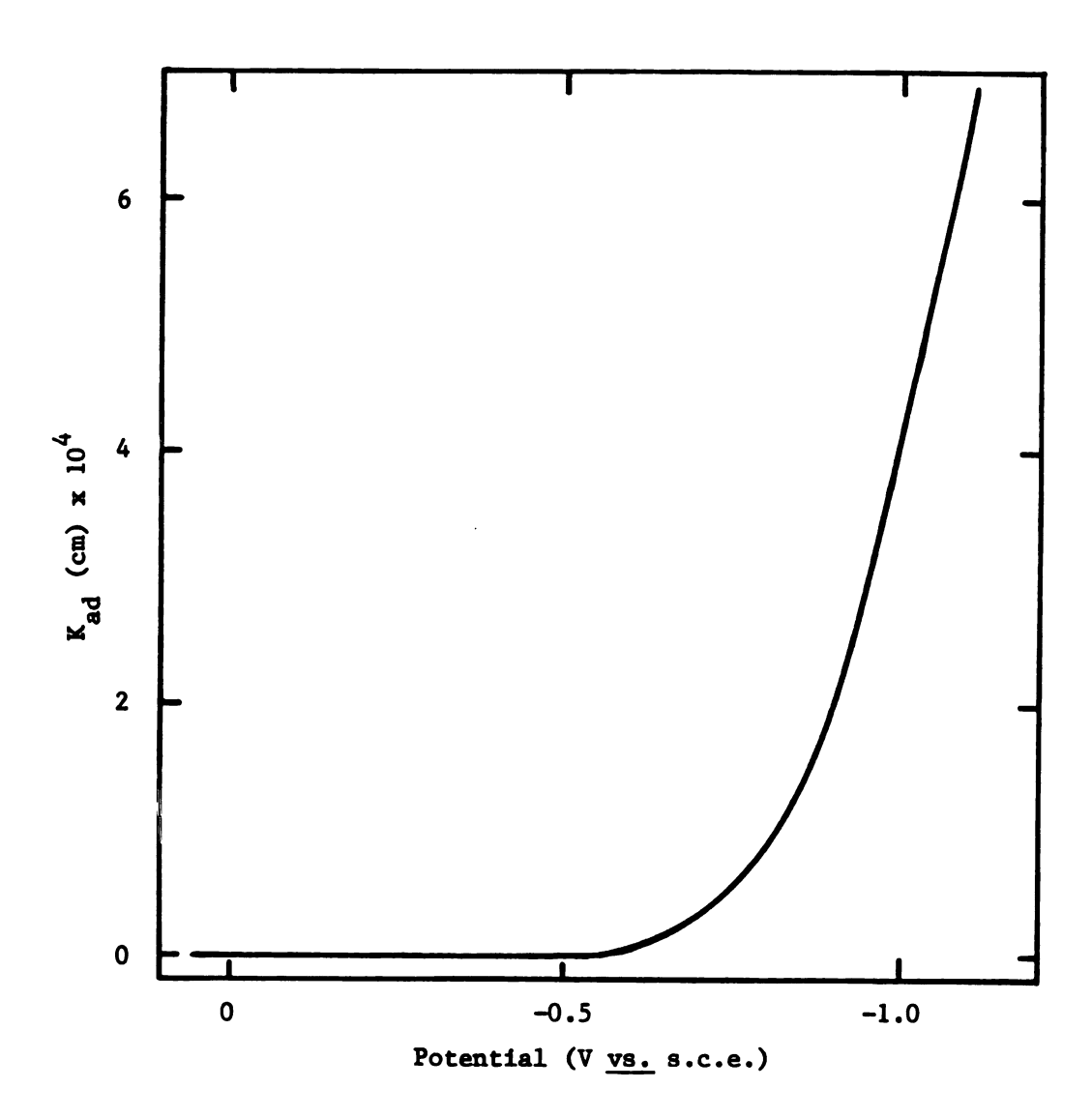


Figure 1.2. Diffuse-layer adsorption coefficient K_{ad} (calculated from equation 1.11) <u>vs.</u> potential for a 3+ ion in 0.1 M KF at a mercury electrode.

diffuse layer extends into the bulk solution. This quantity can also be calculated exactly for systems with an arbitrary number of ions, again showing a very small effect for a 1 mM addition of 3+ ions, while underestimating the value for 3+/3- electrolytes by a factor of 3. Thus, it appears that while the upper limit values are probably somewhat large, those calculated for the 3+/3- system as a lower limit are certain to be much too small.

Intuition and the above calculations predict the depletion of reactant species when the charges on the electrode and the reactant ion are of the same sign. Because the degree of depletion is quite small compared to the amount of adsorption necessary to produce a significant deviation in the simulated transients, it was not considered further.

The extent of any diffuse-layer adsorption depends on the total charge inside the o.H.p., which includes the charge on the metal itself, q^m, and the charge of any adsorbed ions from the supporting electrolyte in the inner layer, q'. It is therefore possible to modify the diffuse-layer adsorption properties through the appropriate choice of a supporting electrolyte. Most halide ions have the effect of making the total electrode charge more negative at positive potentials, but have only a small effect at negative potentials. On the other hand, some quaternary ammonium cations (e.g., tetraethylammonium ion) are strongly adsorbed at negative potentials. Clearly, in the study of the redox properties of a 3+ reactant at negative potentials, the use of an adsorbing cation in the supporting electrolyte will reduce or even eliminate the extent of diffuse-layer adsorption. Although these electrostatic interactions are

inevitable, the electrochemist can exert a degree of control on their magnitude.

In addition to this diffuse-layer adsorption, there often exists a chemical interaction between the reactant and the electrode surface. This chemical interaction is known as specific adsorption (25). The extent of this process depends on the species itself as well as on the nature of the electrode material. At low surface coverages, one might expect the same sort of behavior as would be expected for diffuse-layer adsorption. While specific adsorption is not as prevalent as diffuse-layer adsorption, the Henry's law isotherm should apply under these conditions as well at sufficiently low coverages.

The diffuse layer adsorption process is seen to be in true equilibrium if one examines only the concentration of reactant close to the surface (i.e., in the diffuse layer itself). When one considers that the "excess" molecules are in fact identical to those molecules which are present simply as an extension of the bulk concentration, it is clear that this must be true. The "change" of a bulk molecule to one which is adsorbed is only an expression of the model, and not the physical reality. This change does, however, induce a separate mass-transport process to replace the molecule which becomes adsorbed.

This situation is in contrast to that for specific adsorption, in which the adsorbed species is indeed different from those in the bulk of the solution (and also the diffuse layer). Here, the bond making/bond breaking processes need not be in equilibrium, but can respond at some finite rate to the demands of the thermodynamics.

The limit of applicability of the Henry adsorption isotherm was

taken to be a surface coverage of about 10%, which for a 1 mM reactant leads to a maximum adsorption coefficient of about 2×10^{-5} cm. This might be valid for specifically adsorbed reactants, but for diffuse-layer adsorption an order of magnitude lower is more likely to be appropriate.

1.5. Summary of Dissertation

The remainder of this dissertation consists of an explanation of the methods used to pursue this investigation followed by analyses of four types of experiments designed to measure fast electron-transfer kinetics, and implications which may be drawn from this work.

Chapter 2 describes the overall methodology of the investigation and details the processes of digital simulation and nonlinear regression, as well as some other numerical procedures used for this work.

Chapters 3 and 4 consist of studies of potential-step experiments applied to irreversible and quasi-reversible reactions. The effects of finite potentiostat risetime and of weak reactant adsorption on the results of the analyses of both chronoamperometric decay transients and normal pulse polarograms are determined. Some conclusions are made about the consequences of using normal pulse polarography for electrode kinetics measurements as well as for chemical analysis. Chapter 5 is a study of coulostatics experiments, focusing on the accuracy of derived rate constants in the presence of weak reactant adsorption and finite charge injection time. Galvanostatic double pulse experiments in the presence of weak reactant adsorption are the subject of Chapter 6. At this point, some conclusions about the

analysis of experimental results for small-step perturbation methods are presented.

Finally, some suggested paths are presented for further research in this area in Chapter 7.

CHAPTER 2

METHODS

This investigation is aimed towards determining the effect of experimental nonidealities on the results of electrode kinetics experiments designed to measure the rates of fast electrode reactions.

The general approach used involves assuming a rate constant, using digital simulation to produce a nonideal transient, and analyzing that transient with nonlinear regression or with a conventional method as if the transient is indeed ideal. It was assumed that all other experimental parameters, such as concentrations, diffusion coefficients, etc., were known and their exact values were used for the analyses. The rate constant derived in this manner can then be compared to the known value of the rate constant to assess the error due to that particular nonideality. This general outline, illustrated in Figure 2.1, was applied to several different electrochemical methods, including potential-step chronoamperometry, small-step coulostatics, and galvanostatic double pulse experiments.

This procedure should mimic the practice of performing an experiment in the laboratory (very likely under nonideal conditions) and then analyzing the resulting data according to the equations describing the ideal experiment. Through the use of digital simulation, it is possible to control the extent of each nonideality in the system, as well as evaluate the errors they cause in the rate parameters.

The remainder of this chapter will examine each step of the procedure in more detail, while dealing only with the aspects of each topic which are common to all the experimental techniques. The

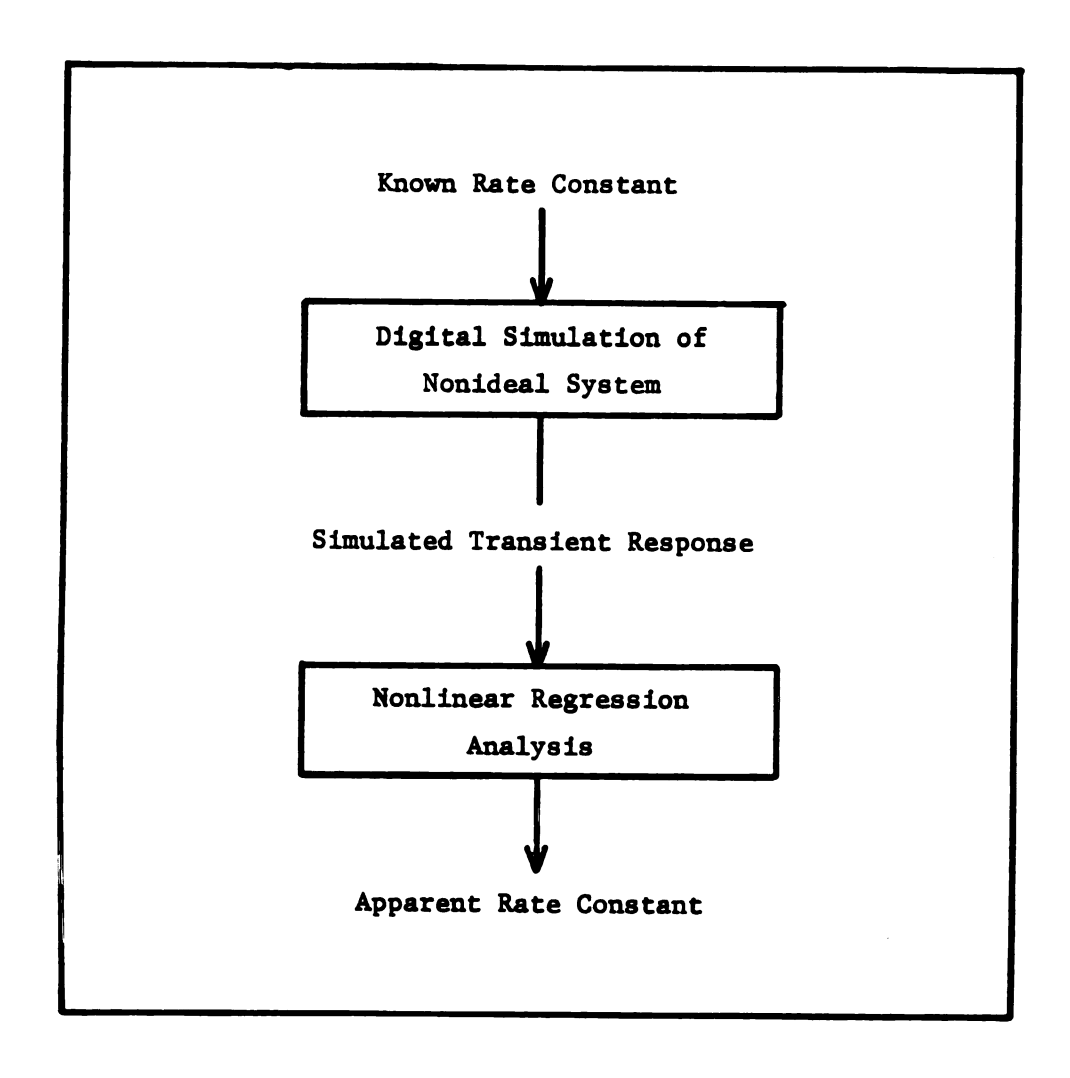


Figure 2.1. Summary of the process used to determine the effects of nonidealities upon the results of electrode kinetics experiments.

specifics of the ideal data analysis and the simulation of each experimental method will be left to the particular chapter which covers
that method.

2.1. Digital Simulation

Since Feldberg introduced the method to electrochemists in 1969 (27), digital simulation has been used in a variety of investigations. As the simulation of electrochemical transients is a major part of this work, a general explanation of the process (28-30) will be presented.

Experiments designed to measure electrode kinetics are described by solutions of Fick's second law of diffusion with initial and boundary conditions appropriate to the particular method used. When the boundary conditions are not too complex, the method of Laplace transformation can be used to solve the partial differential equation. Unfortunately, for the nonideal conditions of interest here, exact solutions of Fick's second law are very difficult to derive in closed form. Numerical methods are the other obvious choice, and the digital simulation scheme chosen for this work is known as an explicit finite difference solution. Other more sophisticated types of numerical methods have been used to improve accuracy or for other special purposes, but the added complexity was not needed here, as will be shown later.

When simulating electrochemical experiments, we need to be concerned with the concentration of the species of interest close to the electrode surface both as a function of time and of distance from the interface. This is seen from Fick's second law, where the time derivative of the concentration is proportional to the second derivative of concentration with respect to distance. Additionally, Fick's first law states that the flux of reactant or product to or from the surface is proportional to the first distance derivative of concentration at the surface. Digital simulation relies on concentration values at a discrete set of points near the surface, the distance, Δx , between each of which being known. Calculations are performed for discrete time intervals, Δt , starting at the beginning of the experiment and continuing for as long as necessary.

The general scheme of digital simulation is shown in Figure 2.2 (27). First, initial conditions for the experiment are set up.

Then, for each time interval, the boundary condition equations are used to calculate the concentration and flux of species at the electrode surface. This newly calculated surface concentration gives rise to a concentration gradient, so that the effect of species diffusing from the bulk of the solution can be calculated for each discrete point in the solution. The time variable is then incremented and the boundary conditions are recalculated.

The initial conditions for most experiments are easily implemented in the simulation. For example, the condition that no concentration gradients exist in the solution before the start of the experiment,

$$t = 0, x \ge 0, C = C_{bulk}$$
 (2.1)

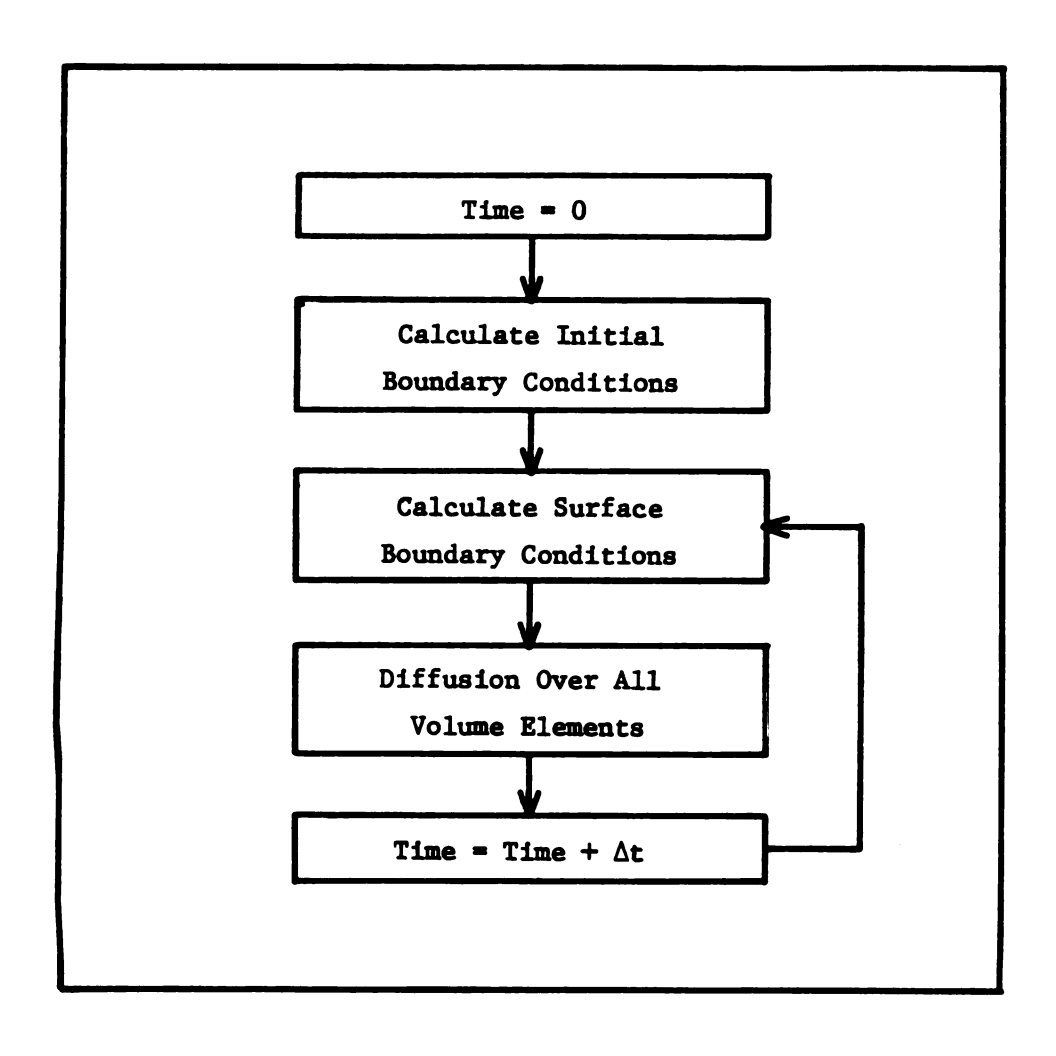


Figure 2.2. Basic elements of digital simulation of electrochemical experiments.

is implemented by setting the concentration at each discrete point in the solution equal to the bulk value. If adsorption is present, the initial surface excess can also be calculated.

The equations for the boundary conditions can become quite complex. In this work, four cases of surface boundary conditions are of interest: kinetically controlled chemically irreversible and reversible systems, both with and without adsorption. (If the reaction is fast enough, the response of the system is controlled solely by diffusion.) The irreversible systems will be used as examples. For the case in which no adsorption is present, the following equations must hold:

$$\Phi = D \left(\frac{\partial C}{\partial x} \right)_{x=0} \tag{2.2}$$

$$\Phi = k_f C_0 \tag{2.3}$$

The first is Fick's first law of diffusion, while the second is a statement of the rate law of the electrode reaction. Writing the equations in terms of the discrete quantity Δx ,

$$\Phi = D(C_1 - C_0)/\Delta x \qquad (2.4)$$

$$\Phi = k_{f}^{C}$$
 (2.5)

These equations can be solved simultaneously for the flux of reactant at the surface and the concentration of reactant at the surface.

$$\Phi = k_f C_1 D / (D + k_f \Delta x)$$
 (2.6)

$$C_{O} = C_{1} - \Phi \Delta x / D \tag{2.7}$$

The resulting expressions can be evaluated at each Δt time increment, using the appropriate rate constant if the potential is some function of time.

When weak adsorption is present, the equations become more complex.

The adsorption process is assumed to be in equilibrium at all times

and can be written for a species Ox as

which leads to an adsorption isotherm of

$$\Gamma = K_{ad} C_{o}$$
 (2.8)

Fick's first law still holds, but the rate law is modified by allowing adsorbed species to react at the surface in addition to molecules
diffusing from the bulk solution, and by the addition of a term
which allows for changing surface excesses:

$$\Phi = k_f C_0 + k_f^a \Gamma - \Delta \Gamma / \Delta t$$
 (2.9)

These equations can be solved for the parameters of interest, the flux Φ , $C_{_{\mbox{O}}}$, and $\Delta\Gamma$:

$$C_{o} = \Gamma \Delta x + \Delta t D C_{1} / [K_{ad} \Delta x + \Delta x \Delta t (k_{f} + K_{ad} k_{f}^{a}) + \Delta t D]$$
 (2.10)

$$\Delta\Gamma = \Delta t D(C_1 - C_0) / \Delta x - \Delta t C_0 (k_f + K_{ad} k_f^a)$$
 (2.11)

$$\Phi = C_0(k_f + K_{ad}k_f^a) - \Delta\Gamma/\Delta t \qquad (2.12)$$

Now, however, the flux of electrons at the surface is no longer equal to the flux of molecules. To calculate the current, we consider only the faradaic flux.

$$\Phi_{far} = C_0 (k_f + K_{ad} k_f^a)$$
 (2.13)

This takes into account the possibility that the total flux includes some molecules coming from the bulk of solution to form or replenish the adsorbed layer. Of course, K_{ad} can also be calculated as a function of potential (and hence, time).

Since there is a rapid equilibrium, the rate constants will always appear as a sum:

$$k_{\text{overall}} = k_f + K_{\text{ad}} k_f^{\text{a}}$$
 (2.14)

The following work has been done assuming that the rate constant for the adsorbed species was zero, in order that the rate constants $\mathbf{k}_{\mathbf{f}}$ might be equated with $\mathbf{k}_{\mathbf{overall}}$ for ease of interpretation. The existence of finite adsorption-desorption kinetics would complicate the calculation considerably; the rate constants would have to be

treated separately.

For the quasi-reversible systems, we include terms for both the oxidized and reduced species and solve them in the same manner, although this is somewhat more complicated, especially with adsorbed reactant present.

Once the concentration C_0 is calculated, the new concentrations at each point in the solution must be calculated. Fick's second law governs diffusion in the bulk solution,

$$\partial C/\partial t = D(\partial^2 C/\partial x^2) \tag{2.15}$$

for planar geometry. This equation can be written in discrete terms for each point i as,

$$\Delta C_i = D\Delta t (C_{i+1} - 2C_i + C_{i-1})/(\Delta x)^2$$
 (2.16)

In practice, the calculation is carried far enough out into the solution that $\Delta C_{\bf i}$ is insignificant. After all the $\Delta C_{\bf i}$ terms have been calculated for each species, the concentrations $C_{\bf i}$ are adjusted to their new values,

$$C_{i} = C_{i} + \Delta C_{i} \tag{2.17}$$

At this point, the time variable is incremented by the element Δt and the calculation of the boundary conditions begins with the new value of C_1 (and possibly E, k, K_{ad} , or any other time-dependent term).

The computation continues in this manner, the flux being converted to current and recorded at the appropriate time interval until the calculation is complete. In this way it is possible to simulate a miriad of types of experiments by making relatively minor changes in the equations. It is this simplicity of modification and generality which makes digital simulation so valuable a tool in electrochemistry.

2.2. Accuracy of Digital Simulation

Since digital simulation is a numerical solution to the relevant differential equations, it can provide only approximate results. The main factors which influence the accuracy of a given calculation are the simulation parameters Δx and Δt . Obviously, the finer the grid of time and distance increments, the closer the simulation approaches the true solution.

The choice of Δx and Δt is constrained by several factors. First, the parameter β , defined as

$$\beta = D\Delta t / (\Delta x)^2 \tag{2.18}$$

must always be less than 0.5 (27). Not meeting this condition will cause the ΔC_1 terms to be too large (larger than the corresponding C_1), so that the concentration values may become negative and oscillate. This is a mathematical constraint, general to all explicit finite difference and finite element solutions.

A second constraint on the choice of the simulation parameters is practical in nature. As Δt or Δx approach zero, more and more

calculations must be performed, and many concentration values must be stored. Computer calculation speed is finite, so that a limitation is imposed on how fine a grid can be used.

A related constraint is the precision (number of significant figures) to which the calculation is carried. Smaller grid increments produce smaller changes and differences, so that accuracy will be limited by the precision of the computation. Of course, the precision can be extended, but at a relatively large cost in computation time.

Given these limitations, one can see that it is unreasonable to expect anything but an approximate solution to the problem. An accuracy of around one percent or less can be achieved in reasonable amounts of computation time, which makes simulations suitable for qualitative studies of the shapes of electrochemical transients, but limits their usefulness in more quantitative applications.

An optimization of the procedure which was found to be successful involves the principle of expanding distance increments (31). Since one is interested mainly in conditions close to the surface, it makes sense to concentrate the calculation in this region. One does not need the same amount of precision far out in the solution, as the concentration gradient is quite small. Although the time increment size is limited by the smallest distance increment, Δx_1 , the number of concentration points which need to be calculated at each time can be greatly reduced.

An exponential expansion function was used for this work,

$$\Delta x_{i} = \Delta x_{1} \exp(\text{const } \cdot i)$$
 (2.19)

The value of the constant can be varied; a value of 0.1 tended to limit most of the simulations to about twenty to thirty concentration values. It is necessary to modify the discrete form of Fick's second law to reflect this unequal spacing,

$$\Delta C_{i} = 2D\Delta t \left(\frac{(C_{i+1} - C_{i})}{\Delta x_{i+1}} - \frac{(C_{i} - C_{i-1})}{\Delta x_{i}} \right) / (\Delta x_{i+1} + \Delta x_{i})$$
 (2.20)

Of course, the equations for the boundary conditions use the value of $\Delta\mathbf{x_1}$.

The use of this method of expanding distance increments yields a computation time savings of about 50%, even though the diffusion equation is more complex. No adverse effect on the overall accuracy of the simulations from the use of this equation were observed unless the concentration grid was severely expanded.

2.3. Parallel Simulation Method (32)

As the diffusion limit of a particular method is approached with larger and larger reaction rates, the shape of the transient depends less and less on the exact value of the rate constant. The rate constant which can then be derived from the transient depends heavily on minor variations in its shape. It is for this reason that some minor deviations from ideality produce no substantial error at slower rates, but induce significant error for faster reactions. Unfortunately, simulation inaccuracy has a similarly large effect on this parameter, sometimes even masking the deviations due to the nonideality itself.

It was found to be necessary to develop a scheme which would eliminate this error, recognizing that conventional methods of optimization were impractical due to computer time limitations.

The simulated systems in this work deal with conditions which cause deviations from some ideal experiment. These deviations are generally minor, and a closed form solution is generally available for the exact case. The method developed to eliminate simulation inaccuracy uses parallel simulations of the nonideal system of interest and the corresponding ideal experiment. All simulation parameters (Δx , Δt , etc.) are identical; the only difference between the resulting transients is due to the effect of the nonideality. The result of the parallel simulation is a sort of error curve which gives the deviation from ideality at each point along the transient. This error curve can then be impressed on the exact ideal transient calculated from the closed form solution to yield a calculated, nonideal transient which reflects only the effect of the nonideality and shows no error from simulation inaccuracy. The process can be summarized by the following equation:

$$x_{\text{calculated}}^{\text{nonideal}} = x_{\text{calculated}}^{\text{ideal}} (\frac{x_{\text{nonideal}}}{x_{\text{ideal}}})_{\text{simulated}}$$
 (2.21)

where X is the measured quantity, usually a function of time.

To verify that this scheme minimizes the dependence of the transients on the simulation parameters, a nonideal system was needed to which an exact solution has been derived. The case of a

linearly rising potential—step experiment (33) was chosen to serve as the nonideal case, while the well-known instantaneous—step experiment (34) was used as the ideal system. Simulations were performed as outlined above, and the results compared to the exact transient calculated from the equation through the use of a standard deviation from simulation.

$$\sigma_{\text{sim}} = \left[\frac{1}{n} \sum_{\text{sim}} - i_{\text{calc}}\right]^{2}$$
 (2.22)

Figure 2.3 shows the results for a typical set of parameters which shows the error, σ_{sim} , in arbitrary units, as a function of the simulation parameter Δx_1 for the standard simulation and the newly developed parallel simulation scheme. It is clear that the new method produces simulations which are more accurate and less dependent on the actual simulation parameters than does the conventional method. This point is further illustrated in Figure 2.4, which displays the error as a function of computation time. Even though the parallel scheme requires twice the time for a given set of simulation parameters, a great savings is gained in the time required for an accurate calculation.

This parallel simulation scheme was used throughout this work when the resulting transient was to be subjected to nonlinear regression analysis. Other analysis methods seem to be less sensitive to variations in the shape of the transient; conventionally simulated transients were used in these cases for convenience.

The overall scheme of this investigation as shown in Figure 2.1

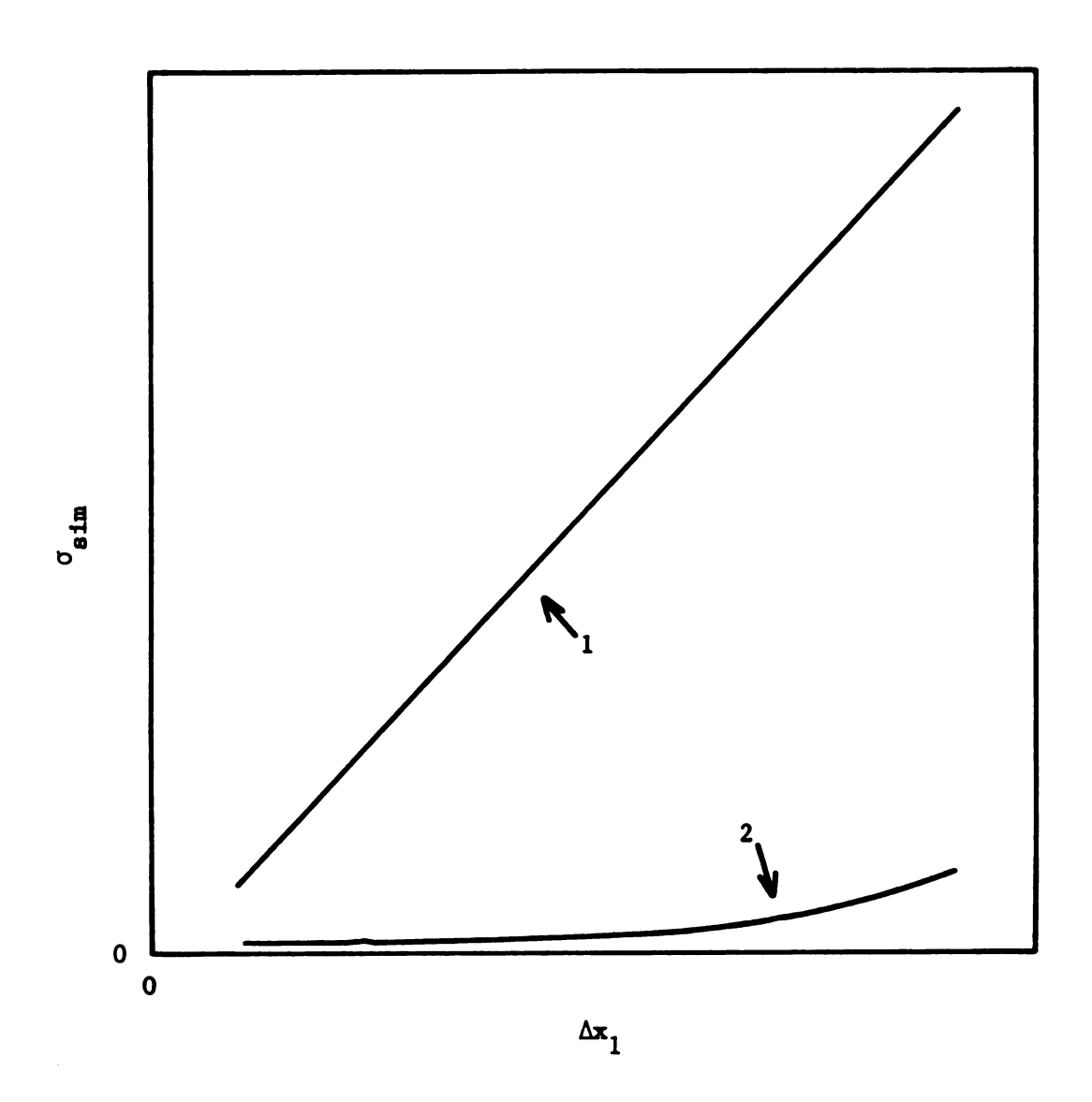


Figure 2.3. Standard deviation of simulation $\underline{vs.}$ simulation parameter Δx_1 for typical systems. Curve 1: conventional simulation. Curve 2: parallel simulation.

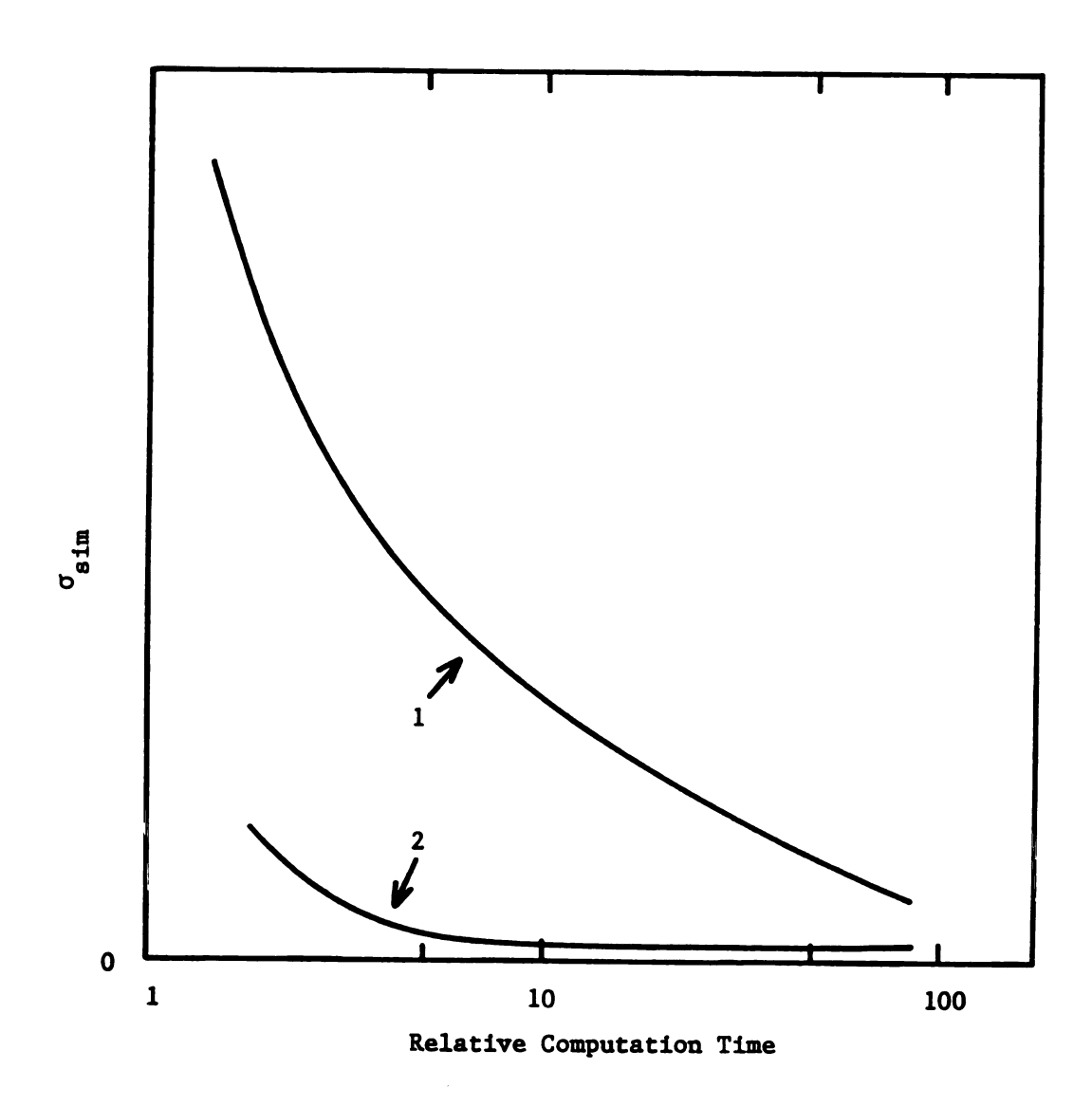


Figure 2.4. Standard deviation of simulation <u>vs.</u> computation time for typical systems. Curve 1: conventional simulation.

Curve 2: parallel simulation.

can now be modified to include the parallel simulations and the impression of the error curve on the calculated ideal transient. The overall process, as modified, is shown in Figure 2.5.

2.4. Details of Simulation Programming

An example of the complete program used to generate the error curve in the above example is presented in the Appendix to illustrate the application of the concepts developed above. The language used in this work was FLECS (35), a structured pre-processor for FORTRAN. Translation of this code to FORTRAN would be a trivial matter for anyone with a knowledge of programming. Structured programming (36) was chosen for ease of coding, maintenance, and modification, and for the clarity of the final result.

The programs were executed in an interactive environment on Digital Equipment Corporation LSI-11 and LSI-11/23 processors (37) under version 4 of operating system RT-11 (37).

2.5. Nonlinear Regression Analysis

After the nonideal system is simulated, the apparent rate constants must be extracted from the transients. Although there are several ways of accomplishing this, nonlinear regression is a generally applicable method which has been used extensively in this work. A brief outline of the technique and its use follows.

There are many examples in electrochemistry and in chemistry in general of the analysis of experimental data by linearizing the

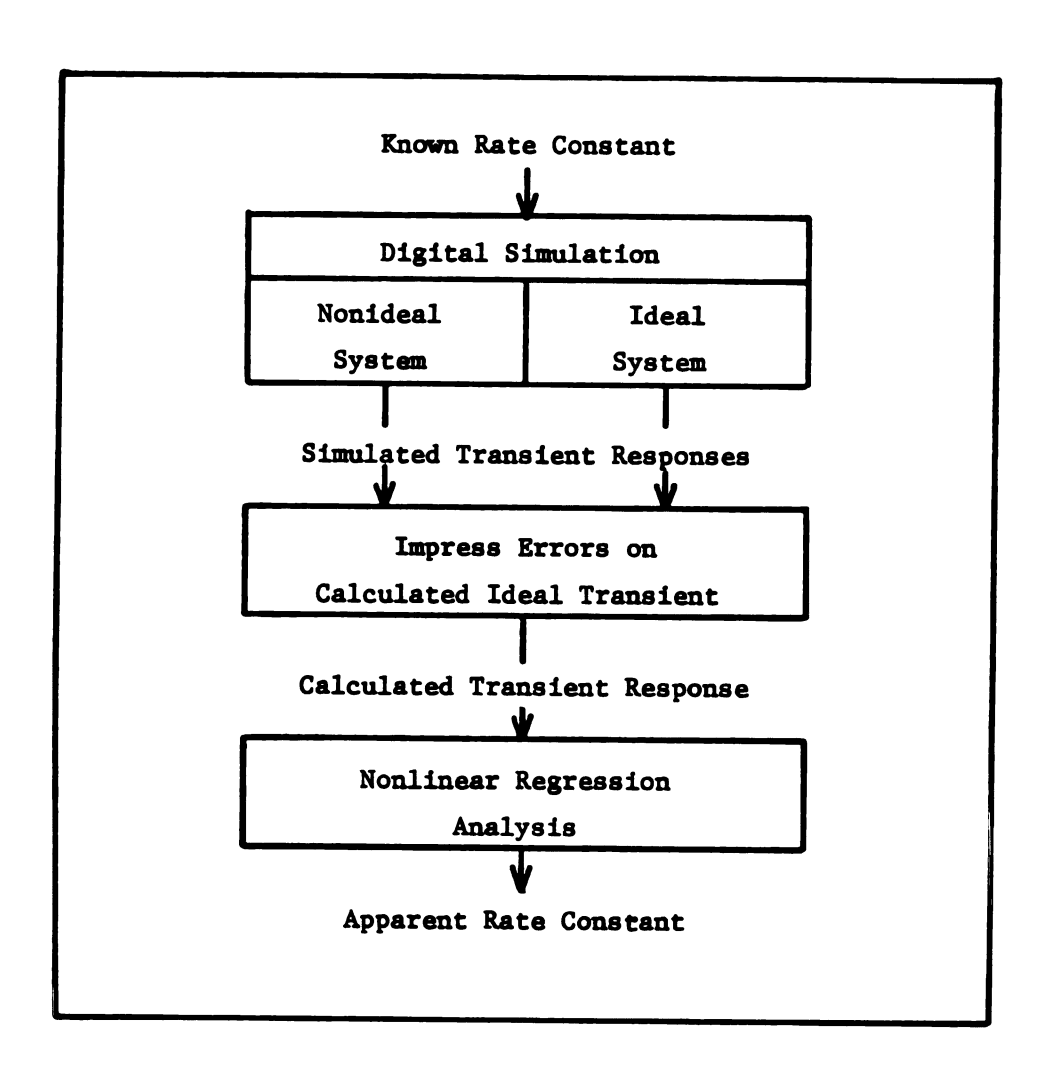


Figure 2.5. Experimental process modified to reflect the parallel simulation method.

dependence of some measured quantity on an independent variable.

This linearized data can then be analyzed with graph paper and a ruler, or with the more sophisticated linear least squares calculation.

This type of manipulation of the data is not always statistically sound, as when the same variable ends up plotted on both axes of the graph, and can lead to erroneous results (38). Additionally, approximations of certain functions often must be made so that the equations may be reduced to a linear form. When these approximations do not hold, the line displays curvature, rendering any calculated slope and intercept meaningless. Even worse is the treatment of such curved plots with polynomial least squares; the resulting virial coefficients have no physical significance whatsoever in most cases, and the resulting equation cannot be used for any sort of reliable extrapolation.

Nonlinear regression (39) is a numerical method which can be used to fit an arbitrary equation to a set of data by adjusting certain key parameters. Many algorithms have been used for the actual adjustment of the parameters, but all attempt to minimize the overall residual. At the minimum residual, the values of the adjustable parameters are those which make the equation best fit the data.

One is able to use the theoretically predicted equation to fit the data as they are measured so as to avoid doubtful approximations in the analysis procedure. Of course, if the data are not actually described by the equation, the results of this method must be in doubt. It is possible to get an indication of the goodness of fit by examining the individual residuals along the curve for evidence

of a systematic pattern (39). A perfect fit has all zero residuals, but we usually see a random scatter around zero due to the random errors of measurement. For a given fit to discriminate among correct and incorrect models, the systematic deviations must be large enough to be seen through the random scatter. Standard deviations from regression can also be calculated and compared to get an indication of which is the better fit.

In this work, we are purposely fitting nonideal, simulated data to ideal models. In most of the cases, the systematic deviations would not be clearly evident were the transients recorded at normal measurement precision; however, the shape would differ enough that errors in the adjusted parameters would still result.

Since the equations do not fit the data, a question arises about the interval over which data is to be analyzed. Using different ranges of data along the same nonideal transient will yield a variation in the results. (The same will be true for analyzing a curved line with linear regression.) For the following work, if an optimum time range for analyzing transients from which to derive rate parameters has been published, that range was used in these analyses. If no optimum range has been specified, a range consistent with a reasonable experimentally accessable measurement time has been used.

The nonlinear regression itself was done by program CFT4A (40). This routine, while not especially efficient, was developed specifically for small computer systems and has been applied successfully for many chemical systems and experiments. No changes were made to the calculational portion of the program, although some I/O and control parameters were added for convenience. CFT4A provides for a separate

subroutine which calculates (by any method) a set of data according to user-provided equations, the set of independent variables, and the current values of the adjustable parameters. This calculated data set is then compared to the experimental set. The equations in this routine can be simple algebraic equations, a complex integration routine, or even a digital simulation procedure.

2.6. Error Function Evaluation

The calculation of the ideal transients often requires the evaluation of the exponential error function,

$$f(x) = \exp(x^2) \operatorname{erfc}(x) \tag{2.23}$$

When x is a real number, a rational function approximation developed by Flanagan (41) was used, which is valid over a wide range of arguments.

In equations describing the ideal transient for some electrochemical methods, however, the argument of the function is a complex number. A procedure has been published (42,43) for the evaluation of the so-called complex error function,

$$g(z) = \exp(-z^2) \operatorname{erfc}(iz), \quad z = x + iy$$
 (2.24)

which is valid for arguments z in the first quadrant (x and y greater than zero). The relationship between the function of interest, f(z), and the calculable function g(z) is trivial:

$$f(z) = g(iz) \tag{2.25}$$

It is also necessary to extend the evaluation of g(z) to other quadrants by means of the following relationships:

$$g(-z) = 2 \exp(-z^2) - g(z)$$
 (2.26)

$$g(conj z) = conj g(-z)$$
 (2.27)

$$conj z = x - iy (2.28)$$

These equations allow the function f(z) to be calculated from variations of the function g(z). Figure 2.6 displays the functions which must be evaluated to obtain f(z) in the four quadrants.

Figure 2.6. Functions of g(z) to obtain f(z) in four quadrants.

sign of x	sign of y	function to evaluate to obtain f(z)
+	+	conj g(-iz)
+	-	g(iz)
-	+	$2\exp\{-(iz)^2\} - g(-iz)$
-	-	conj $\left\{2\exp\{-(\text{conj iz})^2\}-g(\text{conj iz})\right\}$

$$z = x + iy$$
 $i = \sqrt{-1}$
 $conj z = x - iy$
 $f(z) = exp (z^2) erfc (z)$
 $g(z) = exp (-z^2) erfc (iz)$

CHAPTER 3

POTENTIAL-STEP EXPERIMENTS FOR THE STUDY

OF IRREVERSIBLE ELECTRODE REACTIONS

3.1. Description of Experiment

A species which undergoes an irreversible electron-transfer reaction can be conveniently studied with potential-step experiments (44). In these methods, the electrode is in a solution of the species under study at a potential such that no reaction occurs. The potential is then stepped and held constant at the new value. The electron transfer reaction starts at a rate determined by the rate constant $\mathbf{k}_{\mathbf{f}}$, establishing a concentration gradient. The measured current decays as the concentration depletion region grows out into the solution.

In chronoamperometry (10), this decaying current is followed as a function of time, and the entire transient is used to determine the rate constant at that potential. A series of experiments may be performed with varying potential step sizes so that the potential dependence of the rate constant can be evaluated. At large enough overpotentials, though, the rates of the electron-transfer reaction are so large that the decay is controlled entirely by the diffusion of reactant through the solution. These diffusion-limited transients contain no heterogeneous kinetics information, and the onset of diffusion control defines the largest measurable rate constant under those conditions.

Normal pulse polarography (45) involves the same series of potential steps of increasing magnitude, but only the current flowing at one specified time is recorded. If these current values are

plotted against the applied potential (as is commonly done), a curve of a similar shape as a d.c. polarogram results. The data in this form can be analyzed to determine the dependence of the rate constant on potential as well.

For a totally irreversible process

$$0x + ne^{-\frac{k_f}{2}} \text{ Red}$$
 (3.1)

the equation describing the response of the ideal current-time transient to a potential-step perturbation can be shown to be (44)

$$i = nFACk_f \exp(k_f^2 t/D) \operatorname{erfc}(k_f t^{\frac{1}{2}}/D^{\frac{1}{2}})$$
 (3.2)

At the extreme of very large electron transfer rate constants, k_f , the rate of decay is a simple function of time, as given by the Cottrell equation (46),

$$i = nFACD^{\frac{1}{2}}/(\pi^{\frac{1}{2}}t^{\frac{1}{2}})$$
 (3.3)

As the above equations were derived assuming an instantaneous potential—step perturbation, it is of interest to study the effect of finite potentiostat risetime on the results of these experiments.

In addition to this instrumental nonideality, weak reactant adsorption will also be studied.

3.2. Analysis of Data from Potential-Step Experiments

Since all the terms in Equation 3.2 are known except the rate constant and since it is possible to calculate decay transients given values of the variables, nonlinear regression suggests itself as a convenient method for extraction of the rate constant from the experimental current-time transient (47). If either the concentration or the diffusion coefficient is uncertain, a two-parameter analysis may be used. It is not possible, of course, to vary all three parameters since there would be an infinite number of possible solutions.

Other methods of analysis have been used for the extraction of rate constants from these data which involve linearized forms of Equation 3.2 (48,49). These analyses are limited to particular ranges of arguments ("large", "small") of the erfc(x) term. Because non-linear regression is not subject to either the limitations or the approximations of these linear analysis methods, it was the technique used for the analysis of the chronoamperometric transients in all the following work.

A Laplace plane analysis has also been suggested (50) for derivation of values of rate constants from chronoamperometric decay transients. Its main advantages are that it is not necessary to calculate the exponential error function complement term, and that the transformed data are linear, so that a simple linear least squares treatment will suffice. Since it is possible to calculate this function and to perform nonlinear regression quite routinely, there seems to be no advantage in transforming the data to the Laplace plane

for analysis.

An optimal time range for the kinetics analysis of irreversible transients has not appeared in the literature. Recording data at 100 µs intervals is feasible during the experiment if a high-speed transient recorder or a computer is used (51). Twenty current values recorded at this rate or at a rate 10 times slower (2 ms or 20 ms total time) were used in the following analyses. If, however, obviously nonideal features (i.e., a peak in the chronoamperometric decay curve) were observed at the beginning of the transient, the first several points were not used in the analysis.

An alternative method of extracting rate constants from this type of data is to use the Oldham-Parry (48) method, in which the value of the current at a particular sampling time is compared to what it would have been had the transient been purely diffusion limited. This method is generally used when the data are collected as a pulse polarogram, where one simply takes the ratio i/i_{lim} for currents on the rising part of the wave.

Analysis of data by the latter method has several advantages. The concentration terms cancel out; uncertainty in this value does not effect the derived values of the rate constants. Additionally, measurements are easily carried out using pulse polarography, as many commercial instruments include this technique. The disadvantages, however, seem to outweigh these advantages in many instances. Each rate constant is generally derived from only two measurements of the current, and the derivation of any value depends on the correct measurement of the limiting current, i_{lim}. Often, this value

is not accessible for some reason, such as another electrode reaction obscuring the region of interest of the wave, or possibly because of instrumental nonidealities. This will be discussed later.

Chronoamperometric analysis, on the other hand, bases its derivation of the rate constant on many current measurements along a single transient. Adjusting the concentration or the diffusion coefficient simultaneously costs only one degree of freedom; this is easily compensated for by the large number of experimental points. No separate measurement of the limiting current is needed, so that access to this region of the polarogram is not necessary. The disadvantage of chronoamperometry is the somewhat more complicated instrumentation needed to record the current-time transient. The Oldham-Parry analysis can be performed on a hand-held calculator while nonlinear regression analyses require a computer to implement, but this is not a real advantage to the practicing worker as a computer system is often utilized to perform the experiment, and subsequent analysis of the data can easily be performed on-line.

Tyma, et al. (21) have compared the performance of the pulse polarographic analysis and the chronoamperometric analysis for fast, irreversible electrode reactions. Both procedures yielded essentially identical values of the rate constant at each potential, but it was noted that it was easier to spot nonideal conditions just by examining the shape of the polarogram. The methods had roughly the same maximum accessable rate constant. Although evidence of nonideal conditions was noted in this study, no attempt to analyze any apparently nonideal (peaked) polarogram was made.

Due to the fact that the nonlinear regression analysis of chronoamperometric transients seems to provide the most statistically reliable method of deriving rate constants, the following work will
focus on the effect of various nonidealities when the data is analyzed
in this manner. The effect of the nonidealities on the shapes of pulse
polarograms and the rate constants derived from them will be examined
as well.

3.3. Unique Aspects of Simulation

The simulation of irreversible chronoamperometric decay transients and normal pulse polarograms is straightforward; the method outlined in Chapter 2 was used directly.

The model chosen for the applied potential waveform was a simple exponential described by a time constant:

$$E = E_{step}[1 - exp(-t/\tau)] + E_{init}$$
 (3.4)

The actual applied potential profile of a fast potentiostat has been determined (21). The waveform was found to be described by a double exponential curve modified by a triangular deviation super-imposed on the rising part of the waveform. However, a single exponential form also provides an acceptable fit and is more suitable for use here, in that only one parameter is needed to describe the risetime characteristics, rather than four for the experimentally determined profile.

Since the potential is changing throughout the risetime, the

potential dependence of the rate constant $\mathbf{k}_{\mathbf{f}}$ must be considered:

$$k_{f} = k_{std} \exp\left[-\frac{cmF}{RT} (E - E_{std})\right]$$
 (3.5)

The equation used in the simulations produced a rate constant as a function of time given a potential step size, the rate constant at the final potential, and the time constant,

$$k_f = k_{f,E_{step}} \exp\left[\frac{\alpha nF}{RT} \quad E_{step} \exp(-t/\tau)\right]$$
 (3.6)

Thus, for every new time period (every Δt), a new rate constant is calculated to reflect this finite potential risetime.

3.4. Effect of Finite Potential Risetime

The distortions in the chronoamperometric transient produced as a result of non-ideal potential control are illustrated in Figures 3.1a and 3.1b. Figure 3.1a displays the effect when the potentio-stat time constant τ is short enough so that the potential is close to the desired potential before the current is first sampled. As expected, the current is too high at every point along the curve (and, in fact, will never exactly meet the ideal line). Figure 3.1b shows the distortions produced when τ is large enough that the potential is not yet near the control potential when the current is first sampled. Here we see a steep rise in current as the potential exponentially approaches the final potential, and then the usual decay, with currents larger than ideal at every point.

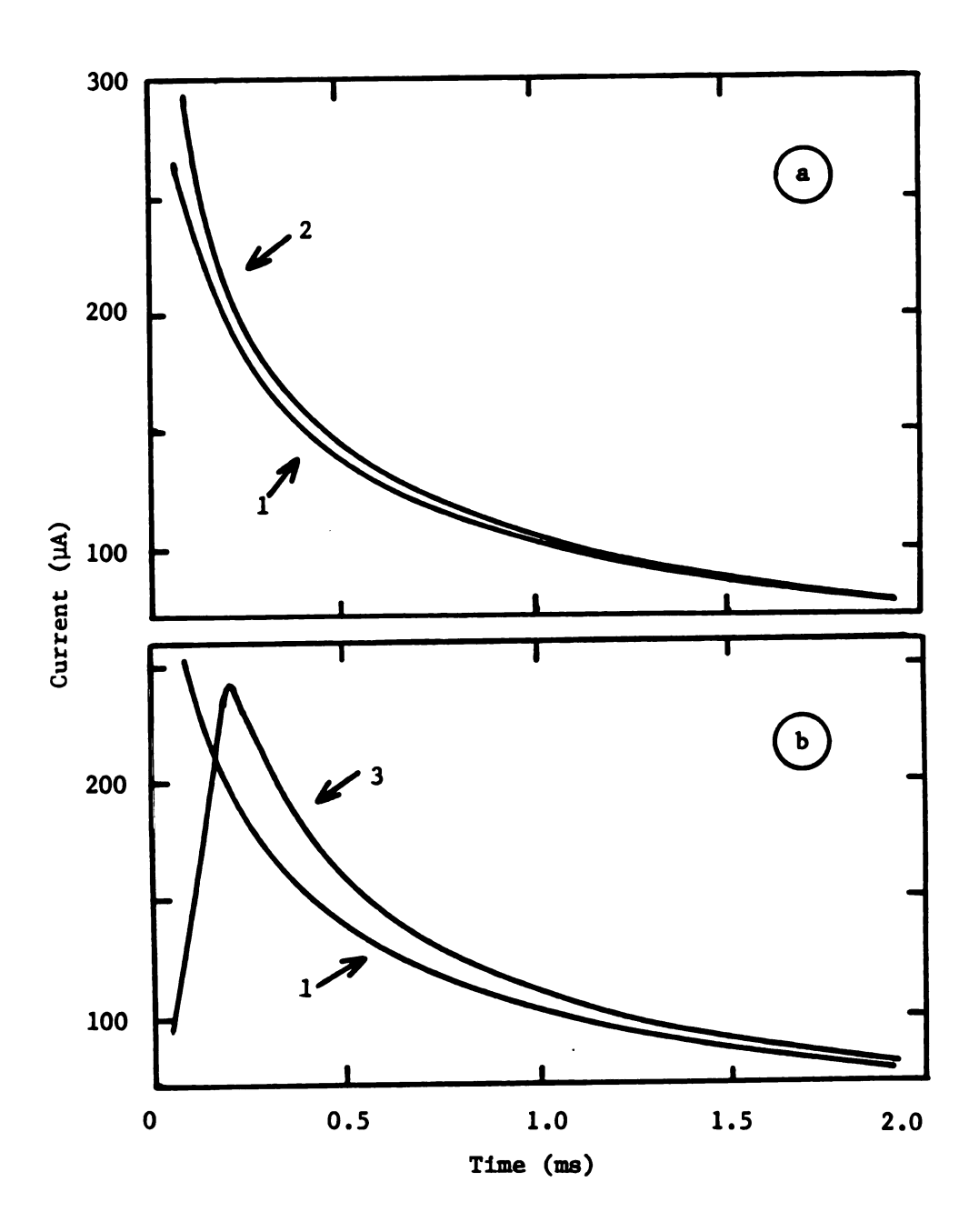


Figure 3.1. Chronoamperometric transients for irreversible reactions illustrating the effects of potentiostat risetime, with k_f = 0.3 cm/s, C = 1 mM, D = 1×10^{-5} cm²/s, E_{step} = -500 mV. Curve 1: ideal system. Curve 2: τ = 20 μ s. Curve 3: τ = 50 μ s.

A comparison of the shapes of the ideal and nonideal transient responses suggests that a rate constant derived from the data on the basis of Equation 3.2 will appear to be larger under finite risetime conditions. In extreme cases, we might even see decay transients which appear steeper than pure diffusion control would allow. Any attempt to derive a rate constant under these conditions using the conventional diffusion model will surely meet with failure. Additionally, any attempt to analyze transients with sampling times so short that a peak appears cannot be expected to yield a valid value for the rate constant.

It is important to consider the effect that the time range over which the data are analyzed has on the resulting values of the rate constant. Although the effect of the nonideality upon the transient diminishes sharply with time, the sensitivity of the apparent rate constant to smaller variations in the shape of the transient increases with time. It is not intuitively obvious which factor, if any, will dominate, and whether the most reliable rate constant will be derived from the short or from the long time range.

A set of chronoamperometric transients was simulated with various potentiostatic time constants for a number of rate constants. Table 3.1 shows the error in the rate constants derived from these transients by means of one-parameter nonlinear regression analyses for a time range of 2 ms (100 μ s sampling time), and the same results when the current is sampled at 1 ms intervals over 20 ms.

Several observations can be made. First, and most obvious, the error in the rate constant increases as the time constant increases.

Table 3.1. Error in Rate Constants Derived^a from Chronoamperometric Transients for Irreversible Reactions^b Due to Finite Potentiostat Risetime.

	k _f (cm/s)			
τ (με)	0.03	0.1	0.3	1.0
Short Time Range ^C				
0.5		+0.2%	+1.0%	+7.5%
1		0.4	2.0	16.7
2		0.8	4.0	43.7
5		2.0	11.1	f
10		4.2	27.1	f
20	+0.9%	7.0	73.1	f
50 ^e	3.1	18.8	f	f
Long Time Range ^d				
0.5		+0.1%	+0.6%	+6.0%
1		0.2	1.2	13.2
2		0.4	2.5	33.3
5		1.1	6.8	f
10		2.2	14.9	f
20	+0.7%	4.4	37.7	f
50	1.9	12.2	f	f

One-parameter nonlinear regression.

 $^{^{}b}$ C = 1 mM, D = 1 x 10^{-5} cm²/s, E_{step} = -500 mV.

 $^{^{\}rm c}$ 100 μs sampling time, 2 ms time range.

d ms sampling time, 20 ms time range.

e First one or two points dropped before analysis.

f Analysis failed to yield reasonable value of rate constant.

Larger time constants produce more severe distortions in the shape of the transients, hence, larger errors. Second, the relative error is greater for larger rate constants at a given time constant. A comparison of the results for the two time ranges shows that there is a slightly larger amount of error for the transients sampled at short times. Although it is not a large difference, some advantage is gained by using a longer sampling time.

Other results show that the error in the rate constant due to these instrumental nonidealities does not depend on the concentration. For values of reactant concentration ranging from 0.1 to 10 mM, the error was found to be constant, even though the current varied over 2 orders of magnitude.

It was also noted that the size of the potential step has only a mild effect upon the value of the rate constant derived from the nonideal transient for a given risetime. For example, analysis of a system with τ = 2 μ s and k_f = 0.3 cm/s yielded rate constants of 0.3122 and 0.3156 for a 500 mV and a 1000 mV potential step, respectively. In an actual experiment, of course, the time constant τ would depend on the magnitude of the potential step.

It is reasonable to consider that, since the potential does not reach the desired value until some point after the beginning of the experiment, the rest of the transient would be "time-shifted" so that the apparent time zero occurs a short period after the potential begins to rise. If this were the case, the equation which describes the transient could be written

$$i = nFACk_f \exp[k_f^2(t-\Delta t)/D] \operatorname{erfc}[k_f(t-\Delta t)^{\frac{1}{2}}/D^{\frac{1}{2}}]$$
 (3.7)

A two-parameter nonlinear regression analysis (varying k_f and Δt) might be expected to yield a more accurate value of the rate constant than could the aforementioned one-parameter analysis. Table 3.2 compares values of rate constants derived from Equations 3.2 and 3.7 for given time constants and rate constants over both the long and short analysis time ranges.

These results indicate that an improvement in the accuracy of $k_{\rm f}$ is indeed obtained by the two-parameter analysis in most cases; the correction is, however, not perfect, and varies with experimental parameters. For larger rate constants (0.3 and 1.0 cm/s) in the 20 ms transients, hardly any effect is seen. The greatest improvement is found at smaller rate constants and shorter analysis time ranges.

The correction is not perfect because the effect of finite risetime is not simply to "time-shift" the transient to later times; the concentration gradient begins to form, and the surface concentration begins to change, as soon as the potential rises enough to allow the electrode reaction to proceed at a significant rate. Thus, Equation 3.7 is inadequate because it implies an infinitely fast potential step at some time Δt after time zero, and an unperturbed system prior to the step, which is clearly not the case here. An examination of Figure 3.1a or 3.1b shows that the difference in time values at a given current value varies with time throughout the transient.

It does not seem likely that the "time-shift" analysis will be of much utility to the electrode kineticist. The greatest gains in accuracy are obtained under conditions such that the error in the apparent rate constant is small anyway. Additionally, the effect of

Table 3.2. Comparison of Results of Standard and "Time-shift" Analyses of Chronoamperometric Transients with Finite Risetime.

		Error in k _f			
		Short Ti	Short Time Range ^C		me Range ^d
τ (με)	k _f (cm/s)	Standard	Standard Time-Shift		Time-Shift
2	0.1	+0.78%	+0.02%	+0.42%	+0.04%
	0.3	4.1	0.4	2.5	2.3
	1.0	43.7	42.1	33.3	31.4
5	0.1	2.0	0.06	1.0	0.08
	0.3	11.1	1.4	6.7	6.3
10	0.1	4.2	0.18	2.2	0.15
	0.3	27.1	4.2	14.8	15.2
20	0.03	0.92	0.06	0.73	0.01
	0.1	7.0	5.9	4.4	0.30
	0.3	73.1	29.4	37.8	38.3

^aStandard analysis: one-parameter (k_f) nonlinear regression. "Timeshift" analysis: two-parameter (k_f and Δt) nonlinear regression.

 $^{^{}b}$ C = 1 mM, D = 1 x 10^{-5} cm²/s, E_{step} = -500 mV.

 $^{^{\}rm c}$ 100 $\mu {\rm s}$ sampling time, 2 ms time range.

d₁ ms sampling time, 20 ms time range.

such an empirical correction would be difficult to predict under actual experimental conditions, where finite potential risetime is not the only nonideality encountered.

3.5. Effect of Weak Reactant Adsorption

The effect of weak adsorption on the shape of the chronoamperometric transient depends on the relative degree of adsorption before and after the potential-step perturbation. Figure 3.2a shows the deviation from ideality for $k_f = 0.1$ cm/s when there is an equal amount of adsorption before and after the step. Currents are greater for all times; this is a consequence of the surface concentration enhancement, and the resulting faster reaction rate. Figure 3.2b displays the shape of the transient which results under differing degrees of adsorption before and after the step, again with $k_f = 0.1$ cm/s. When there is adsorption at the initial potential, but none at the final potential, currents are now even higher than the previous case at short times because the adsorbed species which are released at the onset of the potential step enhance the concentration at the surface and reduce reactant depletion in the diffusion layer. The effect of this "extra" reactant is seen throughout the transient because of the cumulative response of the concentration gradient. The opposite effect is seen when the reactant only adsorbs on the electrode after the step. The current is seen to be too small at short times because the additional flux from the diffusion layer needed to "coat" the surface depletes reactant in the vicinity of the electrode. Once the adsorbed layer is completed (which is a diffusion-controlled process

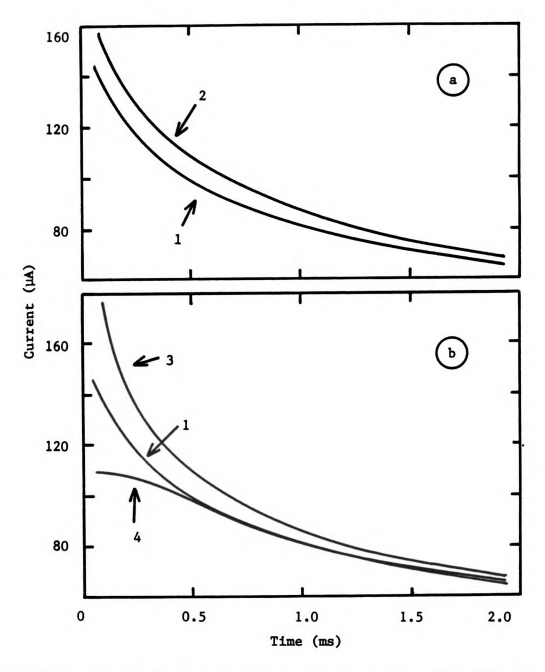


Figure 3.2. Chronoamperometric transients illustrating the effects of weak reactant adsorption, with parameters as in Figure 3.1, except $k_f=0.1$ cm/s. Curve 1: ideal system. Curve 2: $K_{ad}^i=K_{ad}=2x10^{-5}$ cm. Curve 3: $K_{ad}^i=2x10^{-5}$ cm, $K_{ad}=0$. Curve 4: $K_{ad}^i=0$, $K_{ad}=2x10^{-5}$ cm.

because of the rapidly attained equilibrium), the reaction proceeds with the enhanced surface concentration, which will tend to increase the total current. This effect becomes pronounced at longer times, when the current is seen to exceed the ideal value.

In summary, the chronoamperometric decay is steepest when the reactant is adsorbed before the potential step (but not after), and mildest when it is adsorbed only after the perturbation. One would expect larger apparent rate constants from steeper decay curves; this is indeed observed upon analysis of these nonideal transients.

Some chronoamperometric transients were simulated with various values of $k_{\rm f}$ and adsorption coefficients. The results of the nonlinear regression analyses of these transients according to the ideal decay equation (Equation 3.2) are given in Table 3.3. Somewhat greater errors in the rate constant are observed for the short-time analyses, but the difference is not large. The major difference between the two cases, in fact, is that the short time results tend to conform to the earlier, intuitive analysis (i.e., the concept of the rate of decay being directly proportional to the rate constant) than do the long-time results. At longer times (and higher rate constants) the derived values of $k_{\rm f}$ are found to be the largest when the degree of adsorption is equal before and after the step.

This variation in the results as a function of the time period over which the transient is analyzed is due to the fact that the ideal chronoamperometric decay equation does not exactly fit the shape of the decay when adsorption is present for any value of $k_{\mathbf{f}}$. It was seen in Figure 3.2b that after a sufficient period of time, the

Table 3.3. Error in Rate Constants Derived from Chronoamperometric Transients Due to Weak Reactant Adsorption.

	Adsorption Condition		
k _f (cm/s)	Before Step only ^c	After Step only ^d	Before + After step ^e
Short Time Range			
0.01	+15%	-12.8%	+2.0%
0.03	19	-12.3	5.6
0.10	34	-11.6	22
0.30	86	- 2.6	190
Long Time Range ^g			
0.01	+6.0%	- 3.9%	+2.0%
0.03	9.0	- 3.0	6.3
0.10	18	+ 3.0	26

^aOne-parameter nonlinear regression.

b
C = 1 mM, D = 1 x 10^{-5} cm²/s, E_{step} = -500 mV.

$$^{d}K_{ad}^{i} = 0 \text{ cm}, K_{ad} = 2 \times 10^{-5} \text{ cm}.$$

$$e_{K_{ad}}^{i} = K_{ad} = 2 \times 10^{-5} \text{ cm}.$$

 $^{{}^{}c}K_{ad}^{i} = 2 \times 10^{-5} \text{ cm}, K_{ad} = 0 \text{ cm}.$

f 100 µs sampling time, 2 ms time range.

g₁ ms sampling time, 20 ms time range.

current in the nonideal experiment becomes higher than the ideal value. If the analysis looked only at this region of the curve, one might indeed expect a derived rate constant to be too high under these conditions. That the derived rate constants are found to be highest at equal reactant adsorption before and after the step can be understood upon observation of Figures 3.2a and 3.2b. Although the current begins much higher in Figure 3.2b, it returns much faster to the ideal value than does the transient in Figure 3.2a, where equal adsorption before and after is present. At longer times, the deviation from ideal is smaller when there is adsorption only before the step, which would account for the results in Table 3.3.

A more detailed view of the error in the derived rate constant as a function of the adsorption coefficients is given in Table 3.4. The complete variation for a typical rate constant of 0.1 cm/s analyzed over a 2 ms time range is shown. It is obvious that more error is produced by more reactant adsorption, although the error becomes fortuitously small for the conditions where the derived rate constant goes from too high to too low. This point at which the deviations exactly compensate to yield the correct rate constant seems to depend on too many factors to isolate.

Another question which could be asked is whether the error in the rate constant depends only on the amount of adsorbed reactant, Γ , or on the ratio of adsorbed species to bulk species, K_{ad} . A series of transients were generated in which the bulk concentration and adsorption coefficients were varied in such a way as to keep the surface excess constant. The resulting rate constants showed wide variation

Table 3.4. Error in Rate Constants Derived from Chronoamperometric Transients with Varying Amounts of Weak Reactant Adsorption.

		K _{ad} (cm)			
Kad (cm)	0	1 x 10 ⁻⁶	3 x 10 ⁻⁶	1 x 10 ⁻⁵	2 x 10 ⁻⁵
0	0	-0.4%	-1.3%	-5.2%	-11.6%
1×10^{-6}	+1.4%	+1.0	+0.2	-3.7	-10.2
3×10^{-6}	4.3	3.9	3.1	-0.7	- 7.4
1×10^{-5}	15.2	15.0	14.3	+10.7	+ 3.4
2×10^{-5}	33.6	33.7	33.4	30.2	22.0

^aOne-parameter nonlinear regression.

^b100 μ s sampling time, 2 ms time range. $k_f = 0.1$ cm/s, C = 1 mM, $D = 1 \times 10^{-5}$ cm²/s, $E_{step} = -500$ mV.

in the amount of the error, with low concentrations and high adsorption coefficients producing the largest error. Another series of transients were simulated again with varying concentration, but with constant adsorption coefficient (care was taken not to exceed a surface excess greater than about 10% surface coverage). The rate constants derived from these transients were identical, showing that it is the adsorption coefficient, and not the surface excess itself, which dictates the amount of error in the derived rate constants. This is expected given the linear nature of the adsorption isotherm.

3.6. Effect of Coupled Risetime/Adsorption

Weak reactant adsorption and finite potential risetime combine to produce transients which yield rate constants that are in error by an amount which is somewhat greater than would be expected assuming the individual contributions were additive. There seems to be no general rule, however, to allow the prediction of the extent of this coupling.

Table 3.5 shows the effects of an increasing risetime on each of the three adsorption cases, in addition to that when no adsorption is present. As expected, increasing risetime increases the error in the rate constant, but to a somewhat greater extent than when no adsorption is present. The same trends are seen for analyses in both time ranges.

It is interesting to note the compensation of errors produced by finite risetime (which yields positive errors) and the case in which the reactant is adsorbed after the application of the potential step (negative errors). The adsorption is seen to be the controlling

Table 3.5. Error in Rate Constants Derived from Chronoamperometric Transients Due to Both Finite Risetime and Weak Reactant Adsorption.

	Adsorption Conditions				
τ (με)	None	Before Only ^C	After Only	Before and After ^e	
Short Time Range					
0	0	+34%	-11.6%	+22%	
5	+2%	43	-11.0	24	
10	4	51	-10.3	28	
20	7	64	- 9.8	32	
Long Time Range ^g					
0	0	+18%	+3%	+26%	
5	+1%	22	3	28	
10	2	25	4	30	
20	4	30	5	34	
50	12	48	12	50	

^aOne-parameter nonlinear regression.

$${}^{d}K_{ad}^{1} = 1 \times 10^{-11} \text{ cm}, K_{ad} = 2 \times 10^{-5} \text{ cm}.$$

 $b_{k_f} = 0.1 \text{ cm/s}, C = 1 \text{ mM}, D = 1 \times 10^{-5} \text{ cm}^2/\text{s}, E_{\text{step}} = -500 \text{ mV}.$

 $^{{}^{}c}K_{ad}^{i} = 2 \times 10^{-5} \text{ cm}, K_{ad} = 1 \times 10^{-11} \text{ cm}.$

 $^{^{}e}K_{ad}^{1} = K_{ad} = 2 \times 10^{-5} \text{ cm}.$

 $^{^{\}mbox{f}}\mbox{100}\ \mu\mbox{s}$ sampling time, 2 ms time range.

g₁ ms sampling time, 20 ms time range.

factor, with the error in the derived rate constant changing only slightly with increasing risetime. It is possible that the depletion of the solution near the electrode makes the experiment insensitive to the exact risetime conditions.

The opposite adsorption scheme, in which the reactant is released into the solution at the time of the step, shows the largest sensitivity to the potential risetime, probably due to the opposite factors which are operating above. When the adsorption coefficients remain constant throughout the experiment, the errors induced by each nonideality are almost additive.

3.7. Effect of Nonidealities on Normal Pulse Polarography

Finite potential risetime and weak reactant adsorption can have a clearly visible effect on the shapes of pulse polarographic waves when the current is sampled at short enough times. Two things need to be considered when data is collected or displayed in this format, the first and more important of which is the apparent value of the limiting current. The kinetics analysis of the polarogram depends on this value, as do electroanalytical determinations. The second thing to be considered is the actual shape of the wave; deviations could yield nonlinear plots of $\ln k_{\rm f} \ {\rm vs.}$ potential (Tafel plots) or incorrect values of alpha, the transfer coefficient, as well as simple errors in the rate constant.

Figure 3.3a is a comparison of an ideal normal pulse polarogram sampled at 100 μs and the corresponding polarogram which includes the influence of a finite potential time constant of 20 μs . The most

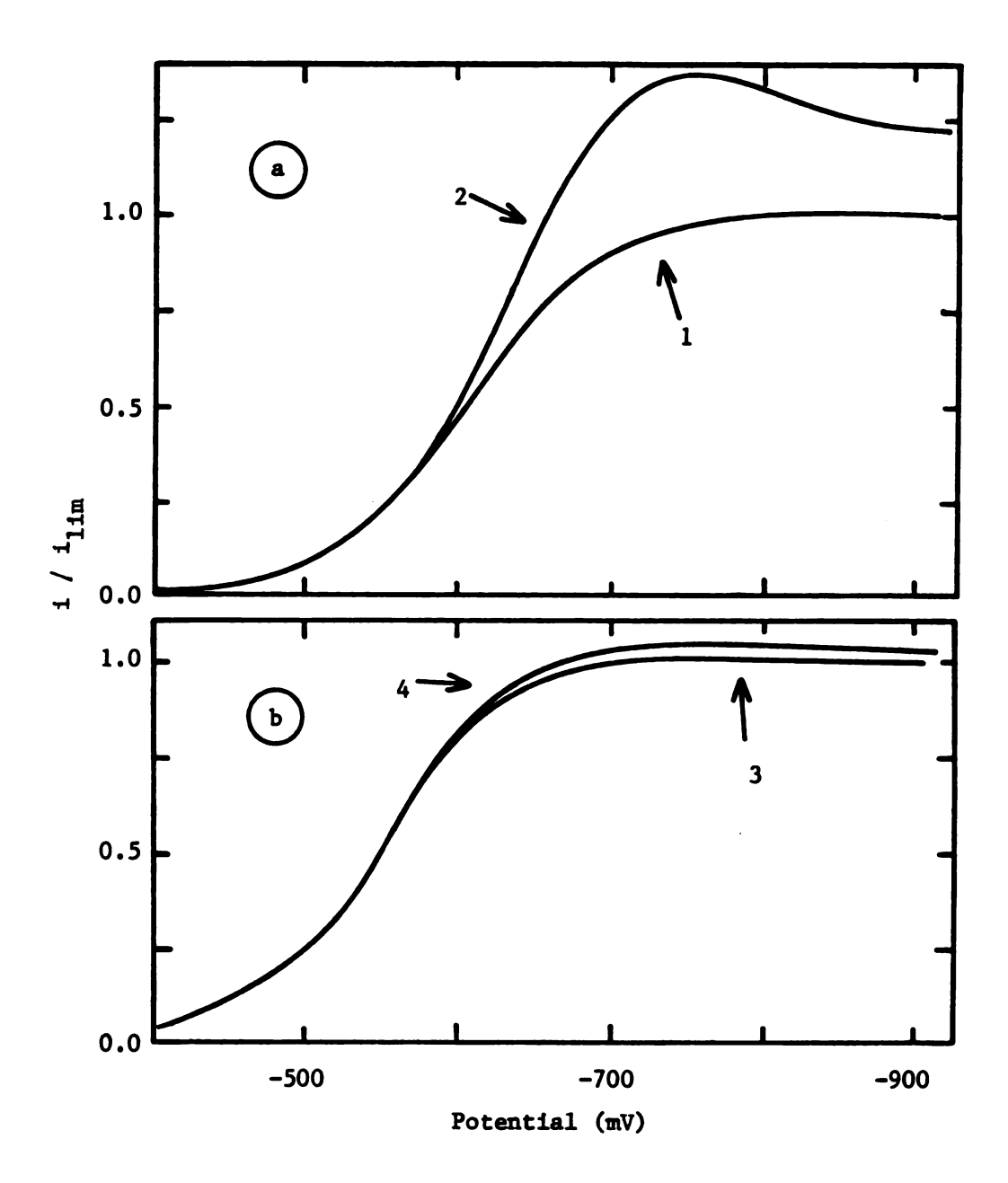


Figure 3.3. Pulse polarograms illustrating the effects of finite risetime, with α = 0.5, C = 1 mM, D = 1×10^{-5} cm²/s. Curve 1: ideal system, 100 μ s sampling time. Curve 2: τ = 20 μ s, 100 μ s sampling time. Curve 3: ideal system, 1 ms sampling time. Curve 4: τ = 20 μ s, 1 ms sampling time.

noticeable feature in the nonideal polarogram is the presence of a peak, similar in appearance to d.c. polarographic maxima. This peak is disturbing because the current does not decay to the true diffusion-limited value (or even to a constant value) even at potentials up to 500 mV or more past the peak. Additionally, the current sampled along the wave is too high beyond about one third of the way up the wave.

These deviations are very sensitive to the sampling time at which the polarogram is recorded. Figure 3.3b shows the identical system and risetime of the previous figure, except that the sampling time is 1 ms. Although the peak can still be discerned, the maximum error is only about 2%, compared to about 35% when sampling at 100 μ s. There is much less error in the rising part of the wave as well.

A problem that arises when one attempts to derive rate constants from these nonideal polarograms is that it is unclear what value of the limiting current to use, since no constant diffusion-limited value can be obtained reasonably near the wave. A comparison between the two data analysis methods for the finite risetime case would be of interest, though, so it was decided to use the current several hundred millivolts from the wave as the limiting current in the analysis.

Table 3.6 shows the results of the pulse polarographic analysis with nonideal currents sampled at 100 µs and the results of the corresponding chronoamperometric analyses. One can see that at the lower rate constants there is more error induced by the polarographic analysis, while the reverse is true for larger rate constants. One might

Table 3.6. Comparison of Results from Pulse Polarographic and Chrono-amperometric Analyses of Transients^a with Finite Risetime^b.

		Error in k _f		
E (mV)	k _f (cm/s)	Pulse Polarographic ^C	Chrono- amperometric ^d	
-450	0.0066	-9.1%	0	
-500	0.017	-5.9	0	
-550	0.045	-4.4	+2.2%	
-600	0.12	0	8.3	
-650	0.30	+3.3	30	

 $^{^{}a}$ C = 1 mM, D = 1 x 10^{-5} cm²/s

 $^{^{}b}\tau$ = 20 µs.

 $^{^{\}text{C}}$ Sampling time = 100 μs , Oldham-Parry analysis.

 $^{^{\}mbox{\scriptsize d}} 100~\mu\mbox{\scriptsize m}$ sampling time, time range 2 ms. One-parameter nonlinear regression.

expect larger errors from the Oldham-Parry analysis (48) simply because the deviations in the transient are highest at the shortest times; the range of sampling times for the chronoamperometric analysis extended to 2 ms, while the polarographic analysis was limited to the values at 100 µs. Additionally, the use of a limiting current value which is too high will cause errors in relatively undisturbed regions of the wave. At higher rate constants, however, there seems to be a compensation effect. The measured current and the limiting current are in error by roughly the same amount, so that the 1/11 value is closer to ideal, and less error in the rate constant results.

Weak reactant adsorption also produces peaks in normal pulse polarograms. Figure 3.4a displays an ideal polarogram sampled at 100 µs and one in which the reactant is adsorbed equally before and after the potential step. Note that the maximum has a different shape than that due to potential risetime; its maximum value comes at lower overpotentials, and, more importantly, the current falls to a true diffusion-limited value one or two hundred millivolts beyond the peak. Electroanalytical applications of normal pulse polarography will not suffer from this nonideality (unless the limiting region of the wave is not accessible for some reason), but errors will arise for electrode kineticists since the current is considerably different from ideal along all but the foot of the wave. As with the finite risetime case, the effect of the nonideality falls off rapidly with increasing sampling time. Figure 3.4b illustrates this point, showing the same system as in Figure 3.4a except that the sampling time was 1 ms.

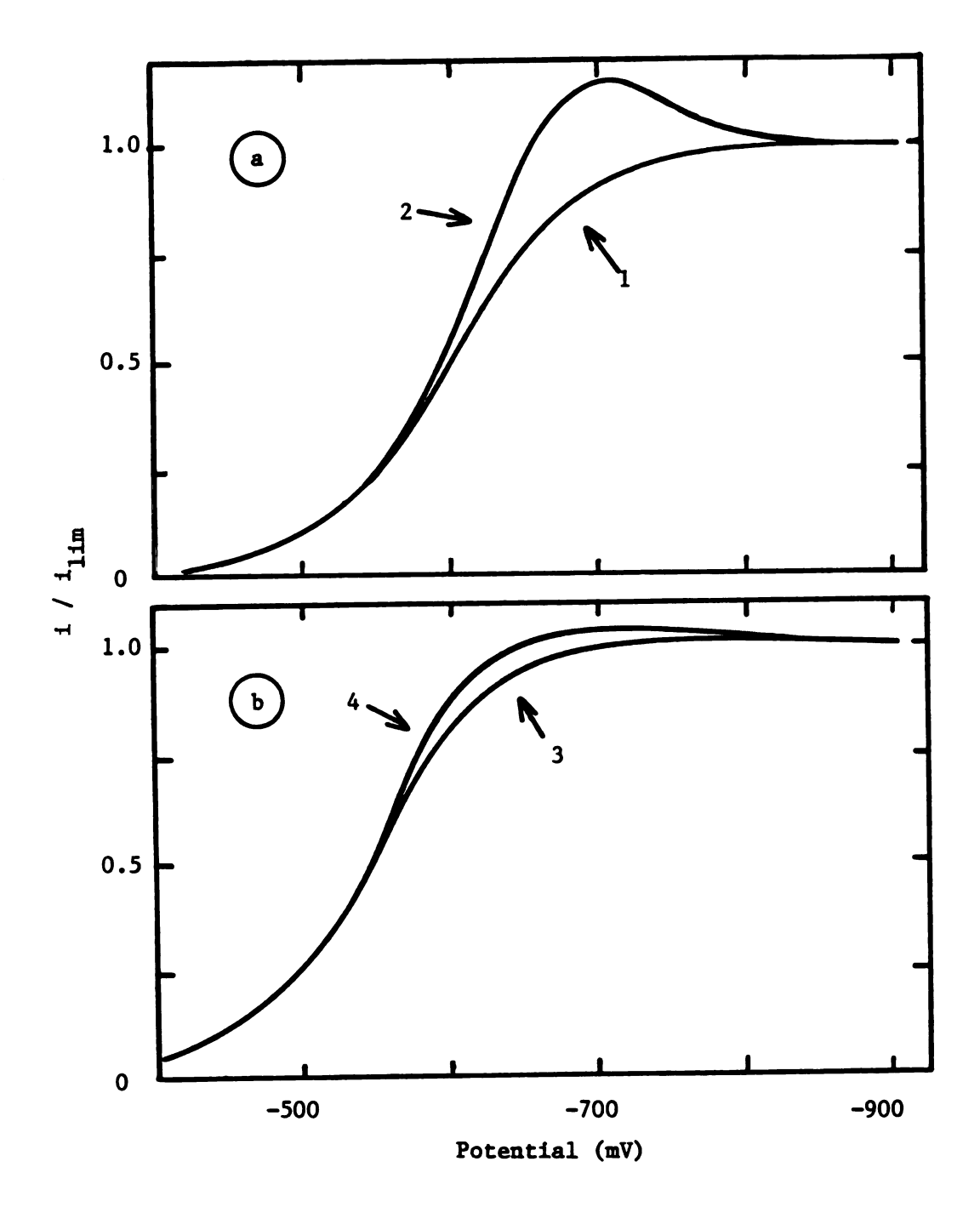


Figure 3.4. Pulse polarograms illustrating the effects of reactant adsorption, with α = 0.5, C = 1 mM, D = 1×10^{-5} cm²/s. Curve 1: ideal system, 100 μ s sampling time. Curve 2: $K_{\rm ad}^{\rm i} = K_{\rm ad}^{\rm i} = 2 \times 10^{-5}$ cm, 100 μ s sampling time. Curve 3: ideal system, 1 ms sampling time. Curve 4: $K_{\rm ad}^{\rm i} = K_{\rm ad}^{\rm i} = 2 \times 10^{-5}$ cm, 1 ms sampling time.

It is interesting to note the effects of varying amounts of adsorption at the initial and final potential. Figure 3.5 shows an ideal polarogram, one in which there is adsorption only at the final potential, and one where adsorption is present only before the step. The latter curve starts out with currents which are too low, the former has larger than ideal currents at the foot of the wave. These curves converge towards the top of the wave to yield identical, somewhat high responses, although with smaller peaks than the equal adsorption case.

Since the true limiting currents are accessible for these weak adsorption polarograms, a kinetics analysis may be carried out to determine the amount of error in the rate constants derived from the nonideal waves. Table 3.7 lists the rate constants derived from these polarograms at selected potentials along the wave, as well as the corresponding values from the chronoamperometric analysis.

At lower rate constants, the error is clearly larger for the pulse polarographic analysis when the adsorption is not equal before and after the step. At equal adsorption conditions, very little difference exists between the methods. At higher rate constants, this difference becomes negligible. It is easy to understand why this occurs. The pulse polarographic analysis uses only the current sampled at $100~\mu s$ to estimate the rate constant, while the chronoamperometric uses that point plus many others at longer times. It has already been shown that the deviations from ideal are largest at short times, so an analysis based only on the shortest time cannot be expected to yield as reliable a value as would one based on many data at longer times.

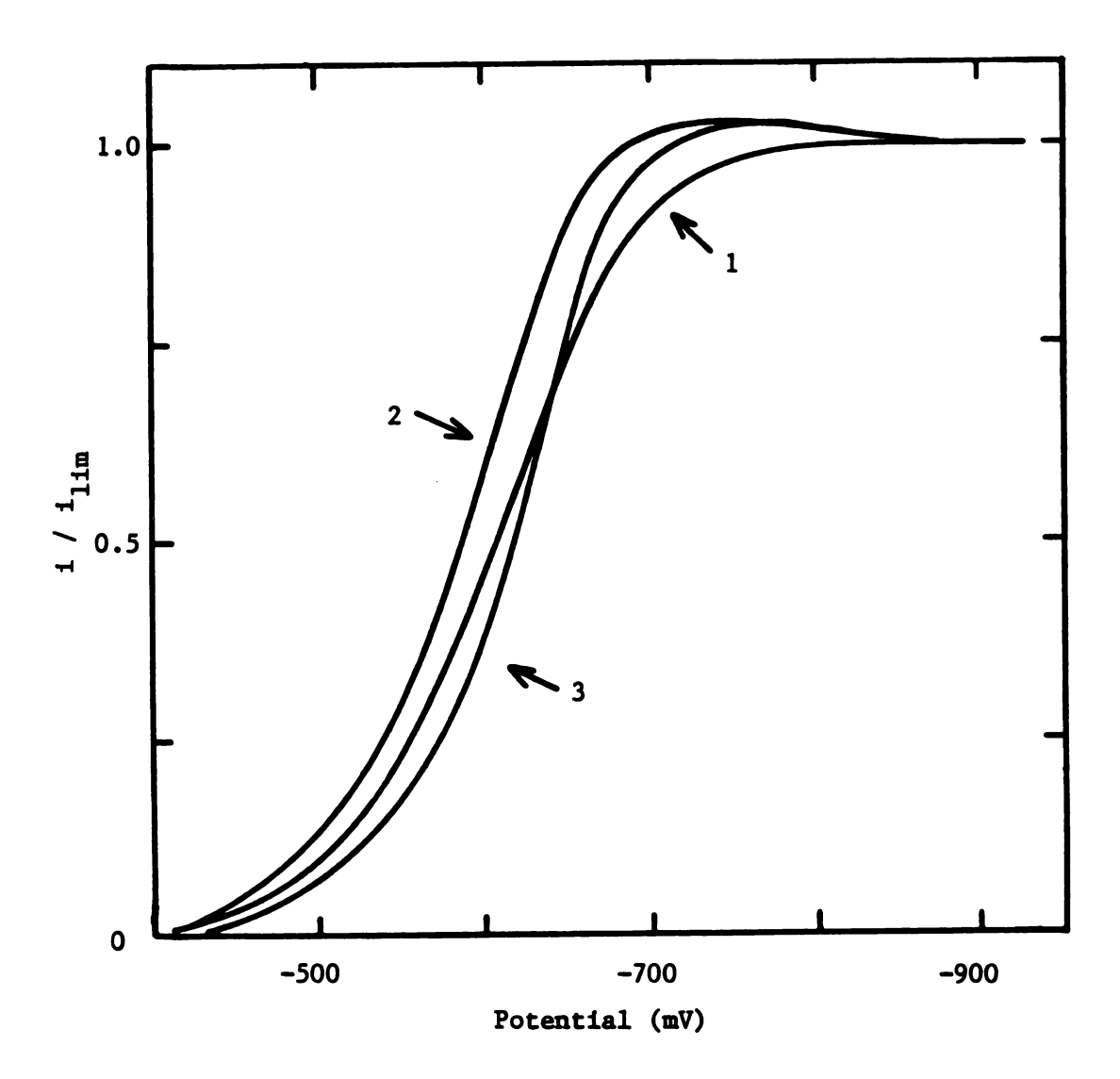


Figure 3.5. Pulse polarograms illustrating the effects of reactant adsorption, with α = 0.5, C = 1 mM, D = 1×10^{-5} cm²/s, 100 µs sampling time. Curve 1: ideal system. Curve 2: K_{ad}^{i} = 2×10^{-5} cm, K_{ad} = 0. Curve 3: K_{ad}^{i} = 0, K_{ad} = 2×10^{-5} cm.

Table 3.7. Comparison of Results from Pulse Polarographic and Chronoamperometric Analyses of Transients with Weak Reactant Adsorption.

				Error	in k		
			Ad	sorption	Condit	ions	
		Before	Only b	After	Only ^C	Before a	nd After ^d
E (mV)	k _f (cm/s)	PPe	CA ^f	PPe	CAf	PPe	CA ^f
-450	0.0066	+32%	+15%	-33%	-12%	0	+2%
-500	0.017	35	18	-29	-12	0	6
-550	0.045	38	22	-31	-13	+6.6%	8.9
-600	0.12	42	38	-28	-12	17	25
-650	0.30	83	87	-13	- 3	160	190

 $^{^{}a}C = 1 \text{ mM}, D = 1 \times 10^{-5} \text{ cm}^{2}/\text{s}.$

$${}^{c}K_{ad}^{1} = 1 \times 10^{-11} \text{ cm}, K_{ad} = 2 \times 10^{-5} \text{ cm}.$$

$${}^{d}K_{ad}^{1} = K_{ad}^{f} = 2 \times 10^{-5}$$
.

 $^{{}^{}b}K_{ad}^{i} = 2 \times 10^{-5} \text{ cm}, K_{ad} = 1 \times 10^{-11} \text{ cm}.$

 $^{^{\}mbox{\scriptsize e}}\mbox{Oldham-Parry analysis, 100}~\mu\mbox{s sampling time.}$

 $^{^{\}rm f}\text{l}$ parameter nonlinear regression, 100 μs sampling time 2 ms time range.

An analysis of polarograms sampled at 1 ms, although the largest accessible rate constant was not as high, was found to produce significantly less error than the 100 µs waves. The error observed was still fairly high, averaging around 100%, and followed the same trends as the shorter time analysis. The errors were roughly comparable to the chronoamperometric analyses; the current at 1 ms was about in the middle of the current-time transients which were analyzed.

Thus, it appears that no increases in accuracy can be gained through the use of the pulse polarographic over the chronoamperometric data analysis when weak adsorption is present. Both procedures seem to suffer from roughly the same relative amount of error in the rate constant under these conditions.

3.8. Correlation of Model with Experimental Data

The types of deviations noted in the previous sections have been observed experimentally in this laboratory (21). It was of interest, therefore, to try to correlate this model of finite potentiostat risetime and weak reactant adsorption with these data in an attempt to derive meaningful values of the rate constant from apparently non-ideal transients when ideal analyses are unable to do so.

A set of chronoamperometric transients was available for $Cr(OH_2)_6^{3+}$ reduction on a mercury electrode (21). When displayed in pulse polarographic format, a maximum was observed in the wave at short sampling times (less than about 500 μ s). These data were analyzed with the ideal chronoamperometric (nonlinear regression) analysis and by the pulse polarographic (Oldham-Parry) method. As can be seen in

Table 3.8, at rate constants above about 0.16 cm/s, points deviated considerably from the Tafel line extrapolated from smaller rate constants, suggesting a failure of the analysis to derive a meaningful value of the kinetics parameter. Below this level, however, there was good agreement between rate constants produced by the two analysis methods.

An alternative analysis method was then used to attempt to extend the range of accessible rate constants under these nonideal conditions. Instead of the ideal equation, a parallel simulation routine was used as the calculation subroutine in the nonlinear regression program. However, there are now four unknowns in the equation: the rate constant, the risetime of the potentiostat, and the adsorption coefficients before and after the application of the step. Since the potential was stepped from a point at which the adsorption coefficient is predicted to be quite small (see Chapter 1), it was assumed that any diffuse layer adsorption at this potential would be negligible, allowing one of the unknowns to be eliminated. The results of the analysis show very good agreement with the two ideal analyses at the lower rate constants; at higher values, however, the derived values are considerably closer to the extrapolated line than either of the other two methods, as shown in Figure 3.6. Indeed, correct rate constants up to 1.47 cm/s seem to have been extracted from these data. There was, however, some problem with two of the intermediate transients; the reason for this is unknown. Table 3.9 contains the resulting values of all three of the parameters. Although the rate constant is derived successfully, there seems to be little sense to

Table 3.8. Rate Constants for $Cr_{(aq)}^{3+}$ Reduction Derived by Pulse Polarographic and Chronoamperometric Analyses.

k_f (cm/s) **Pulse** Chrono-E (mV) Polarographic amperometric -975 0.0109 0.0112 -1000 0.0180 0.0189 -1025 0.0355 0.0329 -1050 0.0535 0.0560 -1075 0.0945 0.0968 0.185 -1100 0.15 -1125 1.464 а -1150 0.589 а -1175 Ъ -1200 b

^aCurrent was too close to diffusion-limited value to obtain meaningful results.

^bAnalysis failed to yield meaningful results.

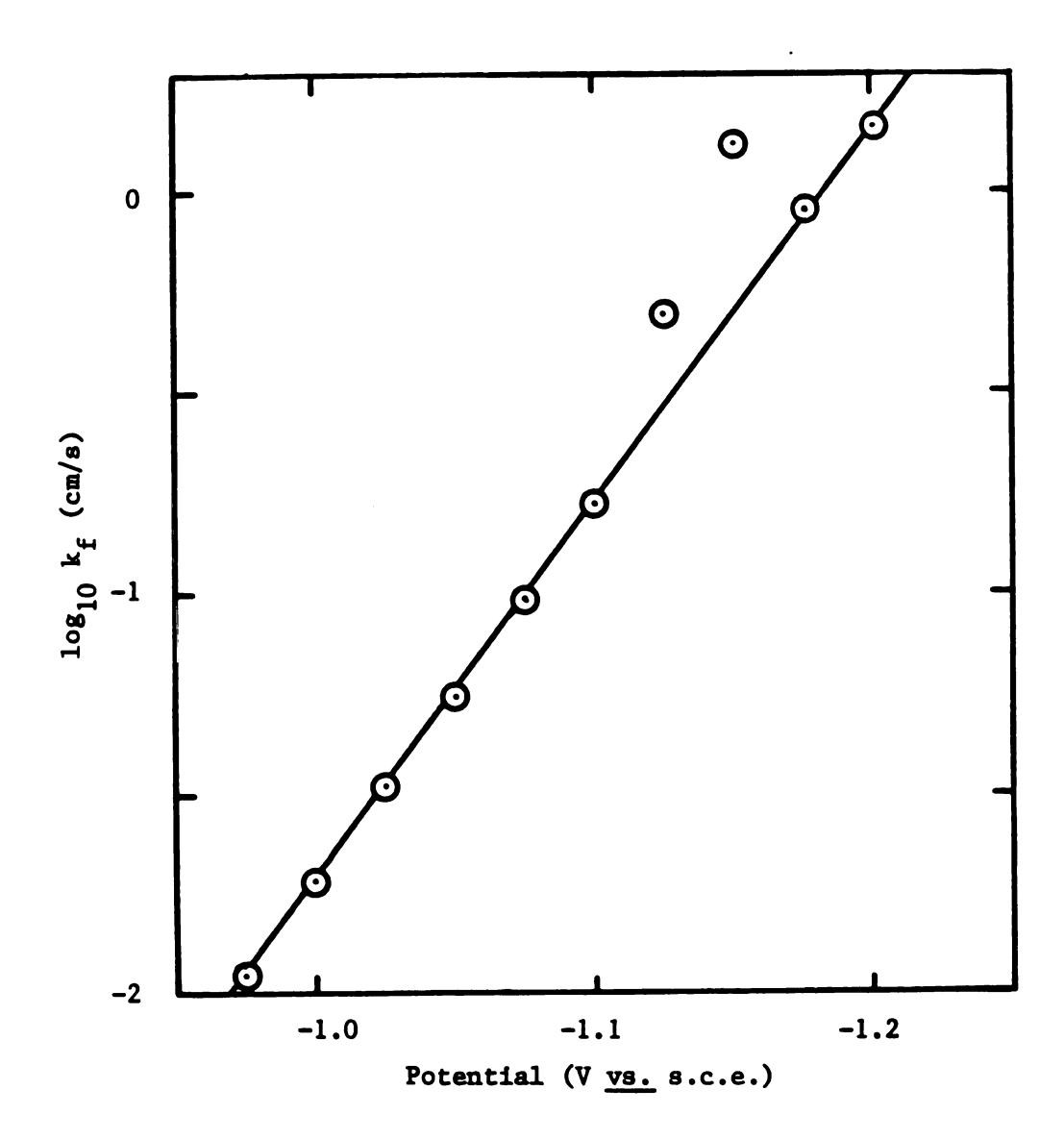


Figure 3.6. Rate constants for $Cr(OH_2)^{3+}_6$ reduction derived from experimental chronoamperometric transients using simulation analysis, <u>vs.</u> potential. Line is least-squares fit of lower six points.

Table 3.9. Results of Simulation Analysis of $Cr_{(aq)}^{3+}$ Data.

	De	rived by Analy	sis
E (mV)	k _f (cm/s)	τ (μs)	K _{ad} (cm)
-975	0.0112	11.5	0
-1000	0.0190	31.5	2.5×10^{-6}
-1025	0.0331	8.6	1.8×10^{-6}
-1050	0.0554	33.9	7.0×10^{-6}
-1075	0.0955	20.7	11×10^{-6}
-1100	0.168	20.7	180×10^{-6}
-1125	0.494	11.2	0
-1150	1.321	9.4	139×10^{-6}
-1175	0.904	47.5	0
-1200	1.47	52.0	12×10^{-6}

be made of the series of adsorption coefficients and risetimes. It is possible that either nonideality can account for the deviations in the transients; one factor may dominate on the basis of trivial differences in the curves.

It is also possible that the exact shape of the transient is extremely sensitive to the shape of the profile of the applied potential. A single exponential model might not be sophisticated enough to adequately fit these data. If this is the case, the actual applied potential profile can be recorded together with the current response to eliminate errors due to the incorrect choice of a risetime model.

Clearly, much more remains to be done in this work. The results of these preliminary experiments are promising, but further systems need to be studied under more well-defined conditions. The major drawback to the use of this method is the long computation time required for this type of analysis - approximately three orders of magnitude longer than the ideal nonlinear regression analysis. This is clearly not the method of choice for data on which the ideal analyses perform well.

CHAPTER 4

POTENTIAL-STEP EXPERIMENTS FOR THE STUDY OF QUASI-REVERSIBLE ELECTRODE REACTIONS

4.1. Description of Experiment

The potential-step experiment for quasi-reversible reactions (34) is analogous to that described in Chapter 3 except that the chemical system to which it is applied now includes a back reaction component:

$$0x + ne^{-k_{f} \atop +} Red$$

$$k_{h}$$
(4.1)

Both large and small potential steps may be used to study the kinetics of this type of process.

In small-step experiments (10), both the oxidized and reduced species are present in the solution while the electrode is maintained at the equilibrium potential. The applied potential is suddenly changed by several millivolts, and the current which flows at this new potential is monitored.

Large-step experiments (10) start with only one species of the redox couple in a solution in which the electrode is held at a potential such that this species is strongly favored on the basis of the Nernst equation. A potential step of several hundred millivolts is applied, causing the reaction to proceed. The current is again monitored as a function of time. The results of these large-step experiments can be treated in the same way as the small-step experiments, or alternatively displayed and analyzed in the form of a normal pulse polarogram.

The equation which describes the current response of a quasi-

reversible system to either a large or small potential-step perturbation is (34):

$$i = nFA (k_f^{C} c_{ox} - k_b^{C} c_{red}) exp(k_f^{2} t/D_{ox} + k_b^{2} t/D_{red}) \cdot erfc(k_f^{\frac{1}{2}}/D_{ox}^{\frac{1}{2}} + k_b^{\frac{1}{2}}/D_{red}^{\frac{1}{2}})$$
(4.2)

Note that when $k_{\mbox{std}}$ is very small, the reverse reaction terms drop out, yielding the equation for the irreversible case.

This equation describes the ideal experiment in which there is no reactant adsorbed at the electrode surface, and in which the potential rises instantaneously to the new value. It is of interest, therefore, to determine the effects of reactant adsorption and finite potentiostat risetime on rate constants derived from these potential-step experiments, both in chronoamperometric small— and large—step procedures, and to compare the large—step chronoamperometric data treatment to that of normal pulse polarograms.

4.2. Conventional Data Analysis

As was the case for irreversible redox systems, nonlinear regression on Equation 4.2 is an obvious method with which to derive heterogeneous rate data. The rate information of interest is contained in the standard rate constant, from which $\mathbf{k}_{\mathbf{f}}$ and $\mathbf{k}_{\mathbf{b}}$ can be derived. Thus, it is possible to perform a one-parameter nonlinear regression analysis of the current-time transient to derive a value of the standard rate constant. Since the experiment is (ideally) carried

out at constant potential, the forward or reverse rate constant could be obtained instead. (This is not the case for coulostatics and galvanostatic double pulse experiments in which only the standard rate constant is accessible.)

Normal pulse polarography (52) can also be performed on quasireversible systems. Now, however, the Oldham-Parry analysis (48)
must be modified to include the effect of the back reaction (46).
Since only forward rate constants are derived through this procedure,
the E_{std} of the redox couple must be known in order to determine
the standard rate constant (this is also the case for the small-step
nonlinear regression analysis).

The advantages and disadvantages of each type of analysis as described in Chapter 3 apply for quasi-reversible reactions as well.

4.3. Unique Aspects of Simulation

The simulation of quasi-reversible systems was a straightforward extension of the irreversible simulations described in Chapter 3.

A single exponential was used as the applied potential waveform, and the Henry isotherm was applied independently to both the oxidized and reduced form of the species.

In small-step experiments, it is not necessary to consider a potential dependence of the adsorption coefficients, so that values of K_{ox} and K_{red} at the equilibrium potential are sufficient to describe the adsorption. The large-step experiments, however, need values of the adsorption coefficient for each species both before and after the step as these parameters exhibit a dependence on potential.

The parallel simulation method was used for simulations of smallstep experiments. Conventional simulations were used for pulse polarographic and large-step experiments because the original goal of these
calculations was simply to observe the morphology of the wave. In
determining the error in rate constants derived from these transients
and polarograms, the values of the rate constants obtained by the same
analysis procedure on ideal and nonideal transients were compared to
help eliminate the effects of simulation error.

4.4. Effect of Risetime on Small-Step Chronoamperometry

Finite potentiostat risetime produces very similar effects in the shape of small-step chronoamperometric transients from both irreversible and quasi-reversible systems. Figure 4.1 shows an ideal transient together with one generated with a potential risetime constant of 50 µs. Because of the relatively long risetime, the potential has not yet reached the desired value by the time the current is first sampled; the shape of the nonideal transient at short times illustrates this. Once the potential is at the desired value, the nonideal transient is larger than ideal, and will remain larger because the slow potential rise causes the diffusion layer around the electrode to be less depleted than it would have been had the experiment been ideal.

A series of small potential-step experiments was simulated using various standard rate constants and potential risetime constants.

Two time ranges were used, as for the irreversible systems. The errors in the rate constants derived from these simulated transients using a one-parameter nonlinear regression analysis are listed in

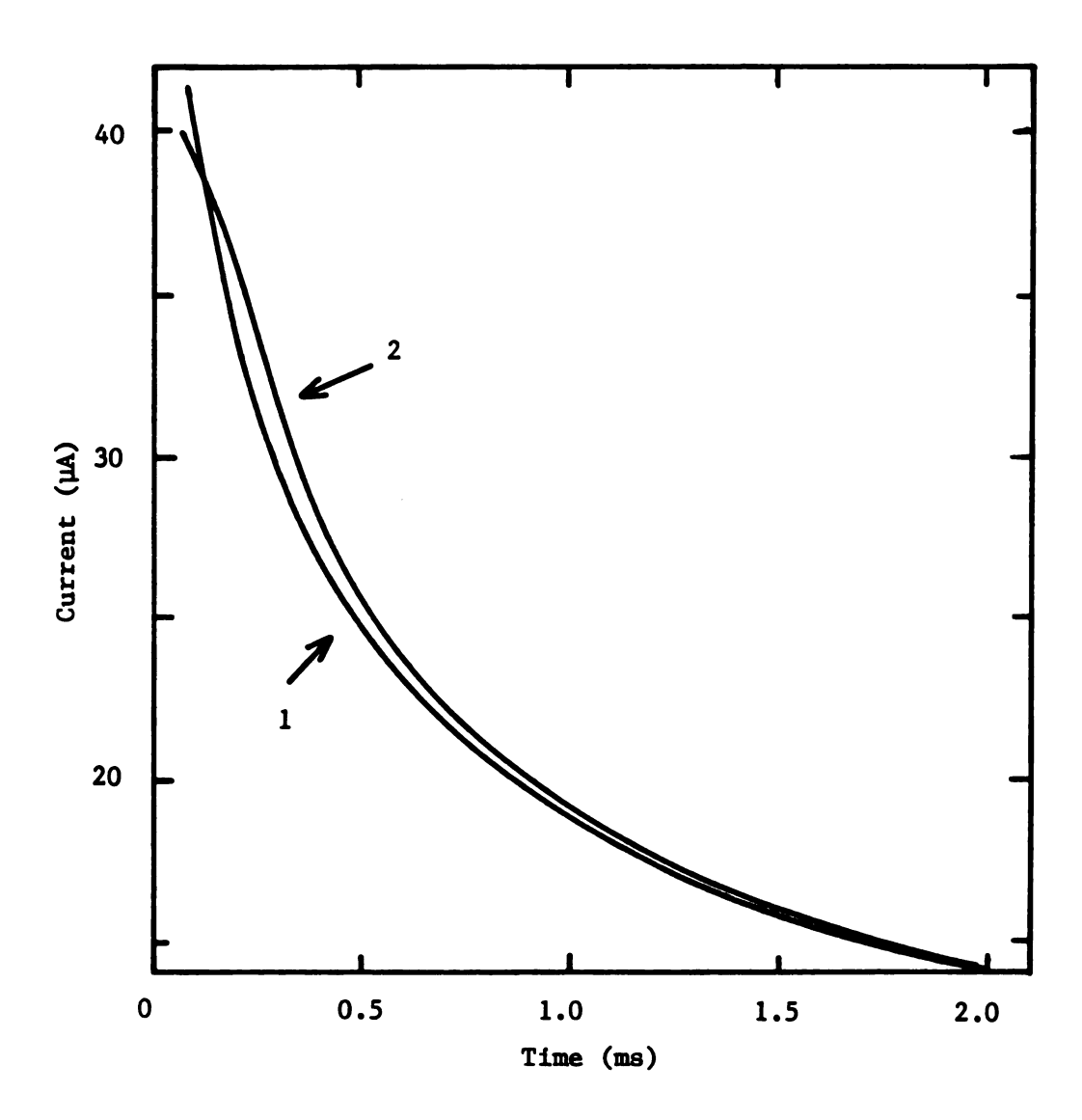


Figure 4.1. Chronoamperometric transients for quasi-reversible reactions illustrating the effects of finite risetime, with k_{std} = 0.1 cm/s, α = 0.5, E_{step} = -10 mV, C_{ox} = C_{red} = 1 mM, D_{ox} = D_{red} = 1×10^{-5} cm²/s. Curve 1: ideal system. Curve 2: τ = 50 μ s.

Table 4.1. These results show that serious errors in the rate constant are found for systems with $k_{\mbox{std}}$ greater than about 0.1 cm/s with reasonable time constants of 5 or 10 $\mu \mbox{s}$, regardless of the time range used.

A comparison of the results for the two time ranges shows that the short time range analysis yields more accurate results under these conditions. This is the opposite of what is found for the analysis of irreversible reactions, in which larger time ranges produced less error, although the degree of this error is roughly comparable overall.

An adjustable experimental parameter in this method is the size of the potential step which is applied to the system, and it is of interest to determine if it is possible to adjust this value to optimize the measurement of the rate constant under nonideal conditions. A series of transients was generated with a range of step sizes from 0.5 mV to 50 mV, keeping all other parameters constant. The error in the rate constants derived from these transients was independent of the step size, except that the error increased dramatically for step sizes over about 30 mV. (In actual practice, however, the time constant probably depends on the size of the potential step.)

It is also of interest to determine whether the concentrations of the reactants affect the accuracy of the derived rate constant under constant risetime conditions. Several series of transients were generated for various values of $C_{\rm ox}$ and $C_{\rm red}$ in a range from 0.1 mM to 10 mM. When the concentration of each of the species was equal, the error in the derived rate constant was independent of the

Table 4.1. Error in Rate Constants Derived^a from Chronoamperometric Transients for Quasi-Reversible Reactions^b Due to Finite Risetime.

		k _{std}	(cm/s)	
τ (με)	0.03	0.1	0.3	1.0
Short Time Range ^C				
1	+0.1%	+0.4%	+2.3%	+29%
2	0.1	0.8	4.7	129
5	0.3	2.0	13.4	e
10	0.7	4.3	35.8	e
20	1.3	9.0	215	e
Long Time Range ^d				
2	+0.1%	+0.5%	+3.8%	+112%
5	0.2	1.2	10.4	e
10	0.4	2.4	24.7	e
20	0.7	5.1	88.8	e
50	1.9	14.7	e	e

^aOne-parameter nonlinear regression.

 $^{^{}b}C_{ox} = C_{red} = 1 \text{ mM}, \quad D_{ox} = D_{red} = 1 \times 10^{-5} \text{ cm}^{2}/\text{s}, \quad E_{step} = -10 \text{ mV}.$

c_{100 µs} sampling time, 2 ms time range.

d₁ ms sampling time, 20 ms time range.

^eAnalysis failed to yield reasonable value of rate constant.

concentration. There was, however, a dependence on the ratio ${\rm C_{ox}}/{\rm C_{red}}$. More error was induced in the rate constant when ${\rm C_{ox}}/{\rm C_{red}}$ deviated from unity in either direction. Even though the actual size of the deviation in the transient wasn't strongly affected by this variation, there simply is less kinetics information available in the transients as the equilibrium potential gets farther from the standard potential. Thus, the kinetics parameter is more sensitive to deviations in the shape of the transient, and larger errors will result for a given size deviation under these conditions.

4.5. Effect of Adsorption on Small-Step Chronoamperometry

The influence of weak reactant adsorption on the shape of the small-step chronoamperometric decay curve is shown in Figure 4.2.

The transient which was generated with both species of the redox couple adsorbed is higher than ideal all along the transient, especially at small times. When only one of the species is adsorbed, the deviation from ideal is roughly half that seen when both species adsorb; there is only a minor difference in the shapes of the transients with only the reactant or product adsorbed. This additional current is due to the reaction of the adsorbed species and to the steeper concentration gradient which is needed to replenish the adsorbed layer.

To obtain an overview of the accuracy of the rate parameters derived from transients generated with weak reactant adsorption, a series of curves were generated with equal adsorption of Ox and Red for various rate constants and adsorption coefficients. The results of the analysis of these transients are shown in Table 4.2. There is

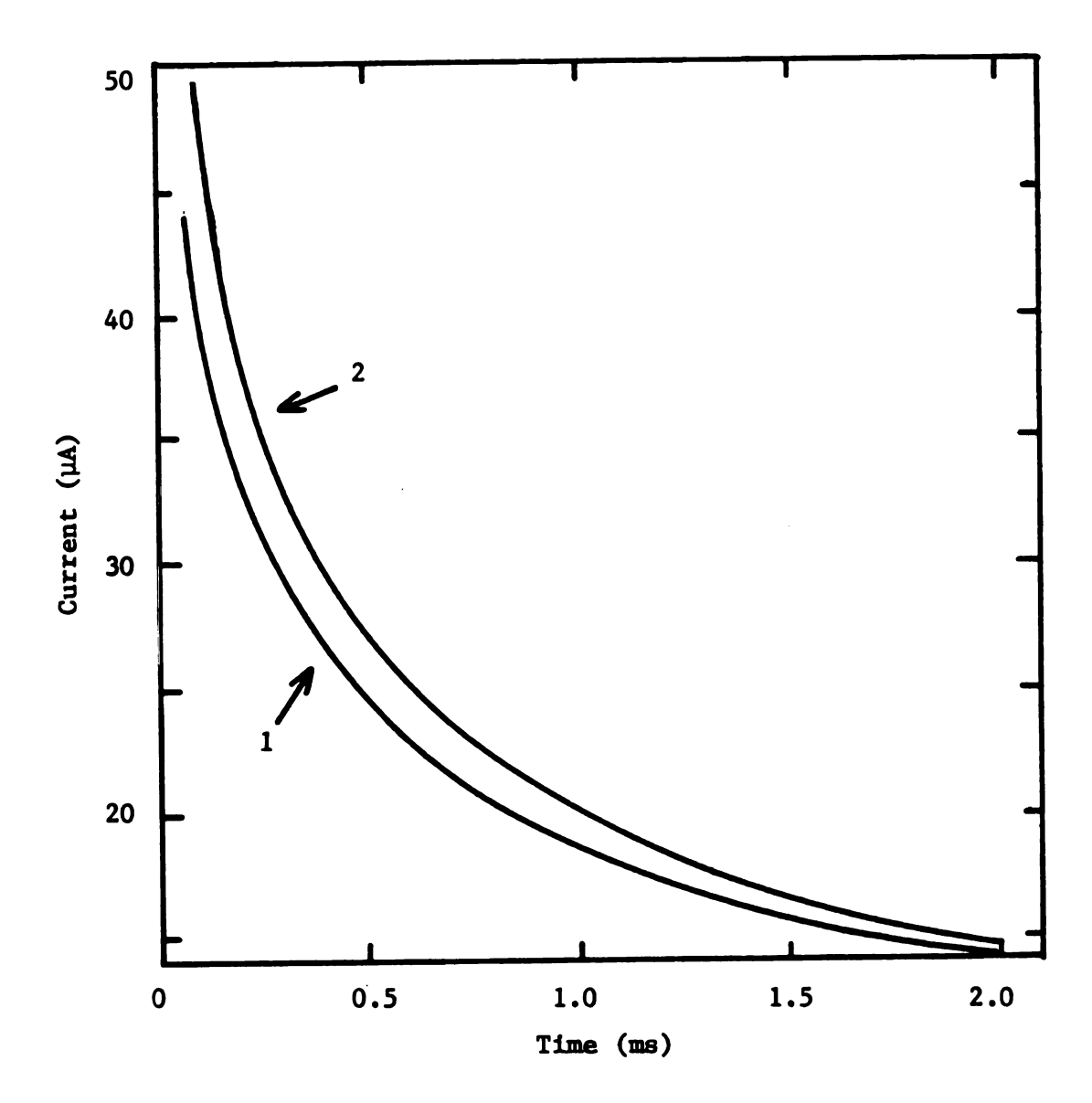


Figure 4.2. Chronoamperometric transients illustrating the effects of reactant adsorption, with $k_{std} = 0.1$ cm/s, $\alpha = 0.5$, $E_{step} = -10$ mV, $C_{ox} = C_{red} = 1$ mM, $D_{ox} = D_{red} = 1 \times 10^{-5}$ cm²/s. Curve 1: ideal system. Curve 2: $K_{ox} = K_{red} = 2 \times 10^{-5}$ cm.

Table 4.2. Error in Rate Constants Derived from Chronoamperometric Transients Due to Weak Reactant Adsorption.

		k std	(cm/s)	
$K_{ox} = K_{red}$ (cm)	0.03	0.1	0.3	1.0
Short Time Range ^C				
1 x 10 ⁻⁶	+0.6%	+2.1%	+6.4%	+28.3%
3×10^{-6}	1.9	6.5	23.4	e
1 x 10 ⁻⁵	6.2	25.2	e	e
2×10^{-5}	12.4	62.7	e	e
Long Time Range				
1 x 10 ⁻⁶	+0.6%	+2.0%	+6.5%	+28.5%
3×10^{-6}	1.9	6.3	24.1	e
1 x 10 ⁻⁵	6.5	26.7	e	e
2×10^{-5}	13.8	93.6	e	e

^aOne-parameter nonlinear regression.

 $^{^{}b}C_{ox} = C_{red} = 1 \text{ mM}, D_{ox} = D_{red} = 1 \times 10^{-5} \text{ cm}^{2}/\text{s}, E_{step} = -10 \text{ mV}.$

 $^{^{\}rm c}$ 100 μs sampling time; 2 ms time range.

d₁ ms sampling time; 20 ms time range.

e Analysis failed to yield reasonable value of rate constant.

virtually no difference between analysis of 2 ms or 20 ms transients, except at the largest levels of adsorption. The error in the derived rate constants is quite severe for small amounts of adsorption $(K_{\text{ox}} = K_{\text{red}} = 3 \times 10^{-6} \text{ cm}, \text{ or a coverage of about 1% of a monolayer in a 1 mM solution) when the rate constant is greater than about 0.1 cm/s.$

The accuracy of the rate constant determination depended only to a very small extent on the size of the potential step which is applied to the cell, as was the case with finite risetime. A potential step size of 10 mV was used for all small potential-step simulations.

It is of interest to expand the study of weak reactant adsorption to situations in which K_{OX} is not equal to K_{red} . Table 4.3 shows the results of the analysis of a series of simulated transients for various values of the adsorption coefficients at a rate constant of 0.1 cm/s. It can be seen that the error increases roughly with the total amount of adsorption, although the effect is not additive for both species. Combined adsorption of both species produces more than the sum of the errors caused by adsorption of the individual species. The slight asymmetry about the $K_{OX} = K_{red}$ diagonal reverses with a potential step of the opposite sign; apparently the adsorption of the reactant species produces larger deviations in the shape of the transient than does adsorption of the product.

Variation of the relative concentrations of the oxidized and reduced half of the redox couple while keeping the adsorption coefficients constant has the same sort of effect as in the finite risetime case.

Table 4.4 shows the results of the analysis of a typical series of

Table 4.3. Error in Rate Constants Derived^a from Chronoamperometric Transients^b Due to Weak Reactant Adsorption $(K_{ox} \neq K_{red})$.

		K _{red} (cr	n)	
0	1 x 10 ⁻⁶	3 x 10 ⁻⁶	1 x 10 ⁻⁵	2 x 10 ⁻⁵
	+0.8%	+2.5%	+8.8%	+18.1%
+1.2%	2.1	3.8	10.3	19.8
3.8	4.7	6.5	13.3	23.4
13.6	14.6	16.9	25.2	37.9
29.3	30.7	33.7	45.0	62.7
	 +1.2% 3.8 13.6	+0.8% +1.2% 2.1 3.8 4.7 13.6 14.6	0 1 x 10 ⁻⁶ 3 x 10 ⁻⁶ +0.8% +2.5% +1.2% 2.1 3.8 3.8 4.7 6.5 13.6 14.6 16.9	+0.8% +2.5% +8.8% +1.2% 2.1 3.8 10.3 3.8 4.7 6.5 13.3 13.6 14.6 16.9 25.2

^aOne-parameter nonlinear regression.

 $^{^{\}rm b}$ 100 μs sampling time; 2 ms time range.

 $c_{k_{std}} = 0.1 \text{ cm/s}, \quad C_{ox} = C_{red} = 1 \text{ mM}, \quad D_{ox} = D_{red} = 1 \times 10^{-5} \text{ cm}^2/\text{s},$ $E_{step} = -10 \text{ mV}.$

Table 4.4. Error in Rate Constant Derived^a from Chronoamperometric Transients^b Due to Weak Reactant Adsorption^c ($C_{ox} \neq C_{red}$).

			C _{red} (mM	i)	
C _{OX} (mM)	0.1	0.3	1	3	10
0.1	+2.1%	+2.6%	+4.2%	+7.2%	+14.2%
0.3	2.2	2.1	2.7	4.2	7.6
1	3.1	2.2	2.1	2.6	4.2
3	4.9	3.0	2.2	2.1	2.7
10	9.0	5.1	3.0	2.2	2.1

One-parameter nonlinear regression.

^b100 µs sampling time, 2 ms time range. $k_{std} = 0.1 \text{ cm/s}$, $D_{ox} = D_{red} = 1 \times 10^{-5} \text{ cm}^2/\text{s}$, $E_{step} = -10 \text{ mV}$.

 $^{^{}c}K_{ox} = K_{red} = 1 \times 10^{-6}$ cm.

nonideal transients with various concentrations C_{ox} and C_{red} . Again, the $C_{\text{ox}}/C_{\text{red}}$ ratio controls the accuracy of the derived rate constant, with a slight asymmetry around the $C_{\text{ox}} = C_{\text{red}}$ diagonal.

These results rule out the possibility of minimizing errors due to weak reactant adsorption by adjusting the concentration of the redox couple. If diffuse-layer adsorption is occurring, however, it may be possible to shift the potential at which the experiment is performed closer to the electrode's p.z.c., sacrificing some sensitivity to the electrode kinetics to lower the extent of the adsorption. The success of this strategy depends on the specific chemical system involved, however.

4.6. Comparison of the Effect of Risetime on Normal Pulse Polarography and Large-Step Chronoamperometry

A finite potentiostat risetime affects the normal pulse polarogram of a quasi-reversible system in much the same manner as is seen for irreversible reactions (Chapter 3). Figure 4.3 shows some simulated pulse polarograms of a species with $k_{\rm std}$ = 0.1 cm/s at a 100 μ s sampling time with the time constant of 20 μ s, 10 μ s, and 0 μ s (ideal case). Again, the current along the nonideal waves is too large at all potentials, with the least deviation at the foot of the wave and far out into the diffusion-limited region. The shape of the deviation is virtually independent of the value of the standard rate constant of the system as can be seen by comparing Figures 3.3a and 4.3.

Other aspects of the shape of the nonideal waves show the same trends as were seen in the previous chapter. The true value of the

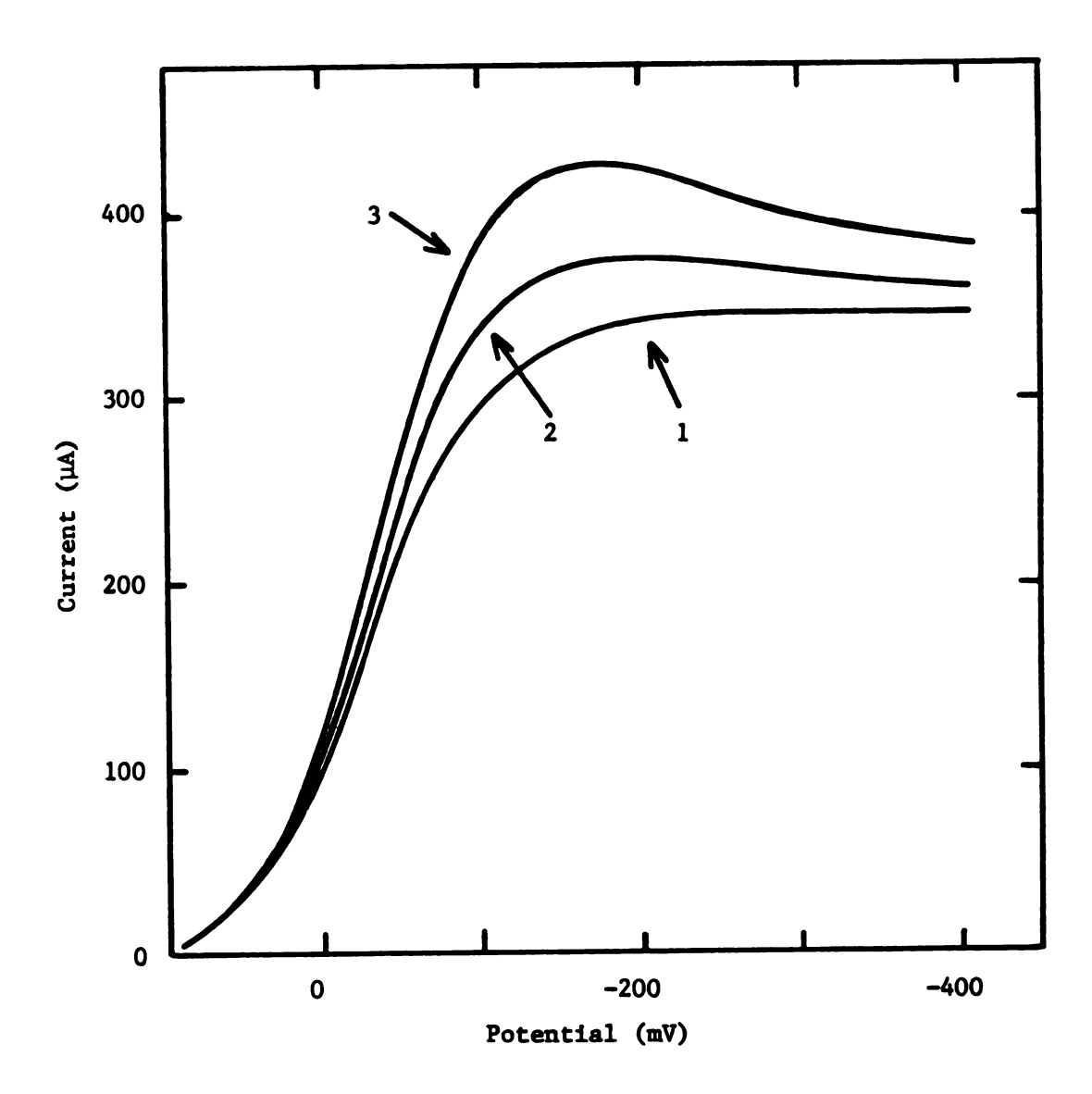


Figure 4.3. Pulse polarograms illustrating the effects of finite risetime, with $k_{std} = 0.1$ cm/s, $\alpha = 0.5$, $E_{std} = 0$ mV, $C_{ox} = 1$ mM, $D_{ox} = D_{red} = 1 \times 10^{-5}$ cm²/s, 100 μ s sampling time. Curve 1: ideal system. Curve 2: $\tau = 10$ μ s. Curve 3: $\tau = 20$ μ s.

limiting current is not approached until many hundreds of millivolts past the wave. The observed current is decreasing continuously past the peak, although this might not be apparent in the presence of an increasing baseline current. There is also a strong dependence on sampling time, with deviations becoming considerably smaller than those in Figure 4.3 when the current is sampled at 1 ms.

The kinetics analysis of these polarograms is complicated by the absence of any apparently normal limiting current region. However, it is possible to use the current at an arbitrary potential after the peak so that results of the pulse polarographic and chronoamperometric analyses may be compared. (Since the choice of the limiting current is arbitrary, though, any analysis based on it must be equally arbitrary.)

Several transients were simulated at various points along the wave for a standard rate constant of 0.1 cm/s and a time constant of 20 μ s. Ten points along each transient were recorded, equally spaced from 100 μ s to 1 ms. Two polarograms were assembled from these data, representing the extremes of the sampling range, and were analyzed using the Oldham-Parry analysis with the back reaction correction. The current-time transients were also analyzed using nonlinear regression to determine the rate constant k_f at each potential. The error in the resulting values of k_f are shown in Table 4.5 for all three sets of data.

The errors in the rate constants derived by the chronoamperometric analysis appear to be the largest, averaging around 40%, while the rate constants derived from the 100 μs polarograms are the most

Table 4.5. Comparison of Chronoamperometric and Pulse Polarographic Analysis of Transients $^{\rm a}$ with Finite Risetime. $^{\rm b}$

			Error in k _f Derived by	y
E (mV)	k _f (cm/s)	Chrono- amperometry ^C	Pulse Polarography 100 μs	Pulse Polarography 1 ms
45.7	0.0411	+47.2%	+3.0%	+13.6%
20.7	0.0668	25.9	-3.4	7.7
- 4.3	0.109	22.5	- 4.2	6.5
-29.3	0.177	30.7	- 0.9	8.5
-54.3	0.288	67.7	+ 9.6	16.1
-79.3	0.468	d	44.0	e
-104.3	0.762	d	e	e

 $[^]a100~\mu s$ sampling time, 1 ms time range. E $_{std}$ = 0 mV. k_{std} = 0.1 cm/s, c_{ox} = 1 mM, c_{red} \approx 0, D_{ox} = D_{red} = 1 x 10^{-5} cm^2/s . b_{τ} = 20 μs .

^COne parameter nonlinear regression.

 $^{^{\}mathrm{d}}$ Analysis failed to yield reasonable values of rate constant.

 $e_{i/i_{lim}}$ too large for meaningful results.

accurate. The reason for this behavior can be seen upon examination of the shapes of the pulse polarograms and the position of the apparent limiting current. Especially on the 100 µs polarograms, the amount of error in the current increases up the wave, so that the values of i/i_{lim} are fortuitously close to ideal. This compensation will occur to some extent whenever a larger-than-correct value of the limiting current is used. Since the error in the limiting current was considerably smaller with the 1 ms polarograms, the effect is not as striking, although the results are still better than the chronoamperometric analysis.

The apparent success of the normal pulse polarographic analysis under conditions in which the data are clearly suffering from some nonideal effect must be viewed with caution. It is not clear whether such an arbitrary method can be relied upon to yield reliable estimates of electrochemical rate parameters under laboratory conditions. The success hinges on selecting the "right" limiting current for the conditions involved, and there would seem to be no way to determine this value from the data alone.

4.7. Comparison of the Effect of Adsorption on Normal Pulse Polarography and Large-Step Chronoamperometry

The adsorption of reactants in large potential-step experiments leads to a relatively large number of cases to be considered, as we need to be concerned with the adsorption of two species both before and after the step. Since these large-step experiments are generally carried out with a very small concentration of product in the solution,

its initial degree of adsorption may be neglected. It has been determined that the adsorption of product has only a minimal effect at the final potential, so that in this work only the adsorption of the reactant needs to be considered.

Even with this limitation, there are three possible variations: the reactant may be adsorbed at the initial potential, the final potential, or at both potentials. As was seen for irreversible reactions in Chapter 3, these variations lead to different shapes in the resulting normal pulse polarograms. These effects are shown in Figure 4.4.

Again, the deviations in the shapes of the polarograms were essentially the same as those seen for irreversible reactions. In all three cases, the ideal limiting current was reached only one or two hundred millivolts after the peak. The largest deviation is seen when the reactant is adsorbed at both the initial and final potentials. Adsorption which occurs only at the final potential leads to currents which are too small on the rising part of the wave, while the opposite is true for adsorption only at the initial potential. These two curves become identical at the top of the wave in the peaked region and beyond.

One interesting aspect of these systems is the behavior of the polarograms as the reversible limit is approached. Flanagan and Anson (6) have examined normal pulse polarograms under Henry's Law adsorption conditions, but with a reversible electrode reaction and a model which considers the depletion of the reactant molecules from the vicinity of the growing electrode due to the adsorption process. They observed waves which were too small, but otherwise normal, when

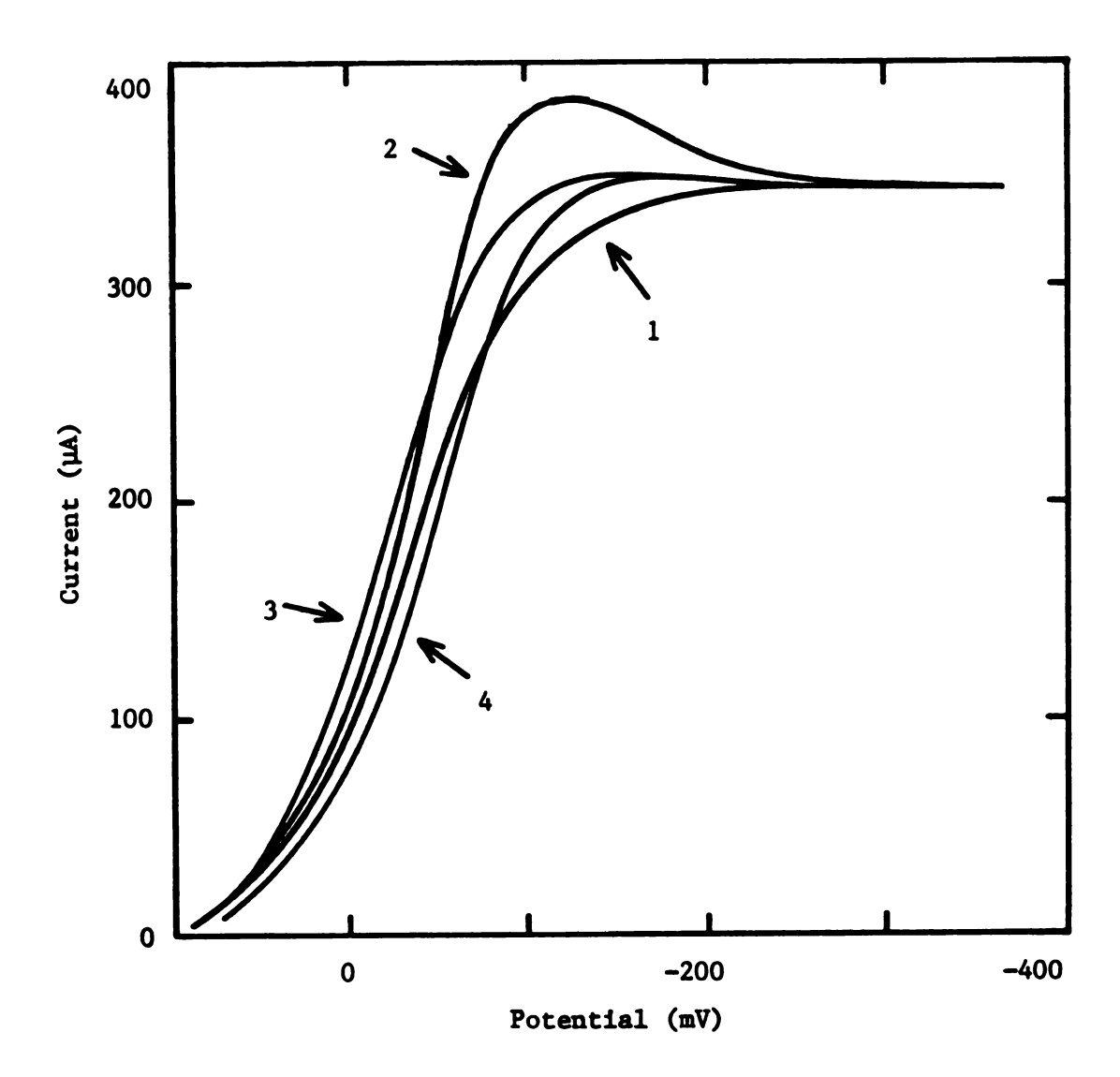


Figure 4.4. Pulse polarograms illustrating the effects of reactant adsorption, with $k_{\rm std} = 0.1$ cm/s, $\alpha = 0.5$, $E_{\rm std} = 0$ mV, $C_{\rm ox} = 1$ mM, $D_{\rm ox} = D_{\rm red} = 1 \times 10^{-5}$ cm²/s, 100 µs sampling time. Curve 1: ideal system. Curve 2: $K_{\rm ox}^i = K_{\rm ox} = 2 \times 10^{-5}$ cm. Curve 3: $K_{\rm ox}^i = 2 \times 10^{-5}$ cm, $K_{\rm ox} = 0$. Curve 4: $K_{\rm ox}^i = 0$, $K_{\rm ox} = 2 \times 10^{-5}$ cm.

reactant and product were equally adsorbed throughout the experiment, which they attributed to reactant depletion. They also observed maxima and a shift in the potential range of the wave with differing degrees of adsorption for the reactant and the product.

Because the adsorption coefficients and concentrations they chose lead to surface coverages equivalent to about 5 - 50 monolayers, it is doubtful that the Henry isotherm would apply. However, if their adsorption parameters are used in the simulation programs employed in this work, maxima at least 10 times larger than they report appear in the wave, which could be due to the depletion phenomenon. Other characteristics seem identical, except for the absence of the depletion effects.

As an example of this effect, Figure 4.5 displays two polarograms with equal degrees of adsorption. One has a standard rate constant of 0.1 cm/s, while the other system has $k_{\rm std}$ = 3 cm/s. For comparison, Figure 3.4a illustrates the effect of the same amount of adsorption on a totally irreversible wave. At 3 cm/s, there is no evidence of any deviation due to the nonideality. This is probably because the reaction proceeds so fast that all the adsorbed species reacts at the very beginning of the experiment, so that all the current observed, even at 100 μ s, is due only to diffusing species, as the theory predicts.

Since the limiting current is readily accessible from the nonideal polarograms, it is possible to derive rate constants from the data without the ambiguities involved in the polarograms distorted by finite potentiostat risetime effects. Again, a series of transients

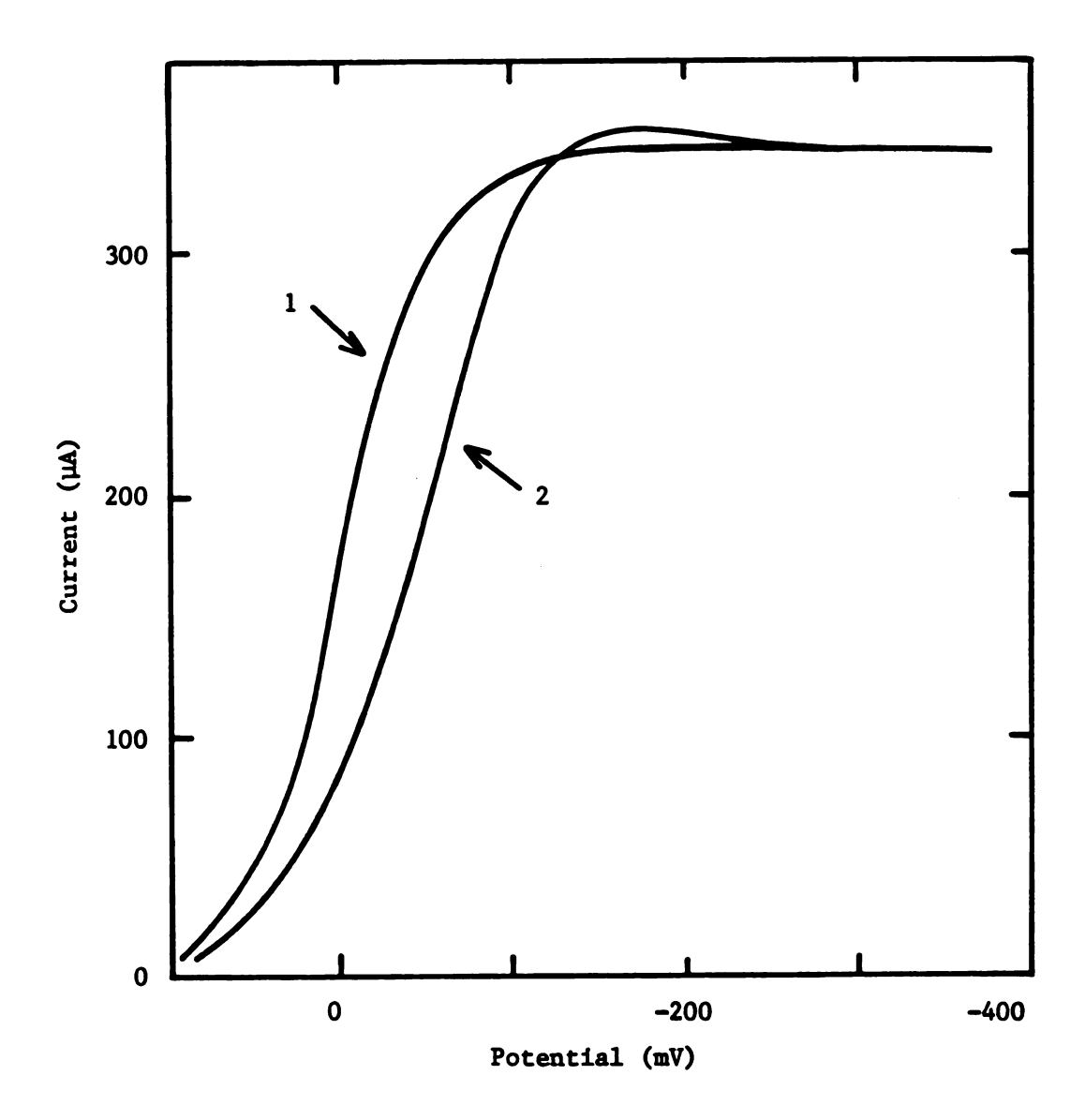


Figure 4.5. Pulse polarograms illustrating the effects of reactant adsorption at the onset of reversibility, with α = 0.5, $E_{\rm std}$ = 0 mV, $C_{\rm ox}$ = 1 mM, $D_{\rm ox}$ = $D_{\rm red}$ = 1×10^{-5} cm²/s, $K_{\rm ox}^{1}$ = $K_{\rm ox}$ = 2×10^{-5} cm, 100 μs sampling time. Curve 1: $k_{\rm std}$ = 3 cm/s. Curve 2: $k_{\rm std}$ = 0.1 cm/s.

was generated for all three adsorption schemes out of which polarograms were constructed. The results of the analyses of both the original transients and of the polarograms are given in Table 4.6.

Here, the difference between the analysis methods is not as distinct as was seen previously. The chronoamperometric analysis yields somewhat more accurate rate constants in almost every case. The overall error in the rate constants is quite large, regardless of analysis method used.

4.8. Implications for the Use of Normal Pulse Polarography

Because of the extensive use of normal pulse polarography in electrode kinetics studies as well as analytical work (53), some comments about the implications of the results of this work will be made.

The normal pulse polarographic mode of large potential-step experiments is quite useful for diagnosing nonideal conditions. The presence of a peak resembling d.c. polarographic maxima is a clear indication of something nonideal in the experiment; the theory describing the ideal experiment predicts no such shape. Furthermore, the exact shape of the maximum yields information on whether chemical or instrumental nonidealities are at fault. Peaks due to adsorption fall off rapidly to yield a constant, diffusion-limited value, while those due to finite potentiostat risetime show an extended region past the peak in which the current constantly decays. This diagnostic information is all that can be extracted from obviously nonideal polarograms; it is clear that data on the rising part, and even at

Comparison of Chronoamperometric and Pulse Polarographic Analyses of Transfents^a with Weak Reactant Adsorption. Table 4.6.

				Error	Error in $k_{ ilde{f}}$ when Reactant + Product Adsorbed:	n Reactant	: + Produc	t Adsorbe	d:		
			Before Only ^b	,b	A	After Only ^C		Ø	Before + After ^d	ter ^d	
E (mV)	$k_{ m f}~({ m cm/s})$	СА ^е	100 µs PP	l ms PP	CAe	100 µs PP	l ms PP	CA ^e	100 µs PP	1 ms PP	•
45.7	0.0411	+70.1%	+78.5%	79.77+	-3.9%	-13.6%	+29.1%	+121%	+111%	+376%	
20.7	0.0668	55.6	8.49	34.8	-8.3	-18.9	17.1	64.9	60.2	98.6	
- 4.3	0.109	52.5	62.2	32.4	-9.2	-20.0	14.7	56.7	87.5	81.1	
-29.3	0.177	. 59.0	68.0	37.6	-7.3	-11.9	20.1	75.2	99.1	124	
-54.3	0.288	80.0	88.2	56.3	-1.1	- 7.6	37.8	193	113	266	
-79.3	0.468	147	164	80	+16.3	-1.5	80	Ŧ.	80	80	
-104.3	0.762	¥	60	60	82.9	60	∞ 0	Ŧ	00	80	
a ₁₀₀ μs	al00 μs sampling time, 1 ms time	e, 1 ms	time range.	x a t	= 0.1 cm/s, E _{ord} = 0 mV, C _{ox}	Estd = 0		= 1 mM, C _{red} ≈ 0,	0 ° 0 □	D ₀ x =	

eOne param- $^{\mathrm{f}}$ Analysis failed to yield a reasonable value of the rate constant. red Dred = 1×10^{-5} cm²/s. 1 bK¹ = 1 K¹ = $^{2} \times 10^{-5}$ cm, 1 Kox = 1 Kred = 1 x 1 cm. 1 1 x 1 10⁻¹¹ cm, 1 cm. 1 Kred = 1 x 1 cm. 1 Kred = 1 x 1 cm. 1 cm. $^{\rm g}_{\rm 1/1_{11m}}$ too large for meaningful results. eter nonlinear regression.

the foot of the wave, are affected by the nonideal conditions.

The implications of this work for electrode kinetics experiments have for the most part already been outlined in this chapter and in the preceding one. The main interest in these experiments is in the rising part of the wave (although errors in the limiting current will influence the results also).

In a crude and not particularly general way, pulse polarography might be useful for distinguishing fast kinetically controlled reactions from those which are reversible (or nearly so), since the maximum is reduced in size as reversibility is approached. The absence of a peak (assuming that all is well with the instrumentation) can be interpreted either as indicating a reversible reaction or simply that there is no reactant adsorption. This limited diagnostic ability might occasionally prove useful, however, in those cases when a reactant is known to be adsorbed at the electrode surface.

The need for a reliable, fast-rise potentiostat in the study of rapid heterogeneous electron transfer-kinetics is especially obvious when one attempts to sample the current at short times. A general rule for the study of fast reactions might be that the risetime of the potentiostat be at least 100 times faster than the time at which the current is sampled.

Diffuse-layer adsorption should not pose a problem if the experiments are carried out in 1 M supporting electrolyte at such a potential that the total charge on the electrode is small, or if the sampling time is at least long enough that maxima are not visible along the wave. There could, however, be serious problems in systems with

lower supporting electrolyte concentrations, or in solutions in most nonaqueous solvents due to unfavorable double-layer conditions (enhanced diffuse-layer adsorption), or increased solution resistance.

Even though the Henry isotherm is probably not valid for significant degrees of diffuse-layer adsorption, the results of this work suggest that any weak reactant adsorption has a strong effect on the shapes of the pulse polarograms sampled at short times. As long as one doesn't attempt to extract rate data from obviously nonideal polarograms, the errors will probably be small. This does, however, form a limitation on the maximum accessible rate constant under a given set of conditions.

The use of normal pulse polarography in chemical analysis has both different procedures and different goals than in electrode kinetics. Here reactant concentrations are often quite small ($<10^{-4}$ M), and the only part of the wave which is of interest is the diffusion-limited plateau. The optimization of sensitivity is usually achieved by decreasing the sampling time to increase the measured current (53).

Because of this need to enhance the sensitivity of the experiment, the risetime of the potentiostat plays a critical role. It must be fast enough to allow the limiting current to be measured accurately as soon as possible after the potential step. Thus, the potentiostat, and the system itself, place a lower limit on the sensitivity of the analysis.

The Henry isotherm for diffuse-layer adsorption is valid at the trace reactant concentration level, even to adsorption coefficients

greater than 2×10^{-5} cm. Analytical systems often have low supporting electrolyte concentrations, are sometimes in nonaqueous solvents, and involve somewhat uncharacterized systems. Diffuse-layer or specific adsorption might be quite strong under these conditions.

A basic problem in these analytical experiments is that the full polarographic wave is rarely recorded in applications such as flow injection analysis (54) or chromatographic detection (55). A potential is chosen which is assumed to be well into the diffusion-limited region, and all the measurements are done at that single potential. If this value is far enough into the plateau, adsorption of the analyte should not influence the experimental results, although instrumental problems may still occur. It is thus quite important to verify that one is indeed in a well-defined (if not ideal) region of the wave for every variation which is made in the chemical system.

A final, positive point can be made regarding the use of normal pulse polarography in analytical applications. Since the nonidealities studied here show very little dependence on the concentration of the reactant, working curves made from carefully made standards should be valid. As long as all conditions leading to the assorted non-idealities remain constant, accurate analyses might still be made, even in the presence of nonideal conditions.

The next two chapters contain a study of two other methods used in the investigation of electrode kinetics. These small-step perturbation techniques will be studied in much the same way as was done for the small potential-step experiments. The results of the three studies will be compared in an effort to determine the most reliable

method for the study of fast electrode reactions in the face of inevitable experimental nonidealities. CHAPTER 5

COULOSTATICS EXPERIMENTS

5.1. Description of Method

The small-step coulostatic experiment, as it is usually practiced, requires both the oxidized and reduced form of a redox couple in solution together with an electrode at such a potential that the system is at equilibrium. An injection of charge takes place (usually in the form of a short current pulse (23) or the discharge of a capacitor) which causes the potential to increase by several millivolts. The system is no longer in equilibrium, as the Nernst equation demands a change in the ratio of oxidized to reduced species concentrations at the surface. The electron-transfer reaction begins in order to adjust this ratio, using electrons which are part of the injected charge. This causes a concentration gradient to be established in the solution near the electrode. Thus, charge leaks off into the solution and the overpotential decays back to the original equilibrium The rate of this decay is controlled by both the rate of the electron-transfer reaction, and by the rate at which molecules can diffuse through the solution.

A general equation which describes the coulostatic overpotentialtime transient has been derived by Reller and Kirowa-Eisner (56), although much earlier Delahay (12) and Reinmuth (13) both derived a more limited case of this equation. For a process

$$0x + ne^{-} \stackrel{k_f}{\underset{k_h}{+}} Red \qquad (5.1)$$

under both activation and diffusion control, the overpotential-time transient is described by the following equation:

$$\eta = \frac{\eta^{0}}{\gamma - \beta} \left[\gamma \exp(\beta^{2} t) \operatorname{erfc}(\beta t^{\frac{1}{2}}) - \beta \exp(\gamma^{2} t) \operatorname{erfc}(\gamma t^{\frac{1}{2}}) \right]$$
 (5.2)

where

$$\beta = \frac{\tau_{d}^{\frac{1}{2}}}{2\tau_{c}} + \frac{1}{\tau_{c}^{\frac{1}{2}}} \left(\frac{\tau_{d}}{4\tau_{c}} - 1\right)^{\frac{1}{2}}$$
 (5.3)

$$\gamma = \frac{\tau_{c}^{\frac{1}{2}}}{2\tau_{c}} - \frac{1}{\tau_{c}^{\frac{1}{2}}} \left(\frac{\tau_{d}}{4\tau_{c}} - 1\right)^{\frac{1}{2}}$$
 (5.4)

$$\eta^{o} = Q_{ini}/(C_{dl} \cdot A)$$
 (5.5)

The charge transfer time constant $\tau_{_{\hbox{\scriptsize C}}}$ and the diffusion time constant $\tau_{_{\hbox{\scriptsize d}}}$ are defined as follows:

$$\tau_{c} = RTC_{d\ell} / (n^{2}F^{2}k_{std}C_{ox}^{1-\alpha}C_{red}^{\alpha})$$
 (5.6)

$$\tau_{d} = \left[\frac{RTC_{d\ell}}{n^{2}F^{2}} \left(\frac{1}{C_{ox}^{\frac{1}{2}}} + \frac{1}{C_{red}^{\frac{1}{2}}}\right)\right]^{2}$$
 (5.7)

It is traditional to identify two limiting cases of Equation 5.2. If $\tau_d << \tau_c$, the overpotential decay is totally charge-transfer controlled, and Equation 5.2 reduces to

$$\eta = \eta^{\circ} \exp(-t/\tau_{c})$$
 (5.8)

At the other extreme, when $\tau_d >> \tau_c$, the rate of reactant diffusion controls the overpotential decay, and Equation 5.2 reduces to

$$\eta = \eta^{0} \exp(t/\tau_{d}) \operatorname{erfc}(t^{\frac{1}{2}}/\tau_{d}^{\frac{1}{2}})$$
 (5.9)

Unfortunately, neither of these limiting cases is particularly useful to the electrode kineticist. The latter situation provides no information about the kinetics of the redox couple under study, while the former is useful only for relatively slow reactions $(k_{std} < 0.1)$ or at concentrations which are too high (>10 mM) to avoid reactant ion migration or disturbances of the double layer.

The above equations assume an instantaneous injection of the required charge at the start of the experiment. This work will assume that the charge is applied in the form of a current pulse of large amplitude and very short duration. This model was chosen over the capacitance discharge method because of its more well-defined nature. Experimentally feasible pulse widths range from about 30 ns to 500 ns, the longer times being required for solutions of high resistance.

As only a relatively small number of electrons are being used in this experiment, the presence of additional molecules of reactant at the electrode surface might be expected to have a significant effect on the coulostatic decay transient, considerably more so than a potential-step experiment, for example, in which a virtually unlimited number of electrons are available. Thus, even very weak reactant

adsorption could cause major deviations from ideality in the shape of the transient.

5.2. Analysis of Data from Coulostatics Experiments

A number of methods have been used to extract kinetics and/or capacitance information from coulostatic overpotential decay curves. Originally, experiments were designed in such a way that simple charge-transfer control applied (12,13). Under these conditions, a plot of $\ln \eta \ \underline{vs}$ time has an intercept which is inversely proportional to the double-layer capacitance, and a slope which is directly proportional to the standard rate constant. Deviations from linearity due to an increasing contribution from diffusion increase with time, leading to curvature in the simple plot. In this case, the initial slope of the curve would be used.

Recently, nonlinear regression on the full decay equation (Equation 5.2) has been used to provide estimates of the double-layer capacitance of the electrode and of the standard rate constant of the redox couple under study (57). This procedure has the advantage of extracting rate data from the experimental transient while the decay curve contains a significant contribution from diffusion.

A comparison of coulostatic data analyses has been published by Kudirka, Daum, and Enke (4) which indicates that nonlinear regression is a superior technique for extracting charge transfer information for experiments in which the ratio $\tau_{\rm c}/\tau_{\rm d}$ was less than about 10. Reller and Kirowa-Eisner (2) have analyzed the errors inherent in both of the above-mentioned procedures, and have determined the

optimal parameters for the determination of the capacitance and/or the standard rate constant. The study suggests that the best accuracy for the determination of the kinetics parameter can be obtained by analyzing data over a time range of twice the charge transfer time constant from the start of the experiment, for experiments with $\tau_{\rm c}/\tau_{\rm d}$ greater than about 0.5.

Additionally, an analysis procedure based upon a transformation of the experimental data to the impedance plane and the use of the Laplace transform of Equation 5.2 has been suggested (58).

In the present work, all analyses were performed via nonlinear regression on Equation 5.2 which, although somewhat time consuming, should give valid results for most values of the ratio $\tau_{\rm c}/\tau_{\rm d}$. However, if a transient is totally diffusion controlled, no kinetics information is available and the analysis (indeed, any analysis) will fail to yield a reasonable value for the standard rate constant.

The optimal time range for the derivation of heterogeneous rate constants using nonlinear regression suggested by Reller and Kirowa-Eisner (2) was used in this work. This interval is equal to twice the charge transfer time constant, which turns out to be an experimentally reasonable window for standard rate constants less than about 5 cm/s. Twenty evenly spaced data points were used for the analysis of the nonideal coulostatics experiments.

5.3. Unique Aspects of Simulation

The simulation of an ideal coulostatic experiment differs from that of the previously discussed potentiostatic experiment. The

overpotential varies with time, being a function of the flux of electrons at the electrode surface. In other respects, however, the potential has the same effect on the flux itself (through the rate constants) as it has in the previous techniques.

The initial overpotential depends on the capacitance of the electrode and the amount of injected charge, as indicated in Equation 5.5. This is calculated as an initial condition in the ideal simulation.

As electrons are transferred across the surface, the rate of decay of overpotential must be given by

$$d\eta/dt = -F\Phi_{far}/C_{dl}$$
 (5.10)

Once the flux has been calculated in the usual manner, the equation can be applied in discrete form to calculate the change in the overpotential during that time increment Δt . The next calculation of the boundary conditions proceeds from this new overpotential.

In the simulation of current impulse charge injection, the initial boundary conditions were calculated during a pre-time zero simulation period. Before this time, the concentration profiles are flat. Charge starts to be injected at a constant rate (i.e., the current is switched on), the overpotential increases, and faradaic processes occur which distort the concentration gradient. At the end of the current pulse, the overpotential is less than that predicted by Equation 5.5, and concentration gradients have been established in the bulk of the solution. This time is defined as time zero. During the charging period,

the

The Par

5.4

cha of

sur

cur

so

sli

rea

to ,

effe time

time

rate

a nur

teris

ject1

the overpotential increases as follows:

$$d\eta/dt = P_{amp}/(C_{dl} \cdot A) - F_{far}/C_{dl}$$
 (5.11)

The duration of the charging period and the current pulse amplitude P_{amp} determine the total amount of injected charge, Q_{inj} .

5.4. Effect of Finite Charge Injection Time

Current impulse charge injection can be thought of as a linear charging of the electrode double layer, during which, ideally, none of this charge has time to "leak off" due to faradaic processes at the surface and the diffusion profile is undisturbed at the end of the current pulse. In an actual experiment charge does leak off, so the charging is not quite linear and the experiment starts at a slightly smaller overpotential and with a concentration gradient already set up in the solution. Intuitively, this would seem to lead to an apparent value of the capacitance which is too high, but the effect on the standard rate constant obtained from the overpotential-time decay curve is not obvious.

The shape of the deviation produced by a finite charge injection time is shown in Figure 5.1. This shape is typical for a range of rate constants and conditions.

The time it takes to apply a given amount of charge depends on a number of factors — among them are the pulse generator characteristics and cell solution resistance. Experimentally feasible injection times for such small amounts of charge as are required (on

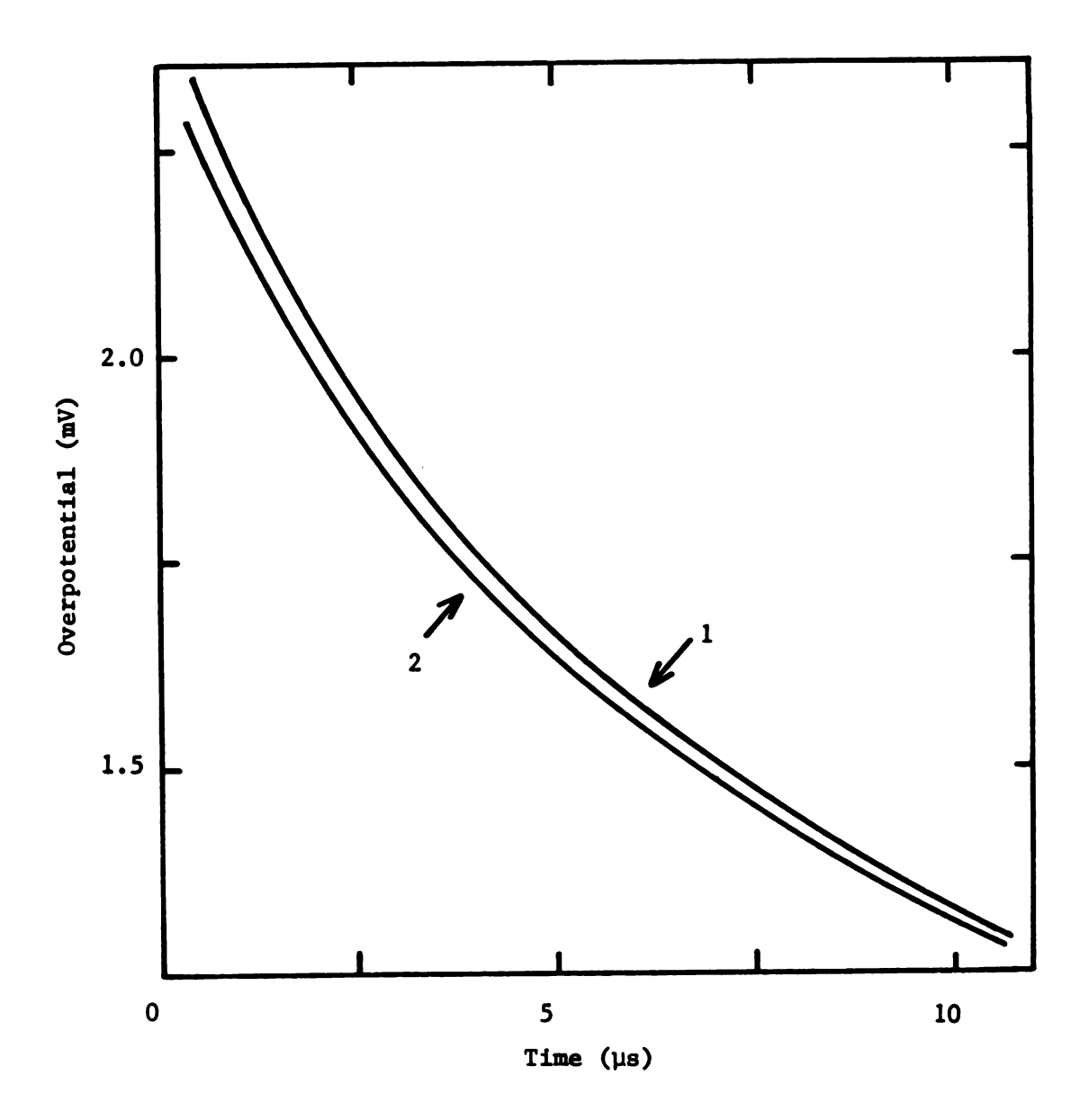


Figure 5.1. Coulostatic transients illustrating the effects of finite charge injection time, with $k_{\rm std} = 1$ cm/s, $C_{\rm d1} = 20~\mu F/{\rm cm}^2$, $Q_{\rm inj} = 1$ nC, area = 0.02 cm², $C_{\rm ox} = C_{\rm red} = 1$ mM, $D_{\rm ox} = D_{\rm red} = 1$ x10⁻⁵ cm²/s. Curve 1: ideal charge injection. Curve 2: $t_{\rm inj} = 500$ ns.

the order of $10^{-3}~\mu\text{Coul}$) for these experiments range from about 10 ns to 200 ns. All transients in this section were generated with injection times in this range, and with standard rate constants between 0.1 and 10 cm/sec.

Table 5.1 displays the error in the standard rate constants obtained for a series of analyses of nonideal transients with various concentrations of oxidized and reduced species, as well as the values of τ_c and τ_c/τ_d for each case.

These data are difficult to interpret due to a number of complications. First, as the rate constant gets smaller, the time range of the experiment expands to maintain a $2\tau_c$ interval. Thus, for a given injection time, one is extracting rate data further and further from the nonideality. The observed effects might be expected to be smaller under these circumstances for this reason alone. Secondly, as the rate constants increase at a given set of concentrations, the ratio τ_c/τ_d decreases. The smaller τ_c/τ_d is, the more effect a small variation in the transient has on the derived value of the rate constant. Finally, one can observe that negative deviations are found in some of the cases studied, and positive deviations in others, 1.e., the derived rate constants are too high. Further, this seems to be a function of the ratio τ_c/τ_d . Negative deviations in the value of the rate constant are observed when this ratio is less than unity, while positive deviations occur at values of τ_c/τ_d greater than one.

This last somewhat curious result prompted some additional experiments under conditions that τ_c/τ_d = 1. The results, also in Table 5.1, show that the correct standard rate constant is derived regardless

Table 5.1. Error in Rate Constants Derived^a from Coulostatic Transfents^b Due to Finite Injection Time.

	ţ	ه				Inje	Injection Time (ns)	(ns)	
xo (風)	red (mM)	std (cm/s)	τ _c (μs)	$\tau_{\rm c}/\tau_{\rm D}$	10	20	50	100	200
-	1	10	0.53	0.047	-8.5%	-15.0%	-28.4%	76.04-	
		3	1.77	0.157	1	- 1.7	- 3.9	- 7.3	-12.0%
		1	5.32	0.47	!	!!!	- 0.3	9.0 -	- 1.2
		0.47		1.0	1	0	0	0	0
		0.3	17.7	1.57	!		+ 0.03	+ 0.07	+ 0.2
		0.1	53.2	4.7	1	!	0.03	90.0	0.1
10	-	က	0.56	0.164	-2.6	6.4 -	-10.7	-18.0	-27.9
		-	1.68	0.491	!	7.0 -	- 1.0	- 1.8	- 3.3
		0.3	5.61	1.64	† † †	!	+ 0.1	+ 0.2	+ 0.5
		0.1	16.8	4.91		!		0.2	0.4
10	10	10	0.053	0.47	6.4-	- 8.2	-14.3		
		က	0.177	1.57	+0.8	+ 2.0	+ 5.8	8.9	18.2
		1	0.532	4.7	ļ	1.2	3.2	6.7	12.4
		0.3	1.77	15.7	i	1	1.2	2.4	9.4
		0.1	5.32	47.	ł	!	7.0	0.8	1.7

a Two parameter (k $_{\rm std}$, $c_{\rm dg}$) nonlinear regression analysis. $10^{-3}~\mu \, \rm coul$, $c_{\rm dg}$ = 20 $\mu \rm F/cm^2$, Area = 0.02 cm².

 $^{D_{D_x}} = ^{D_{red}} = ^{1 \times 10^{-3}} \text{ cm}^2/\text{s}; \quad ^{Q_{inj}} =$

٤

w)

ac

T_C

hig

dou

lec

abl.

ment

but,

of the injection time. The reasons for this result are unknown, but it seems that there must be some sort of compensation effect in the deviation in different parts of the transient. It is probably true that the $2\tau_{\rm C}$ time range over which the data is analyzed is significant. Other results indicate that correct rate constants are derived regardless of the concentration of each species, or the ratio of the concentrations.

A summary of the results obtained for experiments with various injection times is given in Figure 5.2, which shows the relative error in the derived value of k_{std} as a function of the ratio τ_c/τ_d for given values of the ratio t_{inj}/τ_c . As one might expect, larger errors in the rate parameter are observed the larger the value of t_{inj}/τ_c (i.e., the closer the injection time is to the range of data which is analyzed).

The minimization of deviations due to long injection time can be accomplished by attempting to adjust conditions so that the value of $\tau_{\rm c}/\tau_{\rm d}$ is close to unity. For large rate constants, however, this would necessitate increasing the reactant concentration (but not so high that the ions start making a substantial contribution to the double layer). Unfortunately, as the concentration is increased, the charge transfer time constant decreases, and data must be collected over a much smaller time range. Again, experimentally attainable accuracy is determined by a compromise between ideal measurement conditions and physical practicality.

The value of the rate constant is needed to calculate τ_c/τ_d but, of course, it is this parameter which the method is employed

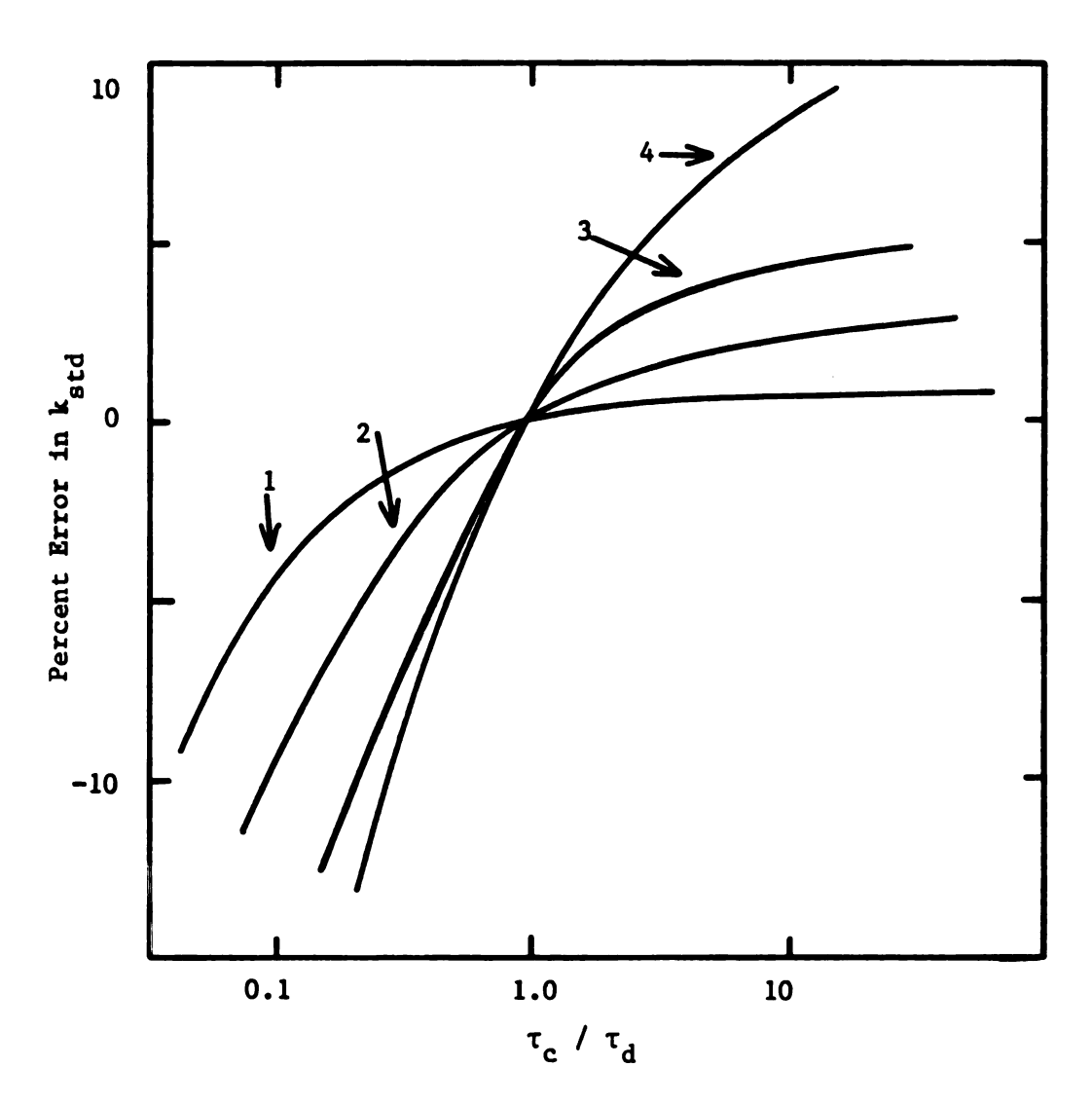


Figure 5.2. Relative error in standard rate constant <u>vs.</u> ratio τ_c / τ_d . Curve 1: $t_{inj}/\tau_c = 0.0188$. Curve 2: $t_{inj}/\tau_c = 0.0565$. Curve 3: $t_{inj}/\tau_c = 0.133$. Curve 4: $t_{inj}/\tau_c = 0.188$.

0 1 tı to measure. Any attempt to optimize an experiment in this manner probably will have to proceed through an iterative process, successively refining the estimate of the standard rate constant until consistent results are attained. It is not clear that this approach would not yield instances of false agreement, though.

From the shape of the deviation from the ideal transient produced by finite injection time, one might expect values of the double-layer capacitance derived from nonideal transients to be too high. Table 5.2 shows the error in values of the double-layer capacitance obtained from the analyses which concurrently yielded the rate constant data in Table 5.1. The capacitance values are indeed too high. The data are summarized in Figure 5.3, which shows the relative error in the value of the capacitance as a function of the ratio $\tau_{\rm c}/\tau_{\rm d}$ at constant $t_{\rm inj}/\tau_{\rm c}$. Obviously, the effect of finite charge injection time upon the apparent value of the capacitance is in general much smaller than was seen for the standard rate constant. For no value of $\tau_{\rm c}/\tau_{\rm d}$ is this error completely eliminated, however.

5.5. Effect of Weak Reactant Adsorption

An excess of reactant at the surface of the electrode during a coulostatic experiment would be expected to produce a transient showing a steeper decay than would be seen if there were no adsorption. The enhanced surface concentration would lead to a greater reaction rate, and hence a faster discharge of the double layer. The extent of the deviation might be expected to be related to the rate of charge transfer compared to that of the diffusion process. For reactions

Error in Double-Layer Capacitances Derived $^{\rm a}$ from Coulostatic Transfents $^{\rm b}$ Due to Finite Injection Time. Table 5.2.

	c	-				Inj	Injection Time (ns)	(ns)	
Xo (MEI)	red (mM)	kstd (cm/s)	τ _c (μs)	$^{\mathrm{T}_{\mathrm{c}}/^{\mathrm{T}_{\mathrm{D}}}}$	10	20	50	100	200
1	1	10	0.53	0.047	+0.5%	+0.9%	+2.1%	+3.7%	
		3	1.77	0.157	1	7.0	0.8	1.5	+2.9%
		-	5.32	0.47	i	ł	0.3	9.0	1.2
		0.47		1		0.1	0.2	0.3	9.0
		က	17.7	1.57	!	!	0.1	0.2	0.4
		1	53.2	4.7		1	0.05	0.1	0.2
10	Т	က	0.56	0.164	9.0	1.1	2.5	4.7	8.6
		H	1.68	0.491		7.0	1.0	2.0	3.9
		0.3	5.61	1.64	!		0.3	0.7	1.4
		0.1	16.8	4.91				0.3	0.5
10	10	10	0.053	0.47	5.6	10.6	23.5		
		က	0.177	1.57	2.1	4.0	9.4	19.4	36.9
		-	0.53	4.7		1.6	2.8	7.4	15.1
		0.3	1.77	15.7	1 1	t !	1.3	2.5	5.0
		0.1	5.32	47	!	1	0.5	0.9	1.8
a Two-pe	aTwo-parameter ($_{st}$ $_{d\ell}$ = 20 $\mu F/cm^2$;	k_{std} , $C_{d\ell}$) nonline; Area = 0.02 cm.	std, $C_{d\ell}$) nonlinear regression. Area = 0.02 cm.	ression.	Pox a	= Dred 1 x 10	10 ⁻⁵ cm ² /s;	Q _{inj} = 10 ⁻³ µcoul;	3 µcoul;

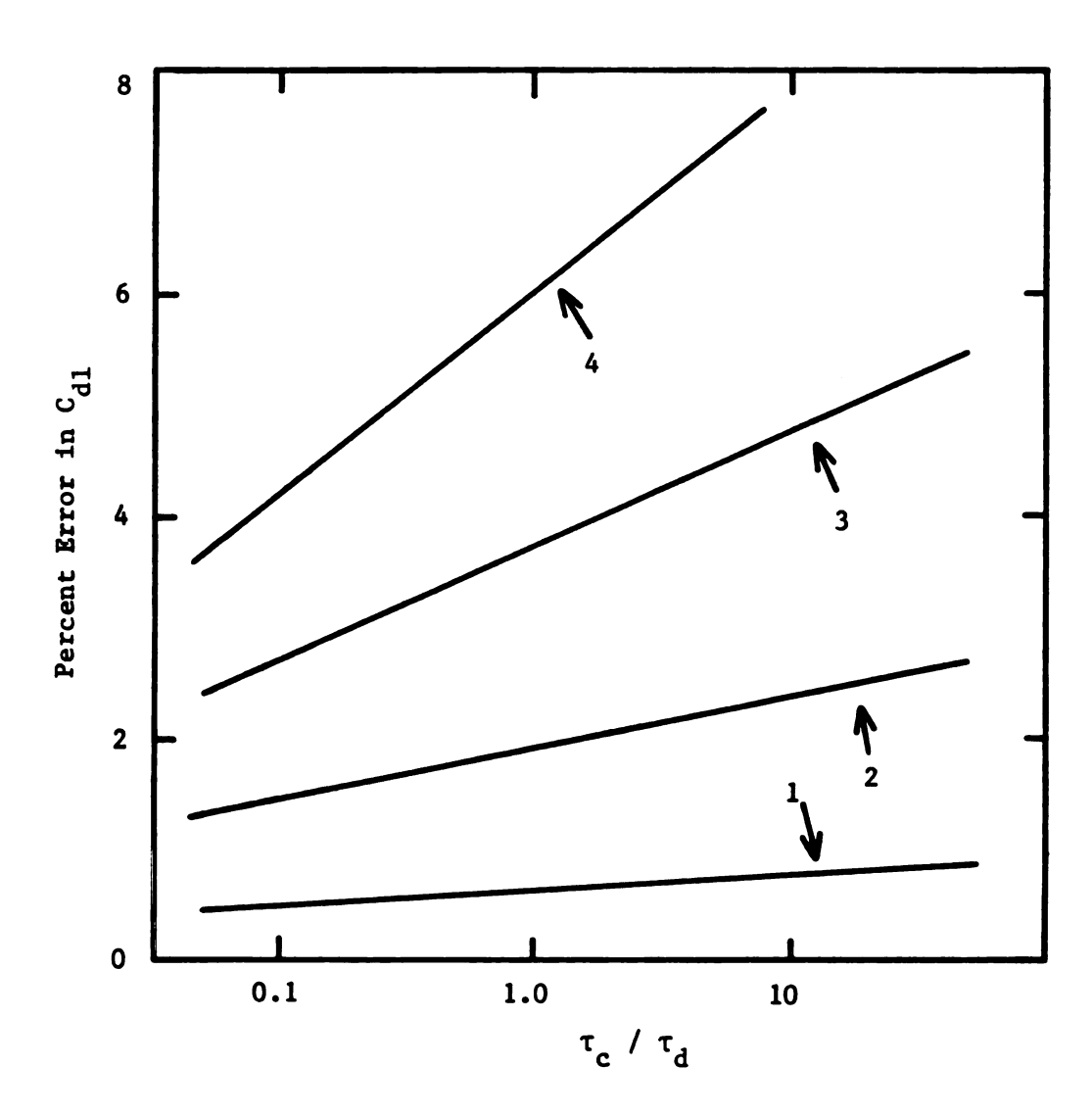


Figure 5.3. Relative error in double-layer capacitance <u>vs.</u>
ratio τ_c / τ_d . Curve 1: t_{inj}/τ_c = 0.0188. Curve 2: t_{inj}/τ_c = 0.0565. Curve 3: t_{inj}/τ_c = 0.133. Curve 4: t_{inj}/τ_c = 0.188.

with small rate constants, there should be very little deviation from the pure charge-transfer control, Equation 5.8. However, the apparent time constant would be smaller than that calculated on the basis of bulk reactant concentrations. Once the influence of diffusion is present, the decay will obey neither Equation 5.8 nor Equation 5.2, which takes both charge transfer and diffusion into account.

The deviations produced by a surface excess equivalent to about 10% coverage are considerably larger than those seen for finite charge injection time conditions. Figure 5.4 shows a family of coulostatic transients which were generated with a standard rate constant of 1 cm/sec and identical adsorption coefficients for the oxidized and reduced species. Note that significant deviations are seen for extremely small surface excesses (0.5% surface coverage) for the moderately fast (1 cm/sec) experiments.

Systems which have differing adsorption coefficients for the oxidized and reduced species show deviations in the transients which are intermediate between the no-adsorption and equal-adsorption cases. Only a slight difference is seen for $K_{ox} = 0$ cm, $K_{red} = 2 \times 10^{-5}$ cm and $K_{ox} = 2 \times 10^{-5}$ cm, $K_{red} = 0$ cm.

The use of Equation 5.2 in the analysis implies that, for given reactant concentrations, a transient can never decay faster than the diffusion limited rate. Some of the transients which were generated for fast reaction rates and high amounts of adsorption appeared to the analysis to be decaying faster than should be possible; the results obtained therefrom are meaningless (and easily identifiable as such, since the k_{std} values are generally in the hundreds; the final result

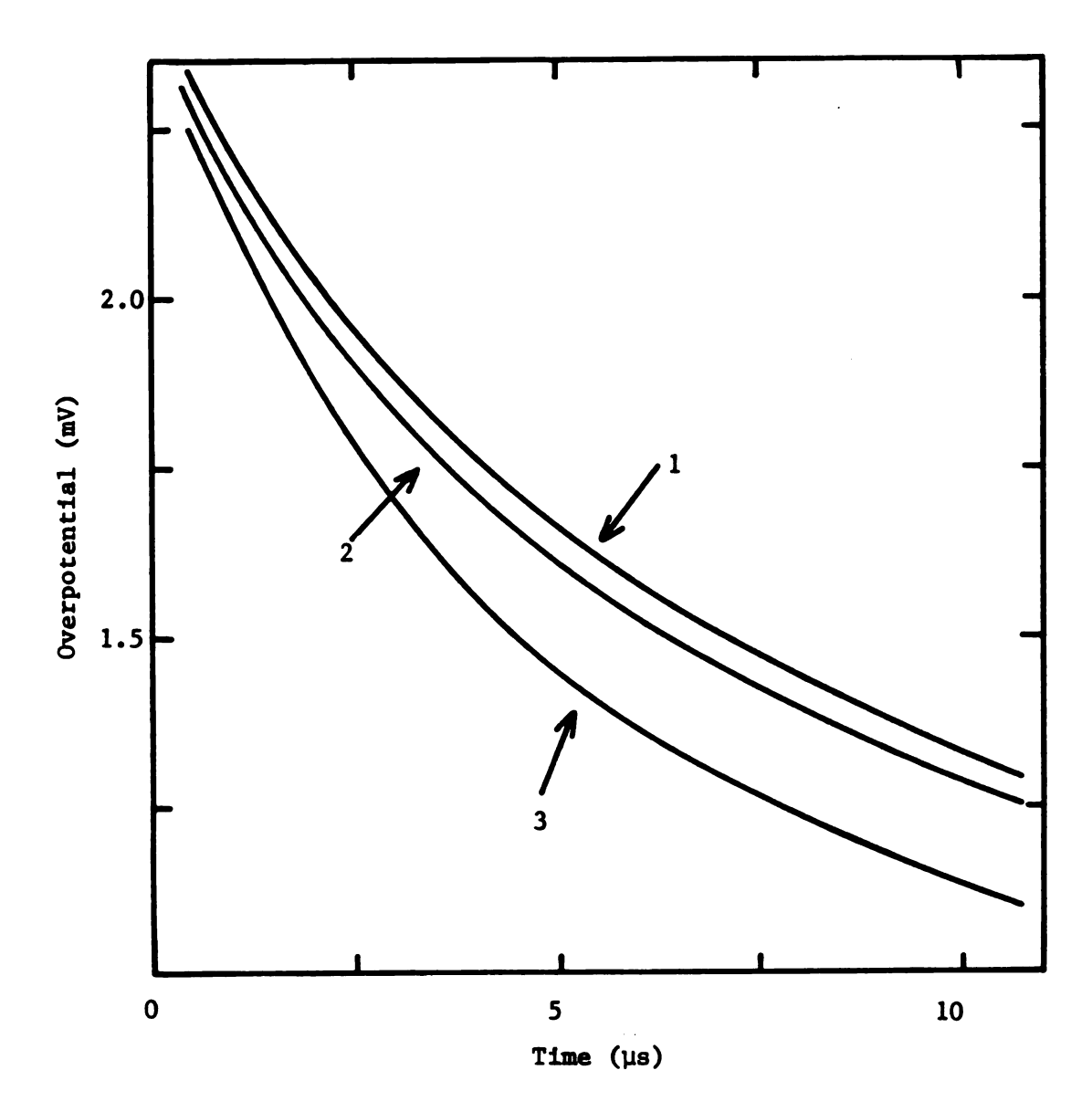


Figure 5.4. Coulostatic transients illustrating the effects of reactant adsorption, with $k_{\rm std}$ = 1 cm/s, $C_{\rm dl}$ = 20 $\mu F/cm^2$, $Q_{\rm inj}$ = 1 nC, area = 0.02 cm², $C_{\rm ox}$ = $C_{\rm red}$ = 1 mM, $D_{\rm ox}$ = $D_{\rm red}$ = 1×10^{-5} cm²/s. Curve 1: ideal system. Curve 2: $K_{\rm ox}$ = $K_{\rm red}$ = 1×10^{-6} cm. Curve 3: $K_{\rm ox}$ = $K_{\rm red}$ = 5×10^{-6} cm.

dep

pro

ana

ini

con

diz In

ref

rel

eff

err

fic

valu

the

of 1

k std resu

adso

in p

are d

depends on the termination routine in the nonlinear regression program). This problem is not unique to the nonlinear regression analysis; a $\log \eta \ \underline{vs}$ time curve will show no linear region, and its initial slope will be meaningless.

Table 5.3 displays the error in the values of standard rate constants derived from transients for various concentrations of oxidized and reduced species, and with various values of K_{ox} and K_{red} . In all cases, $K_{ox} = K_{red}$. The values of τ_c and τ_c/τ_d are given for reference.

Perhaps the most striking trend visible in these data is that the relative error in $k_{\rm std}$ is almost constant for a given adsorption coefficient and rate constant, as long as $C_{\rm ox} = C_{\rm red}$. The relative error increases somewhat as the concentration decreases. Also, there is a larger effect on the rate constant for larger adsorption coefficients, as would be expected.

The fact that the relative error in $k_{\rm std}$ is so dependent on the value of the adsorption coefficient indicates that it is the ratio of surface excess to bulk concentration that is operative, and not the absolute magnitude of the surface excess. For example, a coverage of 10% with bulk concentration of 10 mM produces the same error in $k_{\rm std}$ as does a coverage of only 0.1% when $C_{\rm ox} = C_{\rm red} = 0.1$ mM. This result is somewhat disturbing for it indicates that decreasing the adsorption by decreasing the bulk concentration will be ineffective in producing a more reliable value of the standard rate constant.

The slight increase in the relative error as the concentrations are decreased is probably due to the value of the ratio τ_c/τ_d becoming

Error in Rate Constants Derived $^{\mathbf{a}}$ from Coulostatic Transients $^{\mathbf{b}}$ Due to Weak Reactant Adsorption. Table 5.3.

Tred (mM) (cm/s) (cm/s) τ _c (μs) (μs) (cm/s) τ _c (μs) (cm/s) τ _c (μs) (μs) (cm/s) τ _c (μs) (cm/s) τ _c (μs) (cm/s) (cm/s) (cm/s) τ _c (μs) (cm/s) (cm/s) (cm/s) τ _c (μs) (cm/s) (cm/s) (cm/s) (cm/s) τ _c (μs) (cm/s) (و	ر	<u>د</u>			Adsorpti	on Coeffic	Adsorption Coefficient (cm) $_{ m OX}$	K = K red		
1 0.1 1 53.2 0.047 +11.37 +29.67 +100% +800% 0.3 177 0.157 3.0 6.3 14 50 0.1 532 0.47 2.0 4.0 11 1 1 5.32 0.47 11.2 26 70 c 0.3 17.7 1.57 3.0 6.3 13 37 1 1 53.2 4.7 2.0 4.0 11 1 1 1.68 0.49 21.3 55 250 0.3 5.61 1.64 5.3 11.3 24 10 16.8 4.9 4.0 7.0 10 1 16.8 4.9 4.0 7.0 10 1 0.532 4.7 10.2 19.6 35.4 0.3 1.77 15.7 <th>) (ME) (XE)</th> <th>red (mM)</th> <th>Rstd (cm/s)</th> <th>τ_c (μs)</th> <th>$\tau_{\rm c}/\tau_{\rm D}$</th> <th>5x10⁻⁷</th> <th>1×10-6</th> <th>2×10⁻⁶</th> <th>5×10⁻⁶</th> <th></th> <th>2×10⁻⁵</th>) (ME) (XE)	red (mM)	Rstd (cm/s)	τ _c (μs)	$\tau_{\rm c}/\tau_{\rm D}$	5x10 ⁻⁷	1×10-6	2×10 ⁻⁶	5×10 ⁻⁶		2×10 ⁻⁵
17 0.157 3.0 6.3 14 50 1 5.32 0.47 —— 2.0 4.0 11 1 1 5.32 0.47 11.2 26 70 c 0.3 17.7 1.57 3.0 6.3 13 37 0.1 53.2 4.7 —— 2.0 4.0 11 1 1 1.68 0.49 21.3 55 250 —— 0.3 5.61 1.64 5.3 11.3 24 —— 0.1 16.8 4.9 —— 4.0 7.0 —— 10 1 0.532 4.7 10.2 19.6 35.4 — 0.3 1.77 15.7 2.7 5.3 9.0 — 0.1 5.32 47 —— 1 3 —	0.1	0.1	П	53.2	0.047	+11.3%	+29.6%	+100%	+800%	ဎ	1
1 1 5.32 0.47 11.2 26 70 c 0.3 17.7 1.57 3.0 6.3 13 37 0.1 53.2 4.7 2.0 4.0 11 1 1 1.68 0.49 21.3 55 250 0.3 5.61 1.64 5.3 11.3 24 10 1 0.532 4.7 10.2 19.6 35.4 0.3 1.77 15.7 2.7 5.3 9.0 10 1 0.532 4.7 10.2 5.3 9.0 0.3 1.77 15.7 2.7 5.3 9.0 0.3 1.77 15.7 2.7 5.3 9.0 <t< td=""><td></td><td></td><td>0.3</td><td>177</td><td>0.157</td><td>3.0</td><td>6.3</td><td>14</td><td>20</td><td>+733%</td><td>i i</td></t<>			0.3	177	0.157	3.0	6.3	14	20	+733%	i i
1 1 5.32 0.47 11.2 26 70 c 0.3 17.7 1.57 3.0 6.3 13 37 0.1 53.2 4.7 2.0 4.0 11 1 1.68 0.49 21.3 55 250 0.3 5.61 1.64 5.3 11.3 24 0.1 16.8 4.9 4.0 7.0 10 1 0.532 4.7 10.2 19.6 35.4 0.3 1.77 15.7 2.7 5.3 9.0 0.1 5.32 47 1 3 1 3.			0.1	532	0.47		2.0	7.0	11	26	+70%
0.3 17.7 1.57 3.0 6.3 13 37 0.1 53.2 4.7 2.0 4.0 11 1 1 1.68 0.49 21.3 55 250 0.3 5.61 1.64 5.3 11.3 24 10 1 16.8 4.9 4.0 7.0 10 1 0.532 4.7 10.2 19.6 35.4 0.3 1.77 15.7 2.7 5.3 9.0 0.1 5.32 47 1 3	-	1	1	5.32	0.47	11.2	26	70	ပ	ပ	ပ
1 1.68 4.7 2.0 4.0 11 1 1.68 0.49 21.3 55 250 0.3 5.61 1.64 5.3 11.3 24			0.3	17.7	1.57	3.0	6.3	13	37	81	176
1 1.68 0.49 21.3 55 250 0.3 5.61 1.64 5.3 11.3 24 0.1 16.8 4.9 4.0 7.0 10 1 0.532 4.7 10.2 19.6 35.4 0.3 1.77 15.7 2.7 5.3 9.0 0.1 5.32 47 1 3			0.1	53.2	4.7	!	2.0	4.0	11	20	35
0.3 5.61 1.64 5.3 11.3 24 0.1 16.8 4.9 4.0 7.0 10 1 0.532 4.7 10.2 19.6 35.4 0.3 1.77 15.7 2.7 5.3 9.0 0.1 5.32 47 1 3	10	П	1	1.68	0.49	21.3	55	250	ł	!	ł
0.1 16.8 4.9 4.0 7.0 10 1 0.532 4.7 10.2 19.6 35.4 0.3 1.77 15.7 2.7 5.3 9.0 0.1 5.32 47 1 3			0.3	5.61	1.64	5.3	11.3	24	-	i	
10 1 0.532 4.7 10.2 19.6 35.4 0.3 1.77 15.7 2.7 5.3 9.0 0.1 5.32 47 1 3			0.1	16.8	6.4		4.0	7.0	-	1	
1.77 15.7 2.7 5.3 9.0 5.32 47 1 3	10	10	H	0.532	4.7	10.2	19.6	35.4	1		
5.32 47 1 3			0.3	1.77	15.7	2.7	5.3	0.6	!	!	!
			0.1	5.32	47		1	3			

Two-parameter nonlinear regression. b $^{\rm b}_{\rm D}$ $^{\rm a}$ $^{\rm b}$ $^{\rm b}$ $^{\rm c}$ $^{\rm b}$ $^{\rm c}$ $^{\rm b}$ $^{\rm c}$ $^{\rm b}$ $^{\rm c}$ $^{$

Chalysis failed to yield a meaningful value.

more unfavorable, so that the same deviations in a transient produce a larger and larger uncertainty in the derived value of the kinetic parameter.

The above generalizations do not include the case when $C_{ox} \neq C_{red}$. As can be seen in Table 5.3, the error in k_{std} is substantially higher when $C_{ox} = 10$ C_{red} , even though the values of τ_c/τ_d are almost the same as those for $C_{ox} = C_{red} = 1$ mM. A representative adsorption coefficient of 10^{-6} cm and standard rate constant of 1 cm/sec were used with various bulk concentrations C_{ox} and C_{red} to generate a series of transients which were analyzed to yield values of k_{std} . These results are shown in Table 5.4, and one can note several points of interest.

First, the minimum error in k_{std} is found when $C_{ox} = C_{red}$. As the ratio C_{ox}/C_{red} deviates from unity in either direction, the relative error in k_{std} increases, but not symmetrically. This could be a consequence of going further from the standard potential and decreasing the sensitivity of the experiment to the rate constant. Finally, the trend in k_{std} does not correlate well with τ_c , τ_c/τ_d , C_{ox}/C_{red} , or the total amount of adsorbed species. It was also noted that the injection of charge of the opposite sign produced only minor variations in the derived rate constant, except at very small values of τ_c/τ_d .

Table 5.5 shows the results of analyses of some transients generated using unequal adsorption coefficients, and representative values of the rate constant (0.3 cm/sec) and concentration ($C_{ox} = C_{red} = 1$ mM). The data show a rough symmetry about the $K_{ox} = K_{red}$ diagonal, and it

Table 5.4. Effect of Varying Reactant Concentration on Error in Rate Constant Derived^a From Coulostatic Data^b with Weak Reactant Adsorption.c

				Error	in k std
C (mM)	C _{red} (mM)	τ _c (με)	τ _c /τ _D	$\eta^0 = -2.5 \text{ mV}$	$\eta^0 = +2.5 \text{ mV}$
0.05	1	23.8	0.0191	+93%	+113%
0.1	1	16.8	0.0491	65	
0.2	1	11.9	0.117	40	
0.5	1	7.53	0.295	28	28
1	1	5.32	0.470	26	26
2	1	3.76	0.590	27	27
5	1	2.38	0.583	37	
10	1	1.68	0.491	55	
20	1	1.19	0.381	100	100
1	0.05	23.8	0.0191	+101%	+120%
1	0.1	16.8	0.0491	68	
1	0.2	11.9	0.117	41	
1	0.5	7.53	0.295	28	
1	1	5.32	0.470	26	26
1	2	3.76	0.590	27	
1	5	2.38	0.583	37	
1	10	1.68	0.491	55	
1	20	1.19	0.381	100	100

^aTwo-parameter nonlinear regression.

 $b_{\text{std}} = 1 \text{ cm/s}, \quad D_{\text{ox}} = D_{\text{red}} = 1 \times 10^{-5} \text{ cm}^2/\text{s}, \quad Q_{\text{inj}} = 10^{-3} \text{ } \mu \text{coul},$ $C_{\text{dl}} = 20 \text{ } \mu \text{F/cm}^2; \quad \text{Area} = 0.02 \text{ cm}^2.$

 $c_{K_{ox}} = K_{red} = 1 \times 10^{-6} \text{ cm}.$

Table 5.5. Effect of Varying Adsorption Coefficients on Error in Rate Constant Derived^a From Coulostatic Data.^b

					
			K _{red} (cm)		
K (cm)	None	1 x 10 ⁻⁶	5 x 10 ⁻⁶	1 x 10 ⁻⁵	2 x 10 ⁻⁵
none	0	+2.7%	+14%	+27%	+45%
1×10^{-6}	+3.0%	6.3	18	32	52
5×10^{-6}	11	19	37	55	83
1×10^{-5}	29	34	56	81	120
2×10^{-5}	48	56	86	123	176

^aTwo-parameter nonlinear regression.

 $^{^{}b}k_{std} = 0.3 \text{ cm/s}, \quad C_{ox} = C_{red} = 1 \text{ mM}, \quad D_{ox} = D_{red} = 1 \text{ x } 10^{-5} \text{ cm}^{2}/\text{s},$ $Q_{inj} = 10^{-3} \text{ } \mu \text{coul}, \quad C_{d\ell} = 20 \text{ } \mu \text{F/cm}^{2}, \quad \text{Area} = 0.02 \text{ cm}^{2}.$

was found that values on each side of the diagonal are swapped when charge of the opposite sign is injected. It can also be seen that the deviations produced in \mathbf{k}_{std} do not depend entirely on the sum of the surface excesses.

The interpretation of the above results is not obvious, and no wide-ranging generalizations will be attempted regarding the error in the derived value of $k_{\mbox{std}}$ under differing degrees of adsorption. No attempt will be made to map out every possible combination of concentrations, adsorption coefficients, and rate constants; however, some less general conclusions can be made.

The most obvious result is that the error in k_{std} gets larger as the amount of adsorption increases and as the rate constant itself increases. It was also seen that for a given set of adsorption conditions, the least error is found when C_{ox} = C_{red}. These results indicate that a substantial amount of error in k_{std} is present for even a moderately fast reaction when very weak adsorption is present. Since diffuse-layer adsorption can be of this magnitude, one can expect the technique to yield erroneous results even for non-specifically adsorbed reactants whenever the equilibrium potential is at a point such that there is a significant amount of charge on the electrode. Thus, the concentrations of the oxidized and reduced species probably should be adjusted to bring the equilibrium potential as close as possible to the p.z.c., minimizing the adsorption, although at the expense of sensitivity of the transient to the rate parameter.

The transients which were used to compile Tables 5.3, 5.4, and 5.5 also yielded values for the double-layer capacitance. Tables

5.6, 5.7, and 5.8 display the error in these values in the same format as was used for the three previous tables. In contrast to the rate constant results, the derived value of the double-layer capacitance is smaller than expected in all cases, although the magnitude of the relative error was smaller.

Some other interesting differences can be noted. The clearest indication of the general behavior of the results of the analyses of these nonideal transients can be seen in Table 5.7, and that is the smaller the overall reactant concentration, the less error is observed in the apparent value of the capacitance. The relative error seems to be inversely related to the charge transfer time constant, although the results in Table 5.6 indicate that it is not due to this factor alone.

Table 5.8 shows the effect of varying the adsorption coefficients. Again we see the rough symmetry in the amount of error about the $K_{ox} = K_{red}$ diagonal.

It seems, then, that conditions for the optimization of a coulostatic experiment for measurement of the double-layer capacitance are not the same as for an experiment in which the kinetics parameters are of prime interest. One must lower the concentrations as much as possible to achieve the most accurate estimate of the double-layer capacitance. Since one is generally interested in the capacitance as a function of the electrode potential, it is not practical to adjust the relative concentrations of the reactants so that the equilibrium potential is near the p.z.c. to eliminate diffuse-layer adsorption. If the adsorption is too strong, the transient will decay

Error in Double-Layer Capacitance Derived $^{\mathbf{a}}$ from Coulostatic Transfents $^{\mathbf{b}}$ due to Weak Reactant Adsorption. $^{\mathbf{c}}$ Table 5.6.

						Adsorptio	n Coeffici	Adsorption Coefficient (cm) $K_{ox} = K_{red}$	ox = Kred	
C OX (IIM)	Cred (mM)	kstd (cm/s)	τ _c (μs)	$^{\mathrm{T}}\mathrm{c}^{/\mathrm{T}}\mathrm{D}$	5×10 ⁷	1×10 ⁻⁶	2×10 ⁻⁶	5×10 ⁻⁶	1×10 ⁻⁵	2×10 ⁻⁵
0.1	0.1	н	53.2	0.047	0	0	-0.4%	0	ပ	
		0.3	177	0.157	0	0	-0.1	29.0-	-5.0%	! !
•		0.1	532	0.47		0	0	-0.1	-0.5	-2.4%
1	н	H	5.32	0.47	-0.1%	-0.5%	-2.3	-14.9	ပ	U
		0.3	17.7	1.57	0	-0.1	7. 0-	-2.2	0.9-	-13.1
		0.1	53.2	4.7		0	-0.1	-0.5	-1.6	6.4-
10	1	1	1.68	0.49	-0.4	-1.7	-8.0			
		0.3	5.61	1.64	0	-0.3	-1.1	!	!	! ! !
		0.1	16.8	6.4		-0.1	-0.2			
10	10	1	0.532	4.7	9.0-	-1.6	-4.1		!!!!!!!!!!!!!!!!!!!!!!!!!!!!!!!!!!!!!!!	
		0.3	1.77	15.7	-0.1	-0.4	-1.1			1
		0.1	5.32	47		0	-0.2			

Two-parameter nonlinear regression. bD = D = 1 x 10^5, Q = 10^3 μ coul, C_{dl} = 20 μ F/cm², Area = 0.02 cm². Canalysis failed to yield reasonable value.

Table 5.7. Effect of Varying Reactant Concentration on Error in Double-Layer Capacitance Derived^a From Coulostatic Data^b with Weak Reactant Adsorption.^c

				Error	in C _{dl}
C (mM)	C _{red} (mM)	τ _c (μs)	$\tau_{\rm c}/\tau_{\rm D}$	η ⁰ =-2.5 mV	η ⁰ =+2.5 mV
0.05	1	23.8	0.0191	-0.1%	-0.1%
0.1	1	16.8	0.0491	-0.3	
0.2	1	11.9	0.117	-0.3	
0.5	1	7.53	0.295	-0.4	-0.4
1	1	5.32	0.470	-0.5	-0.5
2	1	3.76	0.590	-0.7	-0.7
5	1	2.38	0.583	-1.1	
10	1	1.68	0.491	-1.7	
20	1	1.19	0.381	-2.9	-2.8
1	0.05	23.8	0.0191	-0.1%	-0.2%
1	0.1	16.8	0.0491	-0.3	
1	0.2	11.9	0.117	-0.4	
1	0.5	7.53	0.295	-0.4	
1	1	5.32	0.470	-0.5	-0.5
1	2	3.76	0.590	-0.6	
1	10	1.68	0.491	-1.6	
1	20	1.19	0.381	-2.8	-2.9

 $^{^{\}mathbf{a}}$ Two-parameter nonlinear regression.

 $^{^{}b}k_{std} = 1 \text{ cm/s}, \quad C_{dl} = 20 \text{ }\mu\text{F/cm}^{2}, \quad D_{ox} = D_{red} = 1 \text{ }x \text{ }10^{-5} \text{ }cm^{2}/\text{s}, \quad Q_{inj} = 10^{-3} \text{ }\mu\text{coul}, \quad \text{Area} = 0.02 \text{ }cm^{2}.$

 $^{{}^{}c}K_{ox} = K_{red} = 1 \times 10^{-6} \text{ cm.}$

Table 5.8. Effect of Varying Adsorption Coefficients on Error in Double-Layer Capacitance Derived^a from Coulostatic Data.^b

			K _{red} (cm)		
K (cm)	none	1 x 10 ⁻⁶	5 x 10 ⁻⁶	1 x 10 ⁻⁵	2 x 10 ⁻⁵
none	0	0	-0.8%	-2.1%	-4.2%
1×10^{-6}	0	-0.1%	-0.9	-2.3	-4.5
5×10^{-6}	0	-0.9	-2.9	-3.9	-6.5
1×10^{-5}	-2.3%	-2.4	-4.0	-6.0	-9.4
2×10^{-5}	-4.3	-4.8	-6.8	-9.5	-13.1

^aTwo-parameter nonlinear regression.

 $^{^{}b}k_{std} = 0.3 \text{ cm/s}, \quad C_{ox} = C_{red} = 1 \text{ mM}, \quad D_{ox} = D_{red} = 1 \text{ x } 10^{-5} \text{ cm}^{2}/\text{s},$ $C_{d\ell} = 20 \text{ } \mu\text{F/cm}^{2}, \quad Q_{inj} = 10^{-3} \text{ } \mu\text{coul}, \quad \text{Area} = 0.02 \text{ cm}^{2}.$

faster than the diffusion limited rate, especially at lower concentrations, and the analysis will fail to give a meaningful value for k_{std} . Under these circumstances it would be risky to trust a capacitance value estimated simultaneously with the rate constant. Thus, it seems impossible to obtain a reliable estimate of the double-layer capacitance in the presence of a weakly adsorbed electroactive species if the electron transfer is even moderately fast (>0.1 cm/sec).

CHAPTER 6

GALVANOSTATIC DOUBLE PULSE EXPERIMENTS

6.1. Description of Experiment

The galvanostatic double pulse technique was developed (15,59) as an improvement over the single pulse method in that it allows a precharging of the double layer prior to the actual measurement of the transient signal. This is important because it assures that all the current which is flowing is used in the faradaic (electron-transfer) process. An initial, short, but relatively large amplitude current pulse is applied to the cell, followed immediately by a second pulse of smaller amplitude. Depending on the duration of the first pulse and the relative amplitudes of the two pulses, a minimum in the overpotential-time curve can be observed at some time after the first pulse. This minimum occurs because the first pulse not only charges the double layer, but also sets up a steeper concentration gradient than is required to maintain the flux from the second pulse. excess reactant causes the potential to return towards the equilibrium value until the gradient adjusts to the new flux and the potential begins to increase again.

To perform a galvanostatic double pulse experiment, the worker interactively adjusts the magnitude and duration of the first pulse, keeping the current in the second pulse constant. The pulses are adjusted so that the minimum in the overpotential-time curve falls exactly at the end of the first pulse. The value of the overpotential at this minimum as a function of the duration of the first

pulse is conventionally used to derive the rate data of interest.

The equations which describe the ideal overpotential-time behavior after the first current pulse are somewhat more complicated than those in coulostatics because the concentration gradients both before and after the pulse must be considered. For small overpotentials (15),

$$\eta = \frac{i_1 G(t)}{C_{d\ell}(\gamma - \beta)} - \frac{(i_1 - i_2)G(t - t_1)}{C_{d\ell}(\gamma - \beta)}$$
(6.1)

$$G(x) = \frac{\gamma}{\beta^{2}} \left[\exp(\beta^{2}x) \operatorname{erfc}(\beta x^{\frac{1}{2}}) + 2\beta(x/\pi)^{\frac{1}{2}} - 1 \right] - \frac{\beta}{\gamma^{2}} \left[\exp(\gamma^{2}x) \operatorname{erfc}(\gamma x^{\frac{1}{2}}) + 2\gamma(x/\pi)^{\frac{1}{2}} - 1 \right]$$
(6.2)

$$\beta/\gamma = \frac{k_{std}c_{ox}^{1-\alpha}c_{red}^{\alpha}}{2} \left(\frac{1}{c_{ox}^{D_{ox}^{\frac{1}{2}}}} + \frac{1}{c_{red}^{D_{red}^{\frac{1}{2}}}}\right) + /-$$

$$\left[\left\{ \frac{1}{2} k_{std} \left(c_{ox}^{1-\alpha} c_{red}^{\alpha} \right) \left(\frac{1}{c_{ox}^{\frac{1}{2}}} + \frac{1}{c_{red}^{\frac{1}{2}}} \right) \right\}^{2} - \frac{n^{2} F^{2} k_{std} c_{ox}^{1-\alpha} c_{red}^{\alpha}}{RTC_{d\ell}} \right]^{2}$$
(6.3)

It is also possible to define the time constants of the system. The charge transfer time constant τ_c and the diffusion time constant τ_d are given by the expressions

$$\tau_{c} = RTC_{d\ell} / (n^{2}F^{2}C_{ox}^{1-\alpha}C_{red}^{\alpha}k_{std})$$
 (6.4)

$$\tau_{\rm d} = \pi / \left[\left(\frac{1}{C_{\rm ob}^{\frac{1}{2}}} + \frac{1}{C_{\rm red}^{\frac{1}{2}}} \right) k_{\rm std} c_{\rm ox}^{1-\alpha} c_{\rm red}^{\alpha} \right]^2$$
 (6.5)

The consequences of adjusting the experimental parameters, particularly the current in the second pulse, are the key to the success of this method. One can optimize the experiment for the particular rate constant, concentrations, and double-layer capacitance simply by adjusting the pulses appropriately. This sort of "fine tuning" is not possible in the usual potentiostatics experiments; perhaps a double potential-step method would be useful for establishing a concentration gradient in the solution before the start of the experiment.

6.2. Analysis of Data from G.D.P. Experiments

As stated above, the galvanostatic double pulse experiment is typically performed by adjusting the amplitude of the first pulse until the minimum in the overpotential-time curve occurs exactly at the beginning of the second pulse. This process is repeated, varying the duration of the first pulse, while keeping the amplitude of the second pulse constant. These minimum values of the overpotential can be plotted against the square root of the pulse time to yield an intercept which is inversely proportional to the standard rate constant for the redox couple (15):

$$k_{std} = RTi_2/(n^2 F^2 c_{ox}^{1-\alpha} c_{red}^{\alpha} \eta_{min}^{o})$$
 (6.6)

This relationship is obtained (60) by differentiating Equation 6.1 with respect to time, and setting $(dn/dt)_{t_{min}}$ equal to zero. This yields an expression for the minimum overpotential as a function only of i_2 and t_1 . Setting t_1 equal to t_{min} , expanding the $\exp(x^2)\operatorname{erfc}(x)$ function, and dropping all but the first term of the expansion leads to an expression in $t_1^{i_2}$ with the intercept given by Equation 6.6 above.

Because there are some instrumental difficulties in observing the overpotential at the exact point at which the current is switched, Nagy (60) has developed equations which allow the minimum in overpotential to fall at some defined time after the first pulse ends. The result of this work is a set of alternative equations relating the intercept of the η_{\min} vs. $t_1^{\frac{1}{2}}$ plot to the standard rate constant.

All of these methods involve approximations in the linearization of the overpotential minimum-pulse time data. The obvious alternative to the above procedures is simply to use nonlinear regression to fit the transient to the explicit equation, Equation 6.1. As with coulostatics, the analysis will adjust two parameters, the standard rate constant and the double-layer capacitance. In fact, Nagy (62) has shown that this type of curve-fitting is superior to the conventional analysis in the accuracy of the derived rate constants in the presence of random measurement errors. As long as a minimum is observable, the advantage of precharging the double layer remains (61).

Although no optimal time ranges for the nonlinear regression analysis of galvanostatic double pulse data have been discussed, Nagy (62) has established some guidelines for single pulse galvanostatic

experiments:

$$t_2 = 10 \tau_c \text{ if } \tau_d > 10 \tau_c$$
 (6.7)

$$t_2 = \tau_d \text{ if } \tau_c < \tau_d < 10 \tau_c$$
 (6.8)

$$t_2 = \frac{1}{2}(\tau_c + \tau_d) \text{ if } \tau_c > \tau_d$$
 (6.9)

These time ranges were used for all the following work when analyzing the g.d.p. data by nonlinear regression on Equation 6.1.

The effect of finite galvanostat risetime has been considered in the literature (1), and an explicit equation has been derived assuming a linearly rising current pulse. Nagy (61) states that the non-linear regression analysis of g.d.p. data is quite sensitive to this risetime when the ideal equation (Equation 6.1) is used in the analysis. However, in his study of the effect of measurement precision, he found that the results which were obtained for the errors in the rate constants were essentially independent of the specific equation which was used in the regression. Finite measurement precision had the same effect on the results whether the galvanostat was considered ideal or not.

Because galvanostat risetime has been previously discussed in the literature (1), it was not considered here. Given the sensitivity of coulostatics to weak reactant adsorption, however, it was of interest to investigate the effects of this chemical nonideality on the results of the g.d.p. experiments. To simplify the procedure, it was assumed that the galvanostat was indeed ideal. In view of the above-mentioned measurement precision study, this should yield

essentially equivalent results as would using a nonideal galvanostat model.

6.3. Unique Aspects of Simulation

The digital simulations of this technique were performed in a manner similar to those in preceding chapters. The constant current condition was identical to the current impulse coulostatics charge injection period, where the change in overpotential with respect to time can be expressed

$$d\eta/dt = i_1/(C_{d\ell} \cdot A) - F\Phi_{far}/C_{d\ell}$$
 (6.10)

The constant current began at time zero, however, and was reduced to the smaller value at the appropriate time. (When the second current is zero, the experiment is identical to current impulse coulostatics.)

Twenty points were recorded at equal intervals along the simulated transients over a time period specified by the above conditions (Equations 6.7-6.9). The parallel simulation scheme was used for all transients which were to undergo the nonlinear regression analysis. Conventional simulations were used for those transients subjected to the conventional g.d.p. analysis. In these few cases, the minimum values were recorded manually as the current parameters were adjusted interactively for the various pulse times.

6.4. Shape of Deviations Due to Reactant Adsorption

The effect of weak reactant adsorption on the galvanostatic double pulse transient is shown in Figure 6.1 for a typical system with varying amounts of adsorption. There are two features of the overpotential-time curves which are immediately noticeable. The overpotential which is attained after the first pulse is lower than expected and is decaying at a faster rate when adsorption is present.

The reasons for this are exactly analogous to those for coulostatics. There is more reactant at the surface when the species is adsorbed, so electrons are lost to the faradaic process faster. This keeps the electrode from charging as fast as it might, and the result is a lower overpotential, even though the number of electrons flowing into the cell is the same.

There are no obvious features which distinguish these nonideal transients from those which are ideal. The minimum is shifted, and the decay is steeper, but in the performance of an experiment these would be interpreted as a maladjusted current pulse sequence rather than any chemical nonideality. Indeed, after suitably adjusting the current in each pulse, it is not at all obvious that adsorption is present.

The larger than ideal currents necessary to compensate for the effects of weak reactant adsorption are used in the equation describing the ideal transient (Equation 6.1), so one would expect that the rate constants derived on the basis of this equation might be in error, even if the absolute shape of the measured transient was identical to

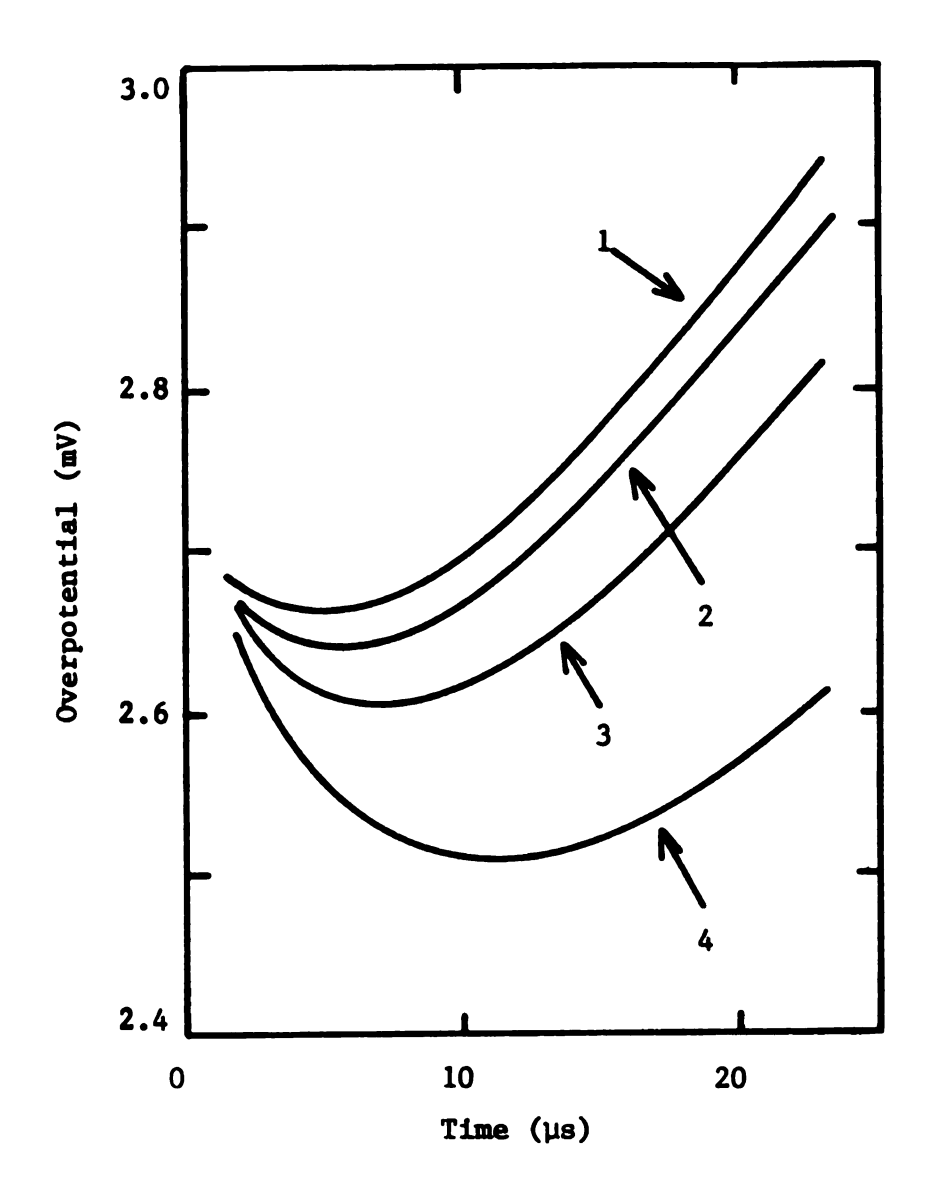


Figure 6.1. Galvanostatic double pulse transients illustrating the effects of reactant adsorption, with $k_{\rm std}=0.3~{\rm cm/s}$, $C_{\rm dl}=20~{\rm \mu F/cm^2}$, $i_1=0.055~{\rm A/cm^2}$, $t_1=1~{\rm \mu s}$, $i_2=0.002~{\rm A/cm^2}$, $C_{\rm ox}=C_{\rm red}=1~{\rm mM}$, $D_{\rm ox}=D_{\rm red}=1{\rm x}10^{-5}~{\rm cm^2/s}$. Curve 1: ideal system. Curve 2: $K_{\rm ox}=K_{\rm red}=1{\rm x}10^{-6}{\rm cm}$. Curve 3: $K_{\rm ox}=K_{\rm red}=3{\rm x}10^{-6}{\rm cm}$. Curve 4: $K_{\rm ox}=K_{\rm red}=1{\rm x}10^{-5}~{\rm cm}$.

the ideal case. Thus, any rate constants derived on the basis of this equation must be in error. It is not clear, however, how much error would be produced, or even whether the derived parameters would be too high or too low.

6.5. Initial Investigations

Galvanostatic double pulse experiments are unique in that there are a large number of parameters which can be adjusted for each chemical system. The pulse parameters control the shape of the resulting transient: The first pulse mainly controls the overall overpotential change at the beginning of the experiment, while the second pulse controls the position of the overpotential minimum and steepness of the measured transient.

It must be determined whether the results of the nonlinear regression analysis are dependent on the adjustable experimental parameters when weak adsorption is present. (If the experiment were ideal, of course, there would be no problem because the equations take these experimental parameters into account.) There are three adjustments which can conveniently be made by the experimenter in setting the pulse parameters: 1) the length of the first pulse, 2) the overall potential change during the first pulse, and 3) the position of the minimum along the transient.

In order to determine the influence of these variations on the results of the nonlinear regression analyses, three sets of transients were generated under identical adsorption conditions. The errors in

the

in fir

lon

kin

and

ext th

to

aı

þ

.

.

ac

for ana the values of $k_{\rm std}$ and $C_{\rm dl}$ derived from these transients are listed in Table 6.1. The first group shows that the effect of varying the first pulse time is quite small, with slightly larger errors from longer pulse times. This is probably due to the reduced amount of kinetics information available at these longer times. The second and third groups in the table show that the overpotential range of the experiment and the position of the minimum along the transient influence the error in the rate constant or in the double-layer capacitance only to a very small degree.

It is now possible to proceed with a systematic variation in the amount of adsorption to observe the errors in the derived rate constants and capacitances. In these simulations, the initial pulse time will be held at 1 μ s for convenience, while the currents will be adjusted to produce a minimum overpotential of about 3 (+/-0.5) mV at a position roughly 10 to 30% along the transient. These small variations should have only minor effects on the results.

6.6. Effect of Adsorption in Nonlinear Regression Analysis

A series of transients was generated to investigate in a general way the effect of weak reactant adsorption upon the results of non-linear regression analyses. For this preliminary work, the concentration of both the oxidized and reduced species as well as their diffusion and adsorption coefficients were assumed to be equal. The adsorption coefficient was varied from 1×10^{-6} cm to 2×10^{-5} cm for a series of rate constants. The results of the nonlinear regression analyses of these transients are shown in Tables 6.2 and 6.3.

Table 6.1. Effect of Adjustable Experimental Parameters on Error in Rate Constant and Double-Layer Capacitance Derived^a From G.D.P. Transients^b with Weak Reactant Adsorption.^c

t ₁ (μs)	t _{min} (µs)	n _{min} (mV)	Error in k	Error in C _{dl}
0.5	2.8	2.6	+69%	-4.3%
1	3.8	2.7	71	-4.3
1.5	2.7	2.5	72	-5.0
2	3.3	2.6	74	-5.3
3	4.7	2.6	77.	-6.0
1	2.5	.48	+67%	-4.4%
1	2.5	.97	70	-4.6
1	2.5	1.94	70	-4.6
1	2.5	3.88	70	-4.6
1	2.5	7.28	71	-4.7
1	2.5	2.7	+71%	-4.7%
1	6.4	2.7	71	-4.6
1	11.4	2.5	71	-4.6
1	17.8	2.3	71	-4.6

^aTwo parameter nonlinear regression.

 $b_{k_{std}} = 0.3 \text{ cm/s}, \quad C_{dl} = 20 \text{ } \mu\text{F/cm}^2, \quad C_{ox} = C_{red} = 1 \text{ mM}, \quad D_{ox} = D_{red} = 1 \text{ } \text{x } 10^{-5} \text{ cm}^2/\text{s}.$

 $^{^{}c}K_{ox} = K_{red} = 1 \times 10^{-5} \text{ cm.}$

Table 6.2. Error in Rate Constants Derived from G.D.P. Transients Due to Weak Reactant Adsorption $(K_{ox} = K_{red})$.

	k _{std} (cm/s)			
K = K (cm)	0.1	0.3	1.0	3.0
1 x 10 ⁻⁶	+2%	+6.3%	+24.5%	+25.2%
3×10^{-6}	6.3	19.8	125	С
1×10^{-5}	22.3	70.1	c	c
2 x 10 ⁻⁵	45.9	135	c	c

a Two parameter nonlinear regression.

 $b_{t_1} = 1 \mu s$, i_1 , i_2 varying, $c_{d\ell} = 20 \mu F/cm^2$, $c_{ox} = c_{red} = 1 mM$, $c_{ox} = c_{red} = 1 \times 10^{-5} cm^2/s$.

^cAnalysis failed to yield a meaningful value.

Table 6.3. Error in Double-Layer Capacitance Derived^a from G.D.P. Transients^b Due to Weak Reactant Adsorption $(K_{ox} = K_{red})$.

				OX 160	
		k _{std} (cm/s)			
$K_{ox} = K_{red}$ (cm)	0.1	0.3	1.0	3.0	
1 x 10 ⁻⁶	+0.01%	-0.1%	-0.4%	-2.8%	
3×10^{-6}	-0.2	-0.7	-4.1	С	
1 x 10 ⁻⁵	-2.3	-4.6	c	С	
2×10^{-5}	-7.0	-9.3	c	c	

^aTwo parameter nonlinear regression.

 $b_{t_1} = 1 \mu s$, i_1 , i_2 varying, $c_{d\ell} = 20 \mu F/cm^2$, $c_{ox} = c_{red} = 1 mM$, $c_{ox} = c_{red} = 1 \times 10^{-5} cm^2/s$.

^CAnalysis failed to yield a meaningful value.

Table 6.2 shows the error in the rate constants which are derived from these nonideal transients. In all cases, the derived rate constants are too high. There were instances in which the overpotential decay was so steep that no meaningful value of either the rate constant or the double-layer capacitance could be derived. This probably indicates that the curves decayed faster than diffusion control would allow under these conditions. It can be seen that only a very small amount of adsorption causes very serious errors in the rate constant at values of 1 cm/s or more. This extreme sensitivity to relatively minor deviations is due to the lack of kinetics information in the shape of the transient. At smaller rate constants, there is still a fairly large amount of error present, except when the adsorption is very small $(K_{ox} = K_{red} = 1 \times 10^{-6} \text{ cm})$.

The errors in the capacitance values which were derived simultaneously with the rate constants are shown in Table 6.3. Here we see that the errors are considerably smaller than for the derived rate constants, but that they do approach 10% for large adsorption coefficients. The probable reason for this is that, although there is very little kinetics information left as diffusion control is approached, the transient is still quite sensitive to variations in the capacitance. The error that is produced is due to the apparently larger extrapolated overpotential at the end of the first pulse, which would imply a smaller capacitance. The tendency for this to occur increases as the redox reaction rate increases, so we observe more error in the capacitance at faster reaction rates.

Even though some of the capacitance values seemed reasonable

when the corresponding rate constants clearly were not meaningful, their values were not reported in Table 6.3. It is thought doubtful to trust one parameter when others derived simultaneously are obviously in error.

Another series of transients was generated to examine the effect of varying the individual adsorption coefficients in a typical system $(k_{std} = 0.3 \text{ cm/s})$. The resulting errors in the derived rate constants are shown in Table 6.4. As in coulostatics and chronoamperometry, we see that the same general rule applies: The more adsorption, whether of the oxidized or the reduced species, the greater the error in the rate constant.

metry of the experiment. Even though the electrode is initially at the equilibrium potential, the current flow causes one half of the redox couple to be a reactant, while the other becomes the product. Thus we see that the adsorption of the reactant has a slightly larger effect on the shape of the transient than does adsorption of the product. The asymmetry in Table 6.4 has been found to be reversed if the current flows in the opposite direction.

The trends in the errors in the double-layer capacitance values are the same as those for the rate constants, with a maximum error of about 10% when the adsorption coefficient of each species is the same, and only about 3% when only one of the species is adsorbed.

Finally, it is of interest to study the effect of varying the concentration of the reactants. It was determined that it is the value of the adsorption coefficient which determines the error, and

Table 6.4. Error in Rate Constant Derived from G.D.P. Transients Due to Weak Reactant Adsorption $(K_{ox} \neq K_{red})$.

		K _{red} (cm)			
K (cm)	0	1 x 10 ⁻⁶	3 x 10 ⁻⁶	1 x 10 ⁻⁵	2 x 10 ⁻⁵
0		+2.8%	+8.3%	+23.7%	+36.4%
1×10^{-6}	+3.1%	6.3	12.2	29.0	43.2
3×10^{-6}	9.5	13.0	19.8	39.3	56.5
1×10^{-5}	27.0	32.3	42.1	70.1	96.1
2×10^{-5}	42.6	49.2	61.9	99.7	135

a Two parameter nonlinear regression.

 $^{^{}b}t_{1} = 1 \mu s$, $i_{1} = 0.065 \text{ A/cm}^{2}$, i_{2} varying, $k_{std} = 0.3 \text{ cm/s}$, $c_{dl} = 20 \mu F/cm^{2}$, $c_{ox} = c_{red} = 1 \text{ mM}$, $c_{ox} = c_{red} = 1 \text{ x } 10^{-5} \text{ cm}^{2}/s$.

not the absolute magnitude of the surface excess when there is equal concentrations of both species in the solution.

Table 6.5 shows the error in both the standard rate constant and the capacitance derived from transients generated while varying the concentration of one half of the redox couple. It can be seen that equal concentrations of the oxidized and reduced species produces the minimum error, with the error increasing as the ratio of the concentrations deviates from unity in either direction. The error in the double-layer capacitance, on the other hand, is smallest at the smallest concentrations.

As was the case with coulostatics, it is not possible to correlate these effects to the experimental variables in any systematic way; the exact amount of error depends on too many factors for correlations to be particularly useful. Some general conclusions can be made, however. The uncertainty in the rate constants derived using nonlinear regression from g.d.p. transients is minimized when the equilibrium potential is the formal potential (i.e., when the concentration of the two species are equal). Attempting to decrease the diffuse-layer adsorption by adjusting the system for a new equilibrium potential closer to the p.z.c. will only work if the adsorption can be made negligible; otherwise, the accuracy gained by the smaller degree of adsorption will be counterbalanced by changing the concentration ratio from unity.

6.7. Effect of Adsorption in Conventional Analysis

Conventional simulations were performed for two systems to compare the performance of the nonlinear regression analysis with the

Table 6.5. Error in Rate Constants Derived from G.D.P. Transients Due to Weak Reactant Adsorption $(C_{ox} \neq C_{red})$.

C (mM)	C _{red} (mM)	Error in k	Error in C _{dl}
1	0.1	+500%	-2.7%
1	0.3	110	-3.4
1	1	70	-4.6
1	3	84	-7.7
1	10	150	-12.

a Two parameter nonlinear regression.

 $b_{t_1} = 1 \mu s$, $i_1 = 0.055 \text{ A/cm}^2$, $i_2 \text{ varying}$, $k_{std} = 0.3 \text{ cm/s}$, $C_{dl} = 20 \mu F/cm^2$, $D_{ox} = D_{red} = 1 \times 10^{-5} \text{ cm}^2/s$. $c_{K_{ox}} = K_{red} = 1 \times 10^{-5} \text{ cm}$.

con tre

lin

wer

bot! ref

dig plo

pro

pl ce

C

p

n

7

s

p

th

fo

conventional $\eta_{\min} \ \underline{vs}$. $t_1^{\frac{1}{2}}$ analysis. One of the systems chosen for this treatment failed to provide any kinetics information under the non-linear regression analysis, while the other yielded rate constants which were in error by about 70%.

Figures 6.2 and 6.3 show the η_{\min} vs. $t_1^{\frac{1}{2}}$ plots for each system both with and without adsorption. The ideal case was simulated for reference because the simulated data were generated using conventional digital simulation routines. The linear regression lines are also plotted on the graph. It is clear that the presence of adsorption produces large deviations in both the slope and the intercept of these plots, as well as some degree of nonlinearity in the data. The intercepts from the linear regression together with the corresponding rate constants derived from these values using Equation 6.6 and their approximate uncertainties are shown in Table 6.6.

These results are strikingly improved over those derived by the nonlinear regression procedure. In the first system, where k_{std} = 0.3 cm/s, we see only a 3% error in the rate constant compared to about 70% from the other analysis. The other system, for which nonlinear regression failed entirely to yield a reliable rate constant, yields a result by this analysis which is in error by roughly 60%. The surprisingly more accurate results afforded by the conventional analysis were seen for a wide range of rate constants and adsorption parameters.

Apparently, the method of adjusting the current pulses to position the minimum at a reproducible time in the experiment is responsible for this improvement. During the first current pulse, not only does

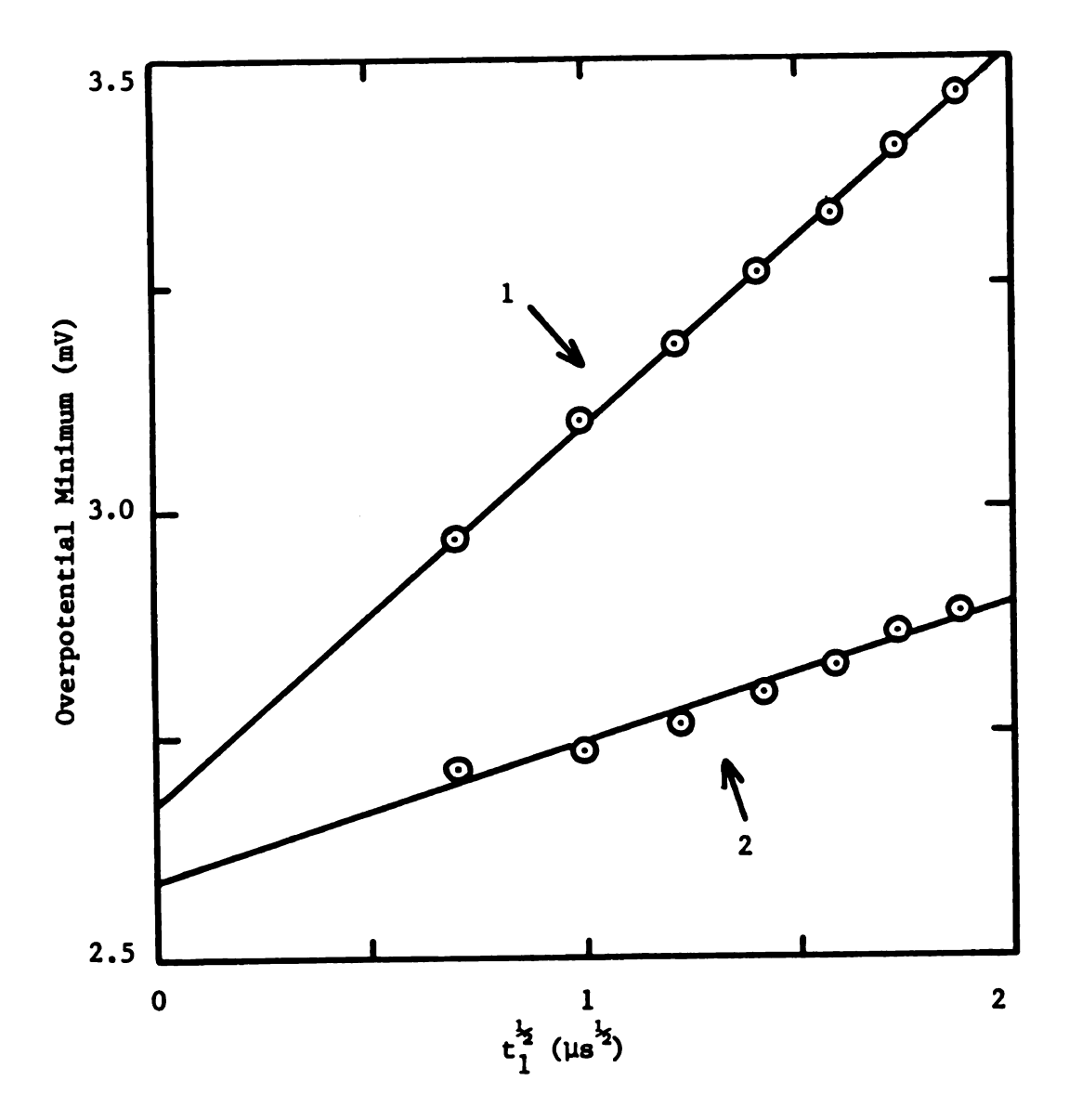


Figure 6.2. Overpotential minimum vs. $t_1^{\frac{1}{2}}$ for conventional g.d.p. analysis, with $k_{std} = 0.3$ cm/s, $C_{d1} = 20 \ \mu F/cm^2$, $t_2 = 0.003 \ A/cm^2$, $C_{ox} = C_{red} = 1 \ mM$, $D_{ox} = D_{red} = 1 \times 10^{-5} \ cm^2/s$. Lines are least-squares best fit. Curve 1: ideal system. Curve 2: $K_{ox} = K_{red} = 1 \times 10^{-5} \ cm$.

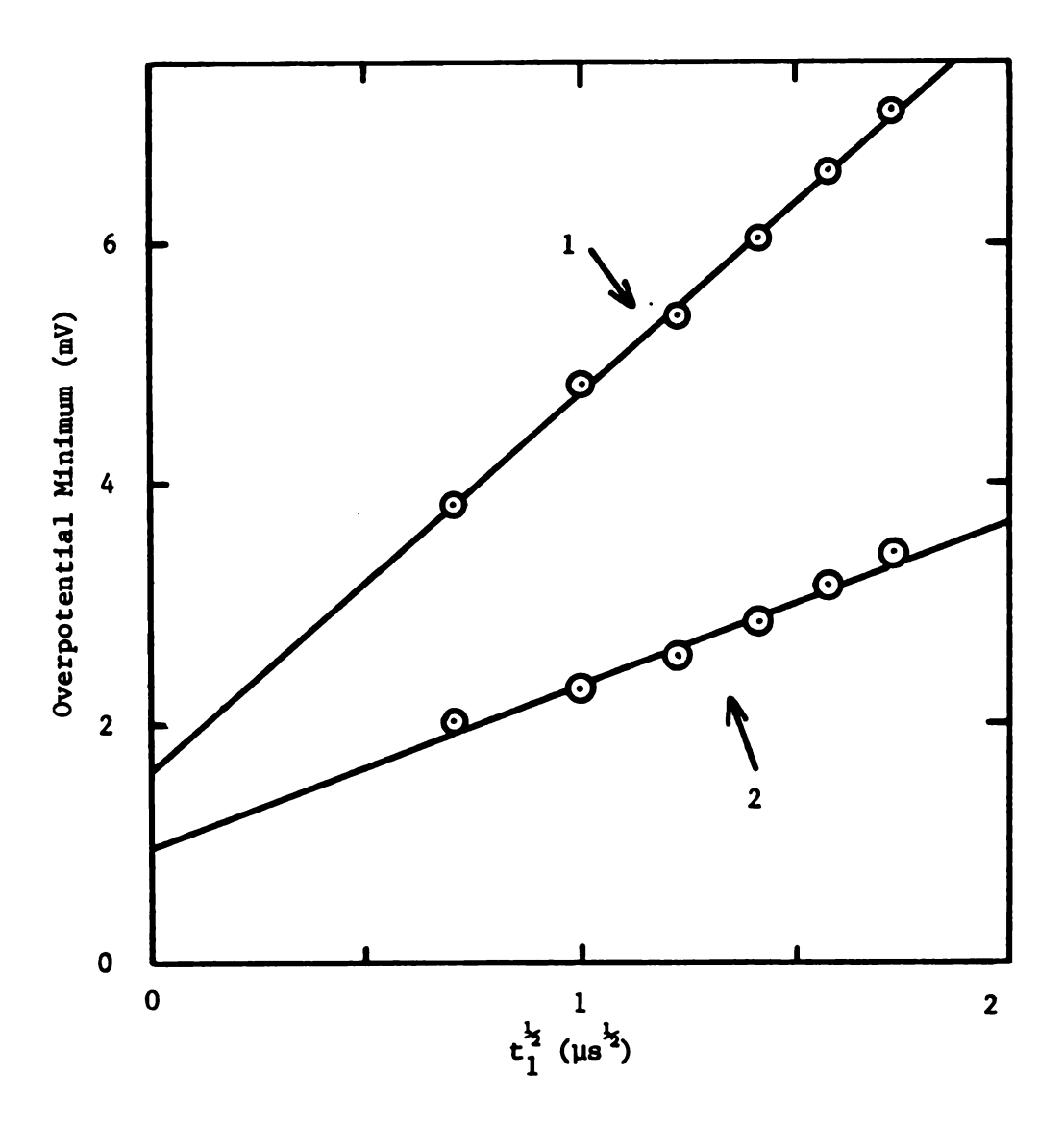


Figure 6.3. Overpotential minimum vs. $t_1^{\frac{1}{2}}$ for conventional g.d.p. analysis, with $k_{std} = 3$ cm/s, $i_2 = 0.02$ A/cm², other parameters as in Figure 6.2. Lines are least-squares best fit. Curve 1: ideal system. Curve 2: $K_{ox} = K_{red} = 1 \times 10^{-5}$ cm.

Table 6.6. Results of Conventional Analysis of G.D.P. Data with Weak Reactant Adsorption.

	Intercept (mV)	Derived k _{std} (cm/s)
$k_{std} = 0.3 \text{ cm/s}$		
Ideal	2.673	0.299 ± .001
Adsorption ^b	2.588	0.308 ± .002
$k_{std} = 3.0 \text{ cm/s}$		
Ideal	1.619	3.289 ± .16
Adsorption	0.982	5.423 ± .67

 $^{^{}a}$ C_{ox} = C_{red} = 1 mM, D_{ox} = D_{red} = 1 x 10^{-5} cm²/s, not parallel simulation.

 $^{^{}b}K_{ox} = K_{red} = 1 \times 10^{-5} \text{ cm}.$

the double-layer charge to the appropriate value, but the faradaic reactions of bulk species and adsorption occur as well. The extrapolation back to time zero which is conventionally done to correct for this concentration polarization during the first pulse evidently also corrects for the reaction of the adsorbed species. The $t_1^{\frac{1}{2}}$ plot linearizes the contribution from the diffusing species, as seen in Figures 6.2 and 6.3 for the ideal system, but the adsorbed species distorts the diffusion profile, rendering curvature in the data. It can be seen that a rough, curved extrapolation yields an intercept even closer to the ideal value, and hence a more accurate rate constant.

6.8. Implications for the Use of Small-Step Methods

It was found that experimental nonidealities in small potentialstep, coulostatics, and galvanostatic double pulse studies of fast
reactions produce a large amount of error when the resulting transients are analyzed with nonlinear regression. In the face of nonideal conditions, the traditional advantage of nonlinear regression
(i.e., the sensitivity of the analysis to minor variations in the
shape of the transient) actuallyworks against the derivation of accurate rate constants from experimental data. As the amount of kinetics information in the transient decreases (for faster reactions),
a deviation of a given magnitude will produce a greater error in the
rate parameter.

These results should serve as a warning to those who routinely use nonlinear regression analyses to reduce their data. The equation

to which the experimental data is fit must accurately reflect the processes which are occurring in the experiment. This is especially important when the curve contains only a small amount of the information of interest. (Of course, the nonideal data examined here could, in principle, be adequately fit by an equation which takes the nonidealities into account. In this case, nonlinear regression would probably be the analysis method of choice.)

The surprising success of the conventional galvanostatic double pulse analysis was indeed a welcome result in the midst of failing nonlinear regression analyses for every other experimental method examined. Ideally, of course, an equation might be derived to allow a valid extrapolation of the η_{\min} vs. pulse time curve to zero time, but even the rough, linear approximation produces much more accurate results than those obtained by nonlinear regression analyses, and even yields estimates of the rate constant under conditions in which nonlinear regression was not able to do even that.

Other methods are also used to study the rates of quasi-reversible reactions, in particular, a.c. polarography. This method was not examined in this study because of the lack of a closed-form solution to the overall current response to the small a.c. potential perturbation. Conventional simulations yielded responses which were too inaccurate to be of use. It would be expected, though, that adsorption of the reactants would interfere with the measurement of fast rate constants here as well. Another method sometimes used to study the rates of fast electrode reactions is cyclic voltammetry. This technique was not examined because preliminary studies (with conventional

simulations) showed only very minor effects due to reactant adsorption; indeed, the observed errors were less than other known errors (e.g., iR drop) for these experiments.

Thus, it seems that the galvanostatic double pulse experiments with the conventional data analysis will yield the best estimates of fast electron-transfer rate constants in the face of inevitable experimental nonidealities.

CHAPTER 7

SUGGESTIONS FOR FURTHER RESEARCH

7.

ra.

ad ev

st Th

pr

Fr

jus

tic

con

scr sit

is

for to

the

app

7.1. Extension to Other Adsorption Isotherms

While this work has illustrated that the influence of weak reactant adsorption becomes pronounced only when one attempts to measure the rate constants of very fast reactions, it is possible that stronger adsorption will influence transient responses to a larger extent even when slower reactions are studied.

There are two isotherms in relatively common use for describing strong adsorption (1): the Langmuir isotherm and the Frumkin isotherm. The Langmuir equation needs two parameters to describe the adsorption properties, as it takes into account a saturation-coverage limit. The Frumkin isotherm takes this one step further (and adds one more adjustable parameter) in considering adsorbate-adsorbate interactions.

Either of these isotherms can be used in more complicated simulations to study the influence of strong adsorption. The study is made considerably more complex than the Henry's law case in that we now need several parameters (and their dependence on potential) to describe the adsorption properties of each species in the system. The situation is further complicated by the fact that specific adsorption is usually not in equilibrium over the time scale of these experiments; for a realistic model, adsorption-desorption kinetics would also have to be considered.

Despite these complications, it should be possible to apply some appropriate simplifying assumptions and obtain useful results from the simulation of these systems. A more realistic model could aid

considerably in the interpretation of experimental results, as described below.

7.2. Alternative Analysis Procedures

As suggested in Chapter 3, these more realistic models could be applied in a nonlinear regression analysis of data which was recorded in such a way as to maximize the extent of the nonideal behavior.

Not only could rate data be recovered, but also information about the adsorption properties of the reactant. Two approaches suggest themselves.

The study of systems with strong adsorption could yield separate kinetics information for the adsorbed reactant and the diffusing reactant. At present, it is difficult to separate the overall faradaic current into the various components, so that the kinetics of the adsorbed species must be studied under conditions which minimize the reaction of the diffusing species. Two methods are used for this: a very small bulk concentration of the reactant (which requires very strong adsorption), or very fast experiments so that very little reactant has time to diffuse toward the surface. A simulation-based analysis might be successful in determining the kinetics of both reactions simultaneously or even the adsorption-desorption kinetics of the species in question.

A second possibility for simulation-based analysis is the compensation for nonideal instrumentation. The actual applied waveform (potential-step, current-step, etc.) could be measured independently of the response transient and used in a simulation analysis. This

approach might also make it relatively easy to do any resistance compensation at the analysis stage instead of guessing before the experiment is performed. By actually measuring the applied waveform, the
need for some instrumental model is eliminated, making the entire procedure more reliable.

Implicit in the above discussion is the assumption that charging currents due to double-layer capacitance in potential-step experiments make no contribution to the analyzed transients. It is hard to ensure this because of iR-drop problems, even though the current may not be sampled until after the applied potential is at the desired value. Although small-step coulostatics and g.d.p. experiments take the double-layer capacitance into account, the theory assumes that it remains constant throughout the experiment, which may not be true in the face of specific adsorption of the reactants. Additionally, a change in the number of adsorbed ions over the course of the experiment could cause nonfaradaic current to flow if the electrosorption valency of the adsorbate was large enough to affect the charge on the electrode. These factors could be examined in more detail to see if they are indeed large enough to produce deviations in the shape of the transients.

The flexibility of digital simulation coupled with the generality of the nonlinear regression analysis gives these procedures much potential. On a mainframe computer, these analyses could become as convenient as a linear least squares calculation.





A SAMPLE SIMULATION PROGRAM

The following program uses the parallel simulation method to produce an error curve to be impressed on a calculated ideal small-step chronoamperometric transient (see Chapter 2). Although comments have been provided in the listing itself, a few explanatory notes will be given.

The listing produced by FLECS includes indentation to show the level of the control structure of an individual statement. The vertical columns of dots allow the level to be traced from page to page. The statement "FIN" serves only to indicate the end of a control level.

In addition to the initialization and the parallel simulations, there are quite a few lines of code dedicated to a convenient user interface. The internal procedure DISPLAY-MODIFY-PARMS allows any number of the variables in the simulation to be adjusted during a session with a minimum of effort.

The octal (base 8) constants (e.g., "33) in WRITE statements to unit 7 (the terminal) are DEC VT-52 compatible escape sequences for controlling the position of the cursor, clearing the screen, etc.

File output statements are not shown in this listing for clarity, although all regular programs include this provision. The extra statements include OPEN/CLOSE logic for new files, a data set header section which records all the simulation parameters, and output statements for the simulated data themselves.

PAGE 1

PROGRAM GSIM C GSIM - CHRONOAMPEROMETRY SIMULATION PROGRAM BY E. SCHINDLER, 5/82 C C * GUASI-REVERSIBLE KINETICS C * LINEAR POTENTIAL RISE C DIMENSION C(100), P(100), CNEW(100), A(14) DIMENSION CI(100), PI(100), DX(100) C REAL KF, KB, KSTD, KFI, KBI BYTE ERR C EQUIVALENCE (A(1), KSTD), (A(2), ESTEP) EQUIVALENCE (A(3), COX), (A(4), DOX) EQUIVALENCE (A(5), CRED), (A(6), DRED) EQUIVALENCE (A(7), ALPHA), (A(8), AREA) EQUIVALENCE (A(9), DX1), (A(10), QQQ) EQUIVALENCE (A(11), BETA), (A(12), DTOUT) EQUIVALENCE (A(13), TFINAL), (A(14), TRISE) C DEFAULT PARAMETER VALUES

DATA A/. 1, 0., 1. E-6, 1. E-5, 1. E-6, 1 1. E-5, . 5, . 02, 5. E-6, . 1, . 4, 1. E-4,

1 2.01E-3, 1.E-5/

FLECS/RT-11 V28.01

PAGE 2

C C INITIALIZATION SECTION C WHILE (. TRUE.) DISPLAY-MODIFY-PARMS NVE=10 NVEI=10 DTNOR=BETA+DX1++2/AMAX1(DRED, DOX) DT=TRISE/200. IF (DTNOR. LT. DT) DT=DTNOR TIME=0. 0 TOUT=DTOUT C . DO (I=1,100) . C(I)=COX . CI(I)=COX

C

EEQUIL=-25. 691*ALDG(CRED/CDX)

. DX(I)=DX1*EXP(QGQ*FLDAT(I))

E=EEQUIL+ESTEP

...FIN

. P(I)=CRED . PI(I)=CRED

FLECS/RT-11 V28.01

. KFI=KSTD*EXP(-ALPHA*E/25.691)

. KBI=KSTD*EXP((1.-ALPHA)*E/25.691)

C .

. WRITE (7,100) "33,"110,"33,"112

FLECS/RT-11 V28. 01

PAGE 3

C	. NONIDEAL SIMULATION ROUTINE
C	•
	. REPEAT UNTIL (TOUT. GT. TFINAL)
	IF (TIME.GT. 2. *TRISE) DT=DTNOR
	WHEN (TIME. GE. TRISE) E=EEGUIL+ESTEP
	ELSE E=EEGUIL+ESTEP*(TIME/TRISE)
C	
	KF=KSTD*EXP(-ALPHA*E/25.691)
	KB=KSTD*EXP((1ALPHA)*E/25.691)
C	
Ċ	SURFACE BOUNDARY CONDITIONS
č	
_	FLUX = (KF*C(1)-KB*P(1)) /
	1. (1, +KF*DX1/DOX+KB*DX1/DRED)
	CO=C(1)-FLUX+DX1/DOX
	PO=P(1)+FLUX*DX1/DRED
С	10-1 (171) EUX-DX17 DXED
Č	DIFFUSION
C	DIFFOSION
C	
	CNEW(1)=C(1)+DOX+DT/((DX(2)+DX1)+.5) *
	1 $((C(2)-C(1))/DX(2)-(C(1)-CO)/DX1)$
	DO (I=2,NVE)
	CNEW(I)=C(I)+DOX+DT/((DX(I+1)+DX(I))+.5) +
	1 $((C(I+1)-C(I))/DX(I+1)-(C(I)-C(I-1))/DX(I)$
	FIN
	DO (I=1,NVE) C(I)=CNEW(I)
С	• •
	CNEW(1)=P(1)+DRED*DT/((DX(2)+DX1)*.5) *
	1 $((P(2)-P(1))/DX(2)-(P(1)-P0)/DX1)$
	DO (I=2, NVE)
	CNEW(I)=P(I)+DRED+DT/((DX(I+1)+DX(I))*.5) *
	1 $((P(I+1)-P(I))/DX(I+1)-(P(I)-P(I-1))/DX(I)$
	FIN
	DD (I=1,NVE) P(I)=CNEW(I)
С	•
_	. IF (ABS(C(NVE-2)-CDX). GT. CDX+. 001) NVE=NVE+1
	IF (ABS(P(NVE-2)-CRED), GT. CRED+, OO1) NVE=NVE+1
	IF (NVE. GT. 100) STOP 'TOO MANY VOLUME ELEMENTS

PACE 4

FLECS/RT-11 V28.01

... FIN

```
C
            IDEAL SIMULATION ROUTINE
            UNLESS (TIME, EQ. O. O)
               KF=KFI
               KB=KBI
            ...FIN
C
C
            SURFACE BOUNDARY CONDITIONS
C
            FLUXI = (KF*CI(1)-KB*PI(1)) /
     1.
             (1.+KF*DX1/DOX+KB*DX1/DRED)
            COI=CI(1)-FLUXI*DX1/DOX
            POI=PI(1)+FLUXI*DX1/DRED
C
C
            DIFFUSION
            CNEW(1)=CI(1)+DOX*DT/((DX(2)+DX1)*.5) *
             ((CI(2)-CI(1))/DX(2)-(CI(1)-COI)/DX1)
     1.
            DO (I=2, NVEI)
                CNEW(I)=CI(I)+DOX+DT/((DX(I+1)+DX(I))+.5) +
                 ((CI(I+1)-CI(I))/DX(I+1) -
     1.
                 (CI(I)-CI(I-1))/DX(I))
     1.
             ...FIN
            DO (I=1, NVEI) CI(I)=CNEW(I)
C
            CNEW(1)=PI(1)+DRED*DT/((DX(2)+DX1)*.5) *
             ((PI(2)-PI(1))/DX(2)-(PI(1)-POI)/DX1)
     1.
            DO (I=2, NVEI)
                CNEW(I)=PI(I)+DRED+DT/((DX(I+1)+DX(I))*.5) *
                 ((PI(I+1)-PI(I))/DX(I+1) -
     1.
                 (PI(I)-PI(I-1))/DX(I))
     1.
             ... FIN
            DO (I=1, NVEI) PI(I)=CNEW(I)
C
            IF (ABS(CI(NVEI-2)-CDX), QT, CDX*, OO1)
                NVEI=NVEI+1
             ... FIN
            IF (ABS(PI(NVEI-2)-CRED). QT. CRED*. QO1)
               NVEI=NVEI+1
             ...FIN
            IF (NVEI. GT. 100)
                STOP 'TOO MANY VOLUME ELEMENTS (I)'
```

PACE 5 FLECS/RT-11 V28. 01 . OUTPUT SECTION C C . IF (TIME+. 5*DT. GT. TOUT) . TOUT=TOUT+DTOUT . . CURR=FLUX+96487. E6+AREA . . RAT=FLUX/FLUXI TYPE*, TIME, CURR, RAT, NVE . . . TYPE C . NEXT TIME INCREMENT . . TIME=TIME+DT ...FIN . PAUSE ...FIN

STOP

```
PACE 6
      FLECS/RT-11 V28. 01
C
      USER INTERFACE SECTION
C
      TO DISPLAY-MODIFY-PARMS
         WRITE-DATA
         REPEAT UNTIL (I.EQ. 0)
             WRITE (7,110) "33,"131,"61,"40,"33,"112
 110
             FORMAT (1X, 6A1, 'ENTER ENTRY TO CHANGE: '$)
             ACCEPT*, I
             CONDITIONAL
                (I.LT.O) WRITE-DATA
                (I. GT. 14) WRITE-DATA
                (I.EG.O) CONTINUE
                (OTHERWISE)
                   TYPE*, 'ENTER NEW VALUE'
                   ACCEPT*, A(I)
                   III=I+"41
                   WRITE (7,120) "33,"131, III, "64, A(I)
                ... FIN
             ... FIN
         ... FIN
      ... FIN
C
C
      TO WRITE-DATA
         WRITE (7, 100) "33, "110, "33, "112,
          KSTD, ESTEP, COX, DOX, CRED, DRED,, ALPHA
          AREA, DX1, QQQ, BETA, DTOUT, TFINAL, TRISE
     1.
         FORMAT (1X, 4A1, 'QUASI-REV CHRONOAMPS': //
 100
          1X, ' 1 STD RATE CON', T22, 1PQ10. 3,
     1.
           1X, ' 2 E STEP', T22, Q10. 3/
     1.
          1X, ' 3
                   CONC DX', T22, Q10. 3/
     1.
           1X, ' 4
                   DIFF COEFF 0X', T22, Q10. 3/
     1.
           1X, ' 5 CONC RED', T22, Q10. 3/
     1.
           1X, ' 6 DIFF COEFF RED', T22, Q10. 3/
     1.
          1X, ' 7 ALPHA', T22, Q10. 3/
     1.
           1X, '8 AREA', T22, G10. 3/
     1.
           1X, ' 9 DELTA X 1', T22, Q10. 3/
     1.
```

1X, '10 EXPANSION FACTOR', T22, 010. 3/

1X, '12 OUTPUT INTERVAL', T22, Q10. 3/

1X, '13 FINAL TIME', T22, Q10. 3/ 1X, '14 RISE TIME', T22, Q10. 3)

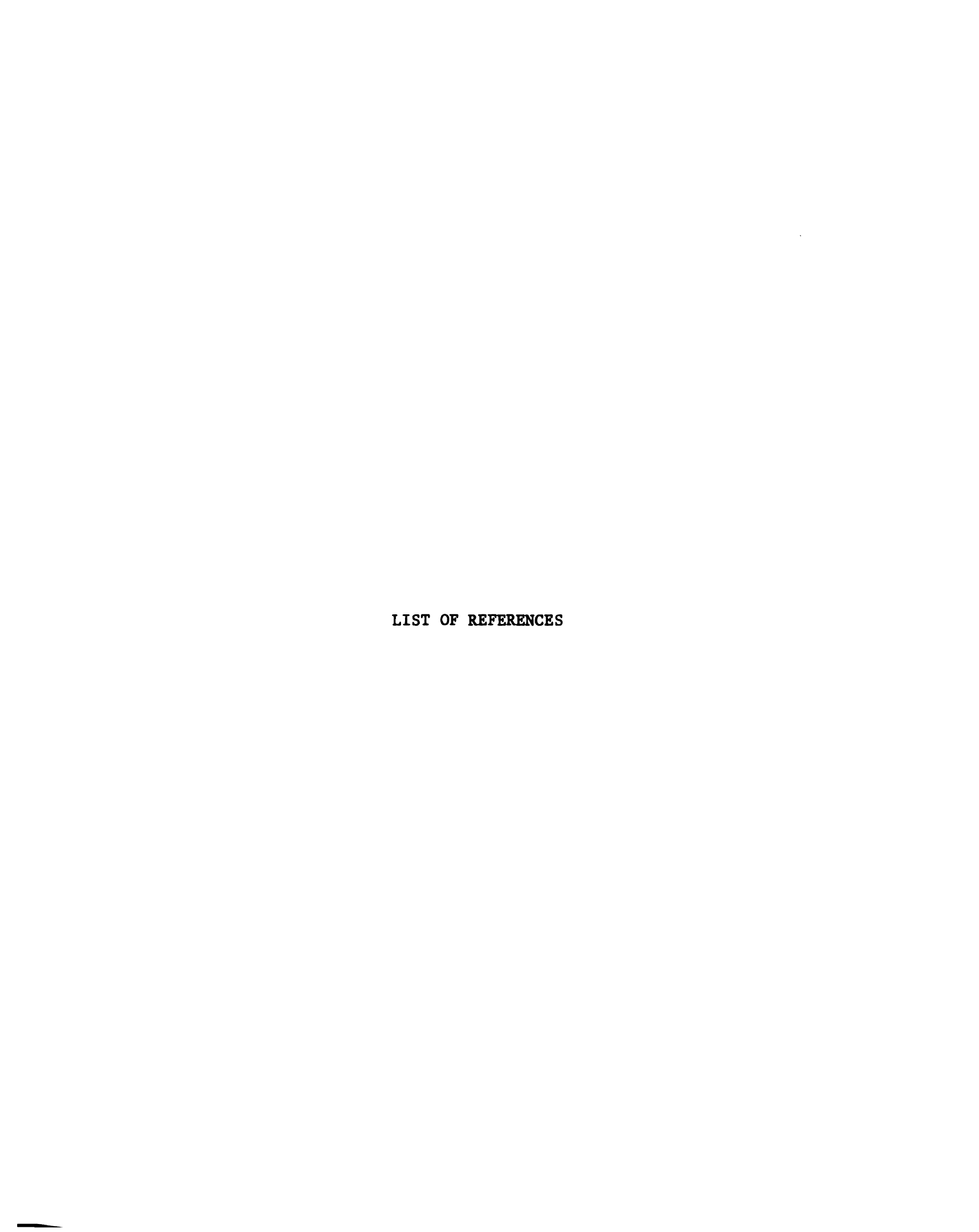
1X, '11 BETA', T22, G10. 3/

1.

1.

1.

...FIN



LIST OF REFERENCES

- 1. Z. Nagy, J. Electrochem. Soc., 125, 1809 (1978).
- 2. H. Reller and E. Kirowa-Eisner, J. Electrochem. Soc., 127, 1725 (1980).
- 3. Z. Nagy, Electrochim. Acta, 25, 575 (1979).
- J. M. Kudirka, P. H. Daum, and C. G. Enke, Anal. Chem., <u>44</u>, 309 (1972).
- 5. F. C. Anson, J. B. Flanagan, K. Takahashi, and A. Yamada, J. Electroanal. Chem., 67, 253 (1976).
- 6. J. B. Flanagan, K. Takahashi, and F. C. Anson, J. Electroanal. Chem., 81, 261 (1977).
- 7. J. B. Flanagan, K. Takahashi, and F. C. Anson, J. Electroanal. Chem., 85, 257 (1977).
- 8. See, for example, J. Albery, Electrode Kinetics, Clarendon Press, Oxford, 1975.
- 9. D. D. Macdonald, Transient Technique in Electrochemistry, Plenum Press, New York, 1977, p. 14.
- 10. P. Delahay, New Instrumental Methods in Electrochemistry, Interscience, New York, 1954, chapter 4.
- 11. H. Gerischer and W. Vielstich, Z. Phys. Chem. (Frankfort), 3, 16 (1955).
- 12. P. Delahay, J. Phys. Chem., 66, 2204 (1962).
- 13. W. H. Reinmuth, Anal. Chem., <u>34</u>, 1272 (1962).
- 14. P. Delahay and T. Berzins, J. Am. Chem. Soc., 75, 2486 (1953).
- 15. H. Matsuda, S. Oka, and P. Delahay, J. Am. Chem. Soc., <u>81</u>, 5077 (1959).
- D. E. Smith, Anal. Chem., <u>35</u>, 610 (1963).
- 17. R. S. Nicholson, Anal. Chem., 37, 1351 (1965).

- 18. R. J. Klingler and J. K. Kochi, J. Phys. Chem., 85, 1731 (1981).
- 19. D. T. Sawyer and J. L. Roberts, Experimental Electrochemistry for Chemists, Wiley-Interscience, New York, 1974, Chapter 5.
- 20. A. Bewick and M. Fleischmann, Electrochim. Acta, 8, 89 (1963).
- 21. P. Tyma, E. W. Schindler, and M. J. Weaver, to be submitted.
- 22. K. B. Oldham, J. Electroanal. Chem., 11, 171 (1966).
- 23. W. D. Weir and C. G. Enke, J. Phys. Chem., 71, 275 (1967).
- 24. A. N. Frumkin, Z. Physik. Chem., 164A, 121 (1933).
- P. Delahay, Double Layer and Electrode Kinetics, Interscience, New York, 1965, Chapter 4.
- 26. See, for example, D. C. Graham, Chem. Rev., 41, 441 (1947).
- 27. S. W. Feldberg in A. J. Bard (ed.), Electroanalytical Chemistry, Vol. 3, Marcel Decker, New York, 1969, pp. 199-296.
- 28. S. W. Feldberg in J. S. Mattson, H. B. Mark, and H. C. MacDonald (eds.), Electrochemistry, Marcel Decker, New York, 1972, pp. 185-218.
- · 29. D. Britz, Anal. Chim. Acta, 122, 331 (1980).
 - D. Britz, Digital Simulation in Electrochemistry, Springer-Verlag, Berlin, 1981.
- 31. T. Joslin and D. Pletcher, J. Electroanal. Chem., 49, 171 (1974).
- 32. E. W. Schindler and M. J. Weaver, submitted to Anal. Chim. Acta.
- 33. M. Przasnyski, J. Electroanal. Chem., 107, 419 (1980).
- 34. See, for example, D. D. Macdonald, Transient Techniques in Electrochemistry, Plenum Press, New York, 1977, p. 81.
- 35. T. Beyer, FLECS/RT-11 User's Guide, Government of Canada, Ottawa, 1980.
- 36. See, for example, R. Conway and D. Gries, An Introduction to Programming, Winthrop, Cambridge, Mass., 1975.
- 37. Microcomputer Processor Handbook, Digital Equipment Corporation, Maynard, Mass., 1979.
- 38. P. N. Rowe, Chemtech, 4, 9 (1974).

- 39. L. Meites, Crit. Rev. Anal. Chem., 8, 1 (1979).
- 40. L. Meites, The Multi-parametric Curve Fitting Program CFT4, Computing Laboratory, Department of Chemistry, Clarkson College, Potsdam, New York, 1976.
- 41. J. B. Flanagan, Ph.D. Thesis, California Institute of Technology, 1978.
- 42. W. Gautschi, SIAM J. Numer. Anal., 7, 187 (1970).
- 43. W. Gautschi, Comm. ACM, 12, 635 (1969).
- 44. See, for example, D. D. Macdonald, Transient Techniques in Electrochemistry, Plenum Press, New York, 1977, p. 77.
- 45. See, for example, A. J. Bard and L. R. Faulkner, Electrochemical Methods, John Wiley and Sons, New York, 1980, p. 186.
- 46. F. G. Cottrell, Z. Physik. Chem., <u>42</u>, 385 (1902).
- 47. P. Delahay in P. Delahay (ed.), Advances in Electrochemistry and Electrochemical Engineering, Wiley-Interscience, New York, 1961, Vol. 1, Chapter 5.
- 48. K. B. Oldham and E. P. Parry, Anal. Chem., 40, 65 (1968).
- 49. J. H. Christie, E. P. Parry, and R. A. Osteryoung, Electrochim. Acta, 11, 1525 (1966).
- 50. A. A. Pilla, J. Electrochem. Soc., 117, 467 (1970).
- 51. J. Mozota, B. Barnett, D. Tessier, H. Angerstein-Kozlowska, and B. E. Conway, Anal. Chim. Acta, 183, 191 (1981).
- 52. M. J. Weaver, private communication.
- 53. A. M. Bond, Modern Polarographic Methods in Analytical Chemistry, Marcel Decker, New York, 1980.
- 54. J. Janata and J. Ruzicka, Anal. Chim. Acta, 139, 105 (1982).
- 55. P. T. Kissinger, C. Refshauge, R. Dreiling, and R. N. Adams, Anal. Lett., <u>6</u>, 465 (1973).
- 56. H. Reller and E. Kirowa-Eisner, J. Electroanal. Chem., 103, 335 (1979).
- 57. H. P. VanLeeuwen, Electrochim. Acta, 23, 207 (1978).
- 58. E. Levart and E. Poirier d'Ange d'Orsay, J. Electroanal. Chem., 19, 335 (1968).

- 59. H. Gerischer and M. Krause, Z. Phys. Chem. (Frankfort), <u>10</u>, 264 (1957).
- 60. Z. Nagy, J. Electrochem. Soc., <u>126</u>, 1148 (1979).
- 61. Z. Nagy, J. Electrochem. Soc., <u>128</u>, 786 (1981).
- 62. Z. Nagy, Electrochim. Acta, 26, 671 (1980).